Tracking Chart – Structural TAC

**31-Special Construction**

| Mod # | Proponent | Chapter | Section | Summary |
|---|---|---|---|---|
| 8357 | Joseph Belcher for Bison | 31 | 3115 | Adds section for exterior elevated flooring systems. |

**No Affirmative Recommendation**

**Commission Action**

☐ AS ☐ AM ☐ I ☐ W ☐ NAR

**Comment**

| | | | | | |
|---|---|---|---|---|---|
| ☐ | 1. Support comment. Comment sufficiently addresses the TAC's concern(s). | | ☒ XX | 2. Do Not Support comment. Comment does not address the TAC's concern(s). | A2 + A3 |
| ☐ | 3. No comment is needed. | | ☐ | 4. Straw Poll. | 3 Yes – 8 No |

# S8357

| | | | | | |
|---|---|---|---|---|---|
| **Date Submitted** | 12/15/2018 | **Section** | 3115 | **Proponent** | Joseph Belcher for Bison |
| **Chapter** | 31 | **Affects HVHZ** | Yes | **Attachments** | No |

**TAC Recommendation** No Affirmative Recommendation
**Commission Action** Pending Review

## Comments

**General Comments** No

**Alternate Language** Yes

### Related Modifications

Related definitions in Section 202

### Summary of Modification

Adds section for exterior elevated flooring systems.

### Rationale

Exterior elevated flooring systems are increasingly seen on rooftops and other exterior locations. The systems are used to create space typically used for assembly occupancies such as restaurants, bars, and nightclubs, and gathering places. The code does not adequately address such systems. This proposal is to address that need.

In many cases, the flooring system is treated as a roof, and overly restrictive provisions are applied. The exterior elevated flooring system is not a roof but is a floor created on a rooftop or other supporting structure. The proposal provides for continuing to treat the systems as a roof by attaching the support pedestals to the roof surface. However, considerable research has shown that these systems due to their air-permeability react to wind forces differently than the typical rooftop. The application of current literature and the use of wind tunnel testing coupled with new provisions on air-permeable cladding in ASCE 7-16 will allow more economical construction of these popular systems with no reduction in safety.

### Fiscal Impact Statement

**Impact to local entity relative to enforcement of code**

No impact on the cost of enforcement of code.

**Impact to building and property owners relative to cost of compliance with code**

The provisions will likely result in savings to property owners desiring to turn rooftops and other exterior spaces into useable areas.

**Impact to industry relative to the cost of compliance with code**

The provisions will allow economical expansion of the conversion of unusable spaces. The provisions will likely result in savings to industry constructing exterior elevated flooring system to turn rooftops and other spaces into useable areas.

**Impact to small business relative to the cost of compliance with code**

The provisions will allow economical expansion of the conversion of unusable spaces benefitting the owners of small businesses. The provisions will likely result in savings to small businesses seeking to add useable areas to their business by installing exterior elevated flooring systems.

### Requirements

**Has a reasonable and substantial connection with the health, safety, and welfare of the general public**

Occupied roofs using elevated flooring systems are becoming more common and the code does not adequately address the systems. This proposal will help to assure the health, safety, and welfare of members of the public using such facilities.

**Strengthens or improves the code, and provides equivalent or better products, methods, or systems of construction**

The change to the code will improve the code by addressing a system not adequately addressed by the code and helping to assure the safety of the public.

**Does not discriminate against materials, products, methods, or systems of construction of demonstrated capabilities**

The change does not discriminate against materials, products, methods, or systems of construction of demonstrated capabilities.

**Does not degrade the effectiveness of the code**

The proposed change does not degrade the effectiveness of the code.

## Alternate Language

## 2nd Comment Period

**8357-A3**

**Proponent** Joseph Belcher **Submitted** 5/26/2019 **Attachments** Yes

**Rationale**

Forgot to attach files.

**Fiscal Impact Statement**

**Impact to local entity relative to enforcement of code**

None.

**Impact to building and property owners relative to cost of compliance with code**

None.

**Impact to industry relative to the cost of compliance with code**

None.

**Impact to Small Business relative to the cost of compliance with code**

The provisions will allow economical expansion of the conversion of unusable spaces benefitting the owners of small businesses. The provisions will likely result in savings to small businesses seeking to add useable areas to their business by installing exterior elevated flooring systems.

**Requirements**

**Has a reasonable and substantial connection with the health, safety, and welfare of the general public**

None.

**Strengthens or improves the code, and provides equivalent or better products, methods, or systems of construction**

None.

**Does not discriminate against materials, products, methods, or systems of construction of demonstrated capabilities**

None.

**Does not degrade the effectiveness of the code**

None.

## Alternate Language

## 2nd Comment Period

**8357-A2**

**Proponent** Joseph Belcher **Submitted** 5/26/2019 **Attachments** Yes

**Rationale**

See uploaded file. The system says the Rationale exceeds the allowed 2000 characters. MS Word Count says the Rationale statement is 1981 characters including spaces.

**Fiscal Impact Statement**

**Impact to local entity relative to enforcement of code**

No impact on the cost of enforcement of the code.

**Impact to building and property owners relative to cost of compliance with code**

The provisions will likely result in savings to property owners desiring to turn rooftops and other exterior spaces into a useable area.

**Impact to industry relative to the cost of compliance with code**

The provisions will economically allow the conversion of heretofore unusable spaces into attractive useable spaces. The provisions will likely result in savings to industry constructing exterior elevated flooring system to turn rooftops and other spaces into a useable area.

**Impact to Small Business relative to the cost of compliance with code**

The provisions will allow economical expansion of the conversion of unusable spaces benefitting the owners of small businesses. The provisions will likely result in savings to small businesses seeking to add useable areas to their business by installing exterior elevated flooring systems.

**Requirements**

**Has a reasonable and substantial connection with the health, safety, and welfare of the general public**

Occupied roofs using elevated flooring systems are becoming more common, and the code does not address the systems. This proposal will help to assure the health, safety, and welfare of members of the public using such facilities by providing guidelines to designers, contractors, and code enforcers.

**Strengthens or improves the code, and provides equivalent or better products, methods, or systems of construction**

The change to the code will improve the code by addressing a popular system not addressed by the code and helping to assure the safety of the public.

**Does not discriminate against materials, products, methods, or systems of construction of demonstrated capabilities**

The change does not discriminate against materials, products, methods, or systems of construction of demonstrated capabilities.

**Does not degrade the effectiveness of the code**

The proposed change does not degrade the effectiveness of the code.

This is not alternate language. I forgot to attach the new referenced standards and the research to the Alternate Language submitted earlier.

**Exterior Elevated Flooring System.** ~~An elevated flooring system installed over roofing systems or other supporting structures.~~ An assembly installed over a roof assembly ~~and /~~ or other exterior supporting structure consisting of a walking surface of pedestrian deck panels ~~/~~ or pavers mounted on pedestals using other accessory components, ~~and~~ mechanical fasteners ~~and /~~ or adhesives as required by the manufacturer's installation instructions for attaching pedestrian deck panels ~~/~~ or pavers to pedestals and other accessory components. Exterior elevated flooring systems may have pedestals attached to the roof or other supporting structure or pedestals installed independently of the roof or supporting structure with the restraint of the pavers at the perimeter and ~~or~~ discontinuous edges. Exterior elevated flooring systems are not part of the roof assembly.

**Attached systems.** Attached systems are those where pedestals are attached to the roof or other supporting structure by mechanical fasteners, adhesives, or both.

**Independent systems.** Independent systems are those where pedestals are not attached to the roof but rest on the roof or other supporting structure.

**Pedestrian Deck Panels~~/and~~ or Pavers.** Pedestrian deck panels ~~/~~ or pavers for ~~the purpose of~~ this section are manufactured from materials such as naturally durable wood, ceramic, stone, or concrete suitable for exterior applications.

**Pedestal.** A fixed or adjustable-height support column composed of a ~~plastic~~ support base, ~~plastic~~ vertical structural element, and a ~~plastic~~ load bearing top cap ~~/~~ surface.

**Accessory Components.** ~~These c~~ Components ~~are~~ used in the installation of pedestals and pedestrian deck panels ~~/~~ or pavers of the exterior elevated flooring system. ~~These~~ Accessory components are made of either plastic, ~~or~~ metal, or other approved materials. ~~These~~ Accessory components may be used to provide lateral bracing of the pedestals, to provide vertical support, for leveling the pedestal, ~~and~~ to restrain the pedestrian deck panels ~~/~~ or pavers to the top of the pedestal, or for other system requirements.

**3101.1 Scope.** The provisions of this chapter shall govern special building construction including membrane structures, temporary structures, pedestrian walkways and tunnels, automatic vehicular gates, awnings and canopies, marquees, signs, ~~and~~ towers and antennas, and exterior elevated flooring systems.

## Section 3115

## Exterior Elevated Flooring Systems.

**3115.1 Scope.** This section ~~is applicable~~ applies to exterior elevated flooring systems installed over roof assemblies or other exterior supporting structures such as an exterior deck. Each exterior elevated flooring system consists of pedestrian deck panels ~~/~~ or pavers supported by pedestals placed directly on roof

assemblies or other exterior supporting structures, to provide a level walking surface. Pedestals ~~can~~ may be ~~adjusted~~ adjustable ~~to various heights or installed at~~ or a fixed height.
The pedestals need not be mechanically or adhesively attached to the supporting structure. The exterior elevated flooring system comprised of the pedestrian deck panels ~~/~~ or pavers and pedestals ~~must~~ shall be restrained on all sides and along any ramps and ~~/or~~ walkway areas against horizontal and vertical movement using a perimeter-restraining system.

**3115.1.1 Attached exterior elevated flooring systems.** Attached systems shall be designed and constructed as a roofing system in accordance with Chapter 15 of this code.

**3115.1.2 Independent exterior elevated flooring systems.** Independent systems shall comply with the provisions of Section 3115.

**3115.2 Materials Information Submitted with Permit Application.** In addition to other information required to accompany the permit application, product-specific information shall be provided as follows:

**3115.2.1 Pedestrian Deck panels~~/~~ or pavers.** Documentation describing the weight, dimensions, specifications, and the manufacturing process of the materials. Specifications for ~~cementitious~~materials ~~such as concrete pavers~~ shall include required material strength properties used in analysis or reference to appropriate tests used to determine paver load capacity.

**3115.2.2 Pedestals.** Documentation describing materials, dimensions, specifications, ~~compression strength~~, and manufacturer's installation instructions. Specifications shall include the allowable axial compression capacity of the pedestal.

**3115.2.3 Fasteners.** Documentation describing mechanical fasteners and adhesives as applicable. A statement shall be provided regarding whether or not the fasteners are commonly available or are proprietary.

**3115.2.4 Plastics for outdoor exposure HVHZ.** Plastics for outdoor exposure in the HVHZ shall comply with Florida Building Code-Building Section 2615.2.

**3115.2.5 Packaging and Identification.** A description of the method of packaging and identification of pedestrian deck panels ~~/~~ or pavers, pedestals, and accessory components. Identification provisions shall include the manufacturer's name, the product name, and copy of the installation instructions, as packaged with the product.

**3115.3 Product Approval and Manufacturer's Installation Instructions.**

**3115.3.1 Product approval.** Exterior elevated flooring systems shall have Florida ~~P~~product ~~A~~ approval or local product approval.

**3115.3.2 Manufacturer's installation instructions**. Manufacturer's installation instructions shall include information on the protection of the roof surface during installation, procedures for removing pavers to facilitate reroofing, roofing repairs, and roofing maintenance. In addition to the copy of the manufacturer's installation instructions submitted with the permit application, the manufacturer's installation instructions shall be kept on the job site and made available to inspection personnel.

**3115.4 Structural Requirements for Exterior Elevated Flooring Systems.**

**3115.4.1 General.** Exterior elevated flooring systemsshall withstand the applicable uniform loads of Florida Building Code-Building Table 1607.1, the applicable load combinations, and other applicable loads contained in ~~FBC-B~~ the Florida Building Code-Building, Chapter 16.

**3115.4.2 Pedestrian Deck panels / or pavers.** Where analysis of panels or pavers is not consistent with codified material design procedures, testing for uniform load and concentrated load capacities shall be performed in accordance with ASTM E2322 and CISCA Recommended Test Procedures for Access Floors achieving a load capacity three (3) times the uniform load capacity designated in the specifications.

**3115.4.3 Pedestals.** Where analysis of pedestals is not consistent with codified material design procedures, testing for axial load capacity shall be performed in accordance with CISCA Recommended Test Procedures for Access Floors, 2016, Section 5 achieving a load capacity three (3) times the axial load capacity designated in the specifications.

**3115.4.4 Wind resistance.** Wind resistance of independent exterior elevated flooring systems shall be determined by wind tunnel testing in accordance with ASCE 7 Chapter 31 and Section 30.1.5 where applicable. Testing shall be conducted, and the data analyzed by a registered design professional. Exterior elevated flooring systems shall be evaluated by a registered design professional to withstand applicable wind loads as specified in ASCE 7 Chapters 26 through 30, as applicable, as well as combined load effects of other applicable gravity loads in ~~FBC-B~~ the Florida Building Code-Building, Chapter 16, such as live and dead loads.

**3115.4.5 Deflection.** Pedestrian deck panels or pavers shall meet the deflection requirement of floor members in Table 1604.3 and Section 1616.3.1 in the HVHZ.

**3115.5 Substrate Requirements for Exterior Elevated Flooring Systems.**

**3115.5.1 Bearing Capacity**. Pedestal support surface or roofing membrane shall be able to support a concentrated surface load of 40 psi under the pedestal base.

**3115.5.2 Drainage.** The substrate immediately below the pedestals shall provide positive drainage.

**3115.5.3 Analysis.** Load effects on structural members and their connections that provide support for independent exterior elevated flooring systems shall be determined by methods of structural analysis that take into account equilibrium, general stability, geometric compatibility and both short- and long-term material properties. Roof structures that provide support for exterior elevated flooring systems shall be checked for deflection in accordance with Section 1604.3.6 or Section 1616 for buildings sited in the HVHZ. Roof structures shall be checked in accordance with Section 1611 for ponding. The design shall account for concentrated loads of the pedestals.

**3115.6 Accessibility.** Accessibility shall comply with the Florida Building Code-Accessibility.

**Chapter 35:**

**ASTM:**

E2322-03 (Reapproved 2015) Standard Test Method for Conducting Transverse and Concentrated Load Tests on Panels used in Floor and Roof Construction……..……...……3115.4.2

**CCIS** Ceilings and Interior Systems Construction Association

1010 Jorie Blvd., Suite 30

Oak Brook, IL 60523

Recommended Test Procedures for Access Floors…….3115.4.2, 3115.4.3

**ASCE/SEI: (Add to existing code section references)**

7-16 ……...…….3115.2.3. 3115.4.4

**202**

**Exterior Elevated Flooring System.** An elevated flooring system installed over roofing systems or other supporting structures. Exterior elevated flooring systems may be attached to the supporting structure or installed independently of the supporting structure or a combination thereof.

**Attached systems.** Attached systems are those where pedestals are attached to the roof or other supporting structure by mechanical fasteners, adhesives, or both.

**Independent systems.** Independent systems are those where pedestals are not attached to but rest on the roof or other supporting structure.

**Exterior Elevated Flooring System.** An assembly installed over a roof assembly and/or exterior supporting structure consisting of pedestrian deck panels/pavers mounted on pedestals using other accessory components, and mechanical fasteners and/or adhesives as required by the manufacturer for attaching deck panels/pavers to pedestals and other accessory components.

**Pedestrian Deck Panels/Pavers.** Pedestrian deck panels/pavers for the purpose of this section are manufactured from materials such as naturally durable wood, ceramic, stone, or concrete suitable for exterior applications.

**Pedestal.** A fixed or adjustable-height support column composed of a plastic support base, plastic vertical structural element, and a plastic load bearing top cap/surface.

**Accessory Components.** These components are used in the installation of pedestals and deck panels/pavers of the exterior elevated flooring system. These components are made of either plastic or metal material. These components may be used to provide lateral bracing of the pedestals, vertical support, leveling the pedestal, and to restrain the deck panel/paver to the top of the pedestal.

**3101.1 Scope.** The provisions of this chapter shall govern special building construction including membrane structures, temporary structures, pedestrian walkways and tunnels, automatic vehicular gates, awnings and canopies, marquees, signs, ~~and~~ towers and antennas, and exterior elevated flooring systems.

**Section 3115**

**Exterior Elevated Flooring Systems**

**3115.1 Scope.** This section is applicable to exterior elevated flooring systems installed over roof assemblies or other exterior supporting structures. Each exterior elevated flooring system consists of deck panels/pavers supported by pedestals placed directly on roof assemblies or exterior supporting structures, to provide a level walking surface. Pedestals can be adjusted to various heights or installed at a fixed height.
The pedestals need not be mechanically or adhesively attached to the supporting structure. The exterior elevated flooring system comprised of the deck panels/pavers and pedestals must be restrained on all sides against horizontal movement using a perimeter-restraining system and along any ramps and/or walkway areas.

**3115.1.1 Attached exterior elevated flooring systems.** Attached systems shall be designed and constructed as a roofing system in accordance with Chapter 15 of this code.

**3115.1.2 Independent exterior elevated flooring systems.** Independent systems shall comply with the provisions of Section 3115.

**3115.2 Information Submitted with Permit Application.** In addition to other information required to accompany the permit application, product-specific information shall be provided as follows:

**3115.2.1 Deck Panels/Pavers.** Documentation describing the weight, dimensions, specifications, and the manufacturing process of the materials. Specifications for cementitious materials such as concrete pavers shall include 28-day compressive strength ($f_{c'}$), impact resistance, and density.

**3115.2.2 Pedestals.** Documentation describing materials, dimensions, specifications, and manufacturer's installation instructions.

**3115.2.3 Fasteners.** Documentation describing mechanical fasteners and adhesives as applicable. A statement shall be provided regarding whether or not the fasteners are commonly available or are proprietary.

**3115.2.4 Packaging and Identification.** A description of the method of packaging and identification of deck panel/pavers, pedestals, and accessory components. Identification provisions shall include the manufacturer's name, the product name, and a copy of the installation instructions, as packaged with the product.

**3115.3 Product Approval and Manufacturer's Installation Instructions.**

**3115.3.1 Product approval.** Exterior elevated flooring systems shall have Florida Product Approval or local product approval.

**3115.3.2 Manufacturer's installation instructions**. In addition to the copy of the manufacturer's installation instructions submitted with the permit application, manufacturer's installation instructions shall be kept on the job site and made available to inspection personnel.

**3115.4 Structural Requirements for Exterior Elevated Flooring Systems.**

**3115.4.1 General.** Exterior elevated flooring system shall withstand the applicable uniform loads of FBC-B Table 1607, the applicable load combinations and other loads contained in FBC-B Chapter 16.

**3115.4.2 Wind resistance.** Wind resistance of independent exterior elevated flooring systems shall be determined by wind tunnel testing in accordance with ASCE 7 Chapter 31and Section 30.1.5 where applicable. Testing shall be conducted and the data analyzed by a registered design professional. Exterior elevated flooring systems shall be evaluated by a registered design professional to withstand applicable wind loads as specified in ASCE/SEI 7 Chapters 26 through 30, and the combined load effects of other applicable gravity loads in FBC-B Chapter 16, such as live and dead loads.

The proposed code change is not intended to provide instructions on the specific design of exterior elevated flooring systems but to provide guidance for the design and installation of the systems. There is no guidance in the code for designers or code enforcers. There is considerable research available on the systems and ASCE 7 permits the use of wind tunnel studies, test data or recognized literature for the design of air permeable systems in Chapter 30 (ASCE 7-16 §30.1.5). (See uploaded file.) The proposed change requires the use of wind tunnel testing per ASCE 7 Chapter 31 and §30.1 where applicable.

Alternate Language A-1 expands the section on structural requirements, adds a section on substrate requirements, expands the requirements to be included in the manufacturer's instructions, adds two reference standards for testing of pedestrian deck panels or pavers, and adds deflection criteria. The change is also modified to address the comments of the Structural TAC members and members of the public.

1. The definition was corrected to a single definition at §202.
2. Concentrated loads on the roofing material are addressed at §3115.5.3.
3. Protection of the roofing membrane during installation is addressed at §3115.3.2.
4. The provisions for limiting pedestals to plastic were removed at. §202 - Pedestal.
5. The provisions have been made as material neutral as possible throughout the proposed change.
6. Plastic weathering requirements for the HVHZ were added at §3115.2.4.
7. Reference to the ADA requirements of the code were added at §3115.6.
8. Provisions addressing interaction between the system and the roofing membrane were added at §3115.5.
9. Provisions related to reroofing, repair, and maintenance of the roofing membrane were added to §3115.3.2.
10. HVHZ specific references are provided. Generally, references to Chapter 16 are intended to invoke the Scope of Chapter 16 to direct users to either the non-HVHZ sections or the HVHZ sections as appropriate.

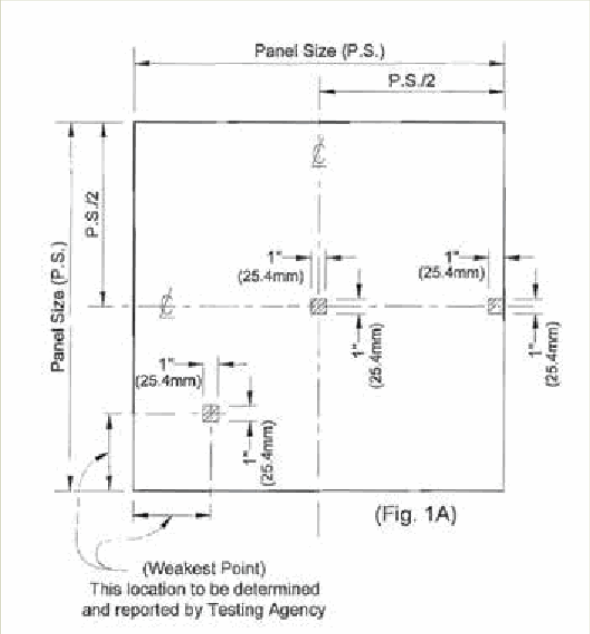


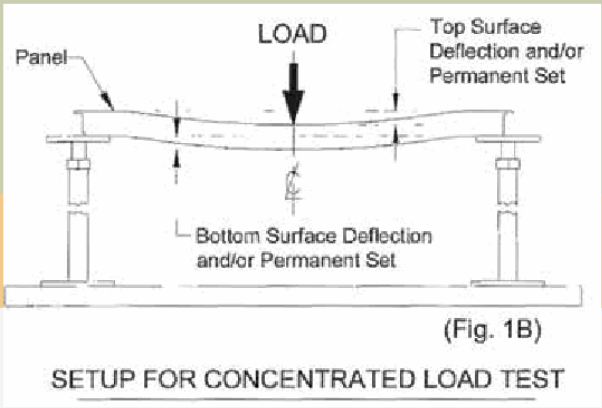


SETUP FOR CONCENTRATED LOAD TEST

# Recommended Test Procedures for Access Floors

CISCA
Ceilings & Interior Systems
Construction Association

This publication,

***Recommended Test Procedures for Access Floors***

was reviewed and no revisions were suggested by the Committee, February, 2016.

***Review Committee:***

**Jim Scissom, Chairman**
ASM Modular Systems Inc.
9500 Industrial Center Drive
Ladson, SC 29456
843-534-1110
jscissom@asmproducts.com

**Jeff Musculus**
Steelcase
PO Box 1967
Grand Rapids, MI 49501
616-698-4685 jmusculu@steelcase.com

**Ryan Hulland**
Netfloor USA
374 Crompton Street
Charlotte, NC 28273
(844) 638-3566
ryan@netfloorusa.com

**Scott Carmichael**
Seal Bond
14851 Michael lane
Spring Lake, MI 49456
800-2524144 X 109
scarmichael@seal-bond.com

**Amy Rapson**
Haworth, Inc.
One Haworth Center
Holland, MI 49423
616-639-3000
amy.rapson@haworth.com

**Bill Reynolds**
Tate, Inc.
7510 Montevideo Dr.
Jessup, MD 20794
410-799-4720
breynolds@tateinc.com

**Mark Krauk**
ASM Modular Systems Inc.
9500 Industrial Center Drive
Ladson, SC 29456
843-534-1110
mark.krauk@asmproducts.com

**BrianVogel**
Haworth, Inc.
One Haworth Center
Holland, MI 49423
616-639-3000
brian.vogel@haworth.com

**Earl Geertgens**
FreeAxez 1810 Underwood Blvd.
Delran, NJ 08075
856-764-0400
earl@freeaxez.com

CISCA
Ceilings & Interior Systems Construction Association

**Ceilings & Interior Systems Construction Association (CISCA)**
CISCA exists to provide a network of opportunities with all industry leaders through education and a forum to allow the interior construction industry to interact, evolve and prosper.

CISCA's vision is to be the acknowledged leader of participating decision-makers in the promotion and support of the interior construction industry. CISCA aspires to be a dynamic, accessible, and valuable network which is market-driven and is transformational in continually leading the ceiling and interior systems industry to new levels of success.

# Recommended Test Procedures for Access Floors Introduction

The publication of CISCA Recommended Test Procedures for Access Floors by the Ceilings & Interior Systems Construction Association (CISCA) represents a significant milestone in establishing a common basis of accepted test methods.

This document is intended to benefit contractors, specifiers, users, and manufacturers. By providing an accepted frame of reference for access floor testing, product characteristics can be judged in a fair context of industry-approved uniform test methods.

CISCA's intent is to provide a method for evaluating access floor characteristics, not criteria requirements. Because differing circumstances demand a range of performance levels, both manufacturers and users benefit from a variety of types of access floors in the marketplace. CISCA is strongly committed to developing test procedures that will appropriately address other performance factors related to all types of access floors.

It is essential, however, that product comparisons be based upon commonly used tests for valid results. These procedures have now been established in an industry-wide spirit of cooperation to achieve our common goal.

## History

CISCA's involvement with access floor test procedures began in 1983, when interior contractor Jim Whittaker, Chairman of the CISCA Seismic Committee, proposed that the manufacturers meet and recommend changes to the Uniform Building Code (UBC). The International Conference of Building Officials (ICBO) then incorporated the CISCA-recommended changes into the 1985 UBC.

When the access floor manufacturers met again in May 1985, this time with the intention of developing a fair method of measurement for concentrated and rolling loads on access floors, the CISCA Access Floor Committee was born. The Committee agreed to develop test methods, not criteria; and further agreed that testing should be done by independent laboratories.

Over the next year, drafts of proposed test procedures were circulated to all known access floor manufacturers for review and comment. In 1987, The CISCA Board agreed to adopt the documents as CISCA's recommended test procedures and to encourage manufacturers to test their access floor products in this manner and report the data on the approved forms. The procedures were approved and published in July 1987.

In 2003, the CISCA Access Floor Committee reconvened to address changes in the marketplace. The committee agreed to tackle the task in two phases. In phase one, immediate issues were addressed and an updated version of Recommended Test Procedures for Access Floors was approved by CISCA's Board of Directors and reprinted in April 2004.

For phase two, the committee went back to work to address the more difficult issues as well as changes in the marketplace. The final document was submitted for approval to the Board of Directors in April 2007.

## Contents

Testing procedures were established for concentrated load, ultimate load, rolling loads, stringer load, pedestal axial load, pedestal overturning moment, uniform load, drop impact load, fire performance and air leakage. These test procedures are user-oriented and represent sound engineering principles.

## Interpretation of Test Results

No particular testing agency is recommended for these tests. Manufacturers are encouraged to select appropriate independent laboratories to test and certify test results.

Because sound engineering principles were used to develop the testing procedures, there should be no requirements to retest components for use in specific installations. For example, pedestals will be tested at the maximum design height; if pedestals are used at lower floor heights, there is no need to retest to assure the desired performance for that lower height. Further, system load tests will be performed utilizing bare panels, eliminating the need to test with each of the wide variety and thicknesses of wearing surfaces utilized in actual installations.

**Note regarding the use and priority of units of measure:**

All units of measure are expressed Inch/Pounds (in/lb) units, with the corresponding SI (Metric) units noted parenthetically. The in/lb units are to be treated as authoritative. Test results conducted pursuant to these procedures may be expressed in either unit, at the option of the proponent.

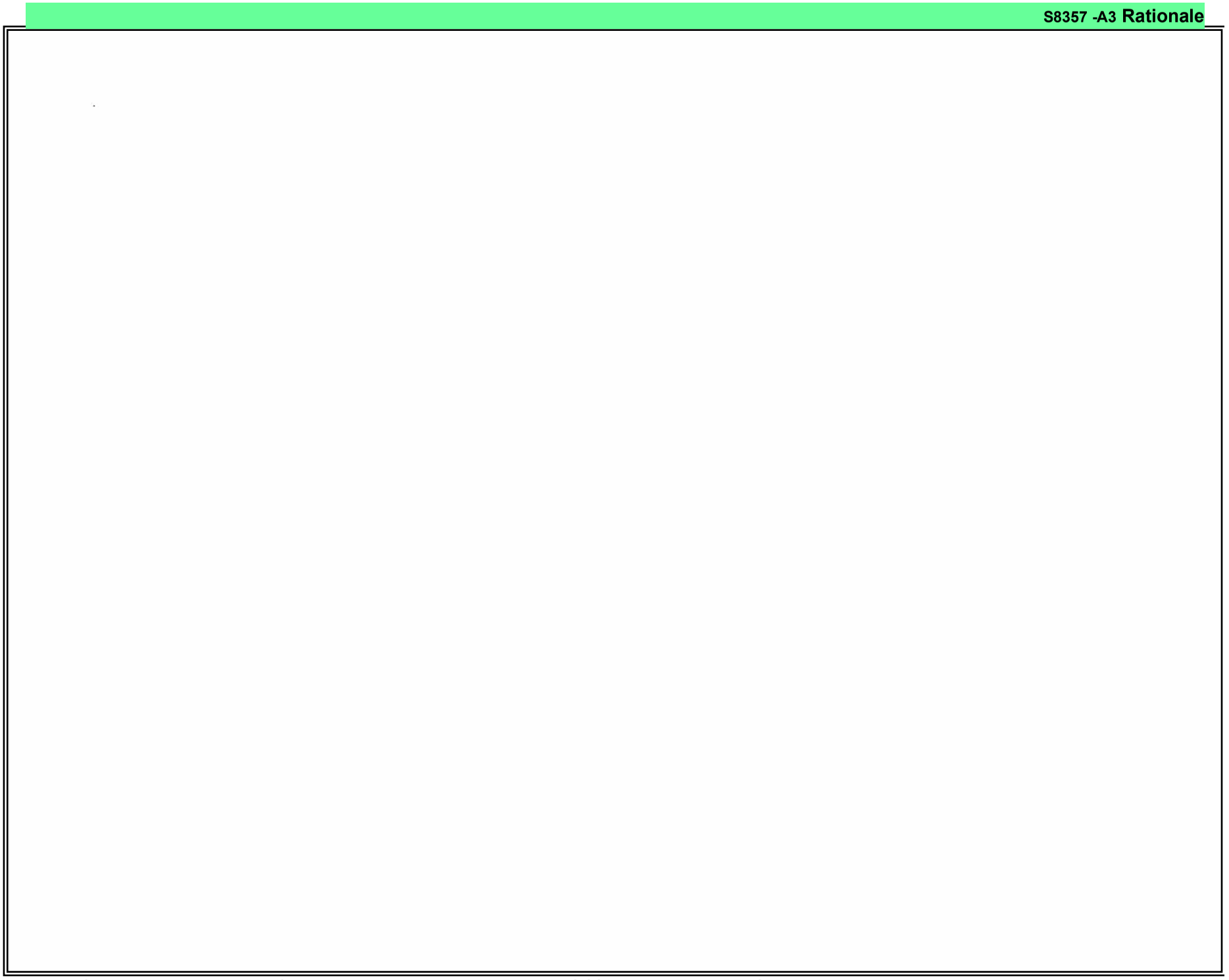

# CISCA Testing Procedures Index

# Section 1
# Concentrated Load

## Purpose:

To determine the maximum deflection(s) and permanent set(s) of an access floor under load.

## Preparation:

1. Test shall be performed on three (3) randomly selected bare panel assemblies. (Four (4) panels are required if panel configuration is not structurally symmetrical.) Panels shall be placed on steel blocks or supports configured to provide support identical to that provided by an installed system. Any coatings, gaskets, pads, clips, fasteners, floor covering, or other materials as required by manufacturer shall be identical to an installed system. Blocks or supports shall not reduce the unsupported edge span below that normally provided with a standard installed system.
2. Panels designed for stringer support shall have stringers spanning the blocks or supports with panel perimeter support and/or interface in an identical manner to the configuration of the installed floor systems. Stringers shall be identical to those of the installed floor system, attached or fitted to the support blocks in an identical manner to the installed floor system, and shall include any coatings, gaskets, pads, clips, fasteners, finishes or other materials as required by the manufacturer in the installed floor system.
3. Height of the test mock-up shall be sufficient to accommodate deflections of stringers and panels and to allow for instrumentation.
4. Concentrated loading shall be applied to the structure though a steel indentor 1" (25.4 mm) square (if applicable, floor covering shall be removed at indentor location). This square indentor may have eased edges at maximum .008" (0.20 mm) radii, but the footprint contact area shall not measure more than 1" x 1" (25.4 mm x 25.4 mm). A round indentor (1.128" [28.65 mm] diameter) may be utilized in lieu of a square indentor provided the footprint contact area shall not exceed one square inch (645 mm2).

## Test Procedure:

1. Each panel shall be loaded at its "weakest point," as determined by the Manufacturer's internal and /or independent / certifying testing agency to be the location which allows the greatest deflection under load. In addition to the "weakest point" panels shall be tested at the centroid and midpoint of edge. In the case of access flooring systems where panels are not contiguous, loads shall also be applied to the "weakest point" of the connecting material (e.g. steel cap) between panels.
2. Each panel shall be pre-loaded for each test to the test load at each location. A pre-load of 50 lb (222 N) shall then be applied and the instrumentation measuring deflection and load shall be set at zero. (Reference zero = 50 lb [222 N] pre-load)
3. Each panel shall be tested for each applied load location. After the pre-load each panel shall be tested at each applied load location by increments not exceeding 200 lb (890 N), with initial load no more than one-half test load. Rate of load application shall not exceed 1500 pounds per minute (6.675 kN/min).
4. Top surface deflection and permanent set shall be measured at each applied load location by recording indentor movement. For products with uneven bottom surfaces and where the deflection and set are measured on the bottom of the panel, the measurements shall be taken at the lowest adjacent horizontal surface.
5. Loads shall be applied at each location for a minimum of one (1) minute and deflection readings taken at the end of that period. The load shall then be relaxed to reference zero (Reference zero = 50 lb [222 N] pre-load) for a minimum one (1) minute and deflection shall be recorded.

## Report:

1. Reference of testing procedure described herein by CISCA A/F section number shall be included in report.
2. All apparatus, equipment, instrumentation, accuracy ranges, etc. shall be described including equipment calibration/certification dates.
3. Materials tested and mock-up configuration(s) should be fully described in verbiage or referenced to manufacturers drawings and/or part numbers, either containing the following information:

   **Panels:**
   - Material(s) of panel construction.
   - Weight, nominal dimensions and thicknesses.

   **Stringers:**
   - Material(s) of construction.
   - Weight, and nominal dimensions and thickness, including fasteners, gaskets, coatings, clips, etc.

   **Other:**
   - Fully describe gasketing, pads, other items utilized in the system.
4. Panel deflection measurements, of the top surface shall be reported to the nearest .001" (0.025 mm) for each applied load.
5. Panel permanent set of the top surface shall be reported to the nearest .001" (0.025 mm) for each applied load.

**Section 1:** – Panel Loading Locations

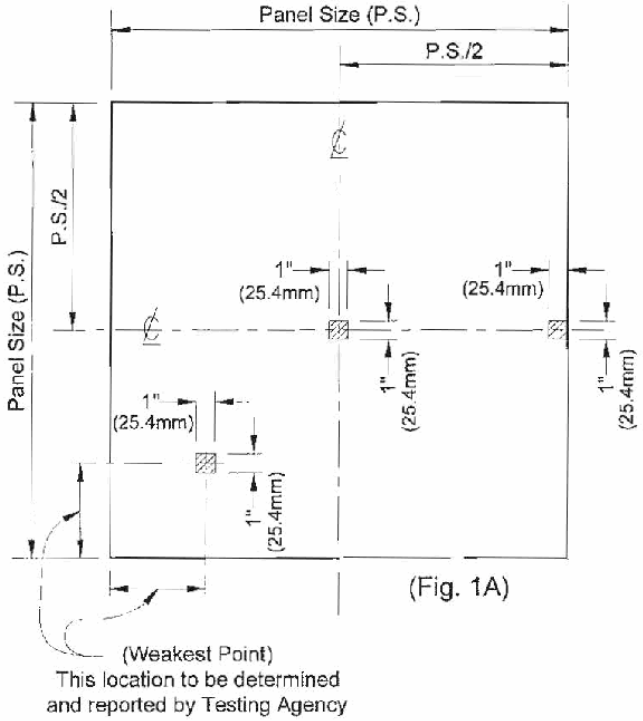


(Fig. 1A)

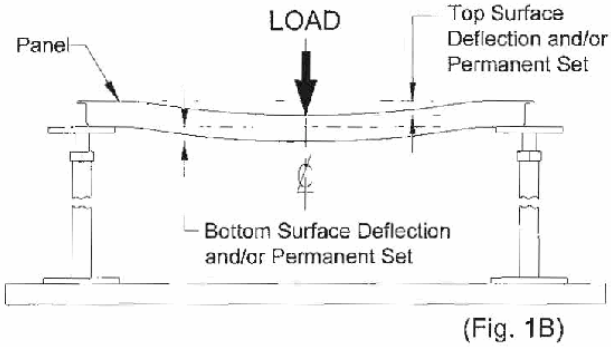


(Fig. 1B)

SETUP FOR CONCENTRATED LOAD TEST

(Fig. 1)

**Section 1:** Concentrated Loads

## REPORT FORMAT

| | Deflection Top Surface | Set Top Surface | Deflection *Bottom Surface | *Set Bottom Surface |
|---|---|---|---|---|
| Panel 1: Center<br>50 lb. (222 N) Pre Load | -0- | -0- | -0- | -0- |
| Concentrated Load _____ lbs. (N). | _____ | _____ | _____ | _____ |
| Panel 2: $C_L$ Edge<br>50 lb. (222 N) Pre Load | -0- | -0- | -0- | -0- |
| Concentrated Load _____ lbs. (N). | _____ | _____ | _____ | _____ |
| Panel 3: Weakest Point<br>50 lb. (222 N) Pre Load | -0- | -0- | -0- | -0- |
| Concentrated Load _____ lbs. (N).<br>(INDICATE LOCATION OF WEAKEST POINT) | _____ | _____ | _____ | _____ |

*BOTTOM SURFACE DEFLECTION AND SET IS OPTIONAL

LOADS AND DEFLECTION(S) MAY BE REPORTED AT ANY INCREMENT LESS THAN OR EQUAL TO 200 lb. (890N).

TOP SURFACE DEFLECTION IS DEFINED AS THE DISTANCE TRAVELED BY THE INDENTOR.

# Section 2
# Ultimate Loading

## Purpose:

To verify the ability of an access floor to accept the manufacturers' published ultimate load.

## Preparation:

1. Tests shall be performed on three (3) randomly selected bare panels supported on an understructure support system identical to that utilized in an installed system. (Four (4) panels are required if panel configuration is not structurally symmetrical.)
2. Any coatings, stringers, gaskets, pads, clips, fasteners, or other materials as required by manufacturer shall be identical to that utilized in an installed system.
3. Finish floor height of the test mock-up shall be 12 inches or the maximum height of the system whichever is less.
4. Ultimate loading shall be applied through a steel indentor 1" (25.4 mm) square. This square indentor may have eased edges at maximum of .008" (0.20 mm) radii, but the footprint contact area shall not measure more that 1" x 1" (25.4 mm x 25.4 mm) square or a round indentor 1.128" (28.65 mm) diameter may be utilized in lieu of a square indentor provided the footprint contact area shall not exceed one square inch (645 $mm^2$).
5. Safety restraining frames or configurations may be utilized in the test procedure to restrain horizontal movement of the tested mock-up if deemed prudent by the testing facility. Frames shall not interfere with vertical movement of the mock-up.

## Test Procedure:

1. Testing shall be conducted with the load applied at the "weakest point" of the panel. The "weakest point" is to be determined by the independent certifying/test agency and is that panel location which results in the lowest ultimate load. In addition, testing may be conducted with loads applied at the panel locations, such as center of panel and mid-point of panel edge.

## Report:

1. Reference of testing procedure described herein by CISCA A/F section number shall be included in report.
2. All apparatus, equipment, instrumentation, accuracy ranges, etc. shall be described including equipment calibration/certification dates.
3. Materials tested, mock-up configuration(s) and restraining frames, if used, should be fully described in verbiage or referenced to manufacturers' drawings and/or part numbers, either containing the following information:

   **Panels:**
   - Material(s) of panel construction.
   - Weight, nominal dimensions and thickness.

   **Pedestals:**
   - Height.
   - Material and cross-section.

   **Stringers:**
   - Material(s) of construction.
   - Weight, nominal dimensions and thickness, including fasteners, gaskets, coatings, clips, etc.

   **Other:**
   - Fully describe gasketing, pads, or other items utilized in the system.

4. The applied load for each panel at the weakest point, edge and centroid, shall be reported. Additionally, the applied load at other tested locations may be reported.

**Section 2:** – Panel Loading Locations

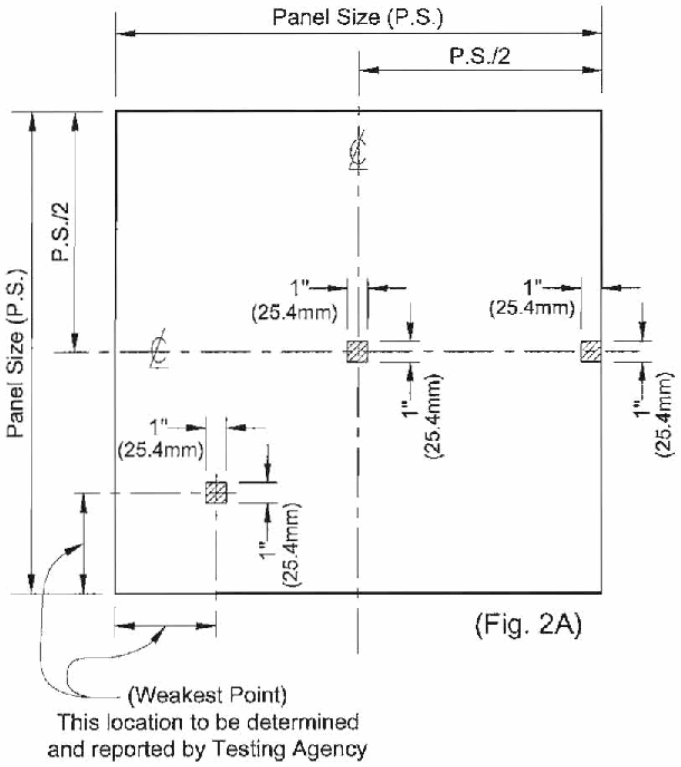


(Fig. 2A)

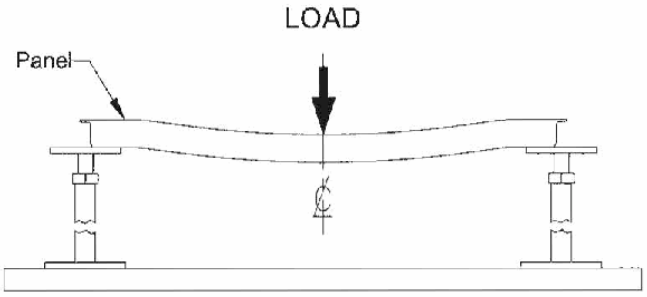


(Fig. 2B)

SETUP FOR ULTIMATE LOAD TEST

(Fig. 2)

**Section 2:** Ultimate Loading – Report Format

| REPORT FORMAT | |
|---|---|
| SYSTEM 1 – Panel Center: | Load _____lbs. (N) |
| SYSTEM 2 – Panel $C_L$ Edge: | Load _____lbs. (N) |
| SYSTEM 3 – Weakest Point: | Load _____lbs. (N) (indicate location) |

# Section 3
# Rolling Loads

## Purpose:

To determine the durability and/or deformation of access floor systems when exposed to commercially anticipated caster traffic using a specified load.

## Preparation:

1. Each test shall be performed on a mock-up consisting of a minimum of three (3) randomly selected bare panels installed on a support understructure system identical to the configuration of a normal field installation with a finished floor height of 12" or the maximum height of the system, whichever is less.
   A restraining frame which laterally supports the mock-up assembly may be utilized to protect equipment or for personnel safety, provided said frame is constructed to not interfere with the panels or supporting understructure and provides clearance from any point of the mock-up prior to the start of test.
   Testing apparatus shall be designed to impose caster rolling loads directly on the mock-up system, with the load traversing in a fixed path on the three panels being tested. Dampening of mock-up, load, caster wheel applicator, load carriage or load bed is prohibited.
2. Loads shall be directly imposed through caster wheels manufactured in accordance with attached drawings.

## Rolling Load Wheel Specifications

### 10 pass test

**Wheel A -**

3" diameter x 1¾6" width (76.2 mm diameter x 46.0 mm width)
Tread type: hard rubber or phenolic material, maximum .062" (1.57 mm) crown

### 10,000 pass test

**Wheel B - For loads up to 1500 pounds (6.675 kN)**

6" diameter x 2" width
(152 mm diameter x 50.8 mm width)
Tread Type: molded urethane tread, maximum 1/16" (1.59 mm) crown

**Wheel C - For loads over 1500 pounds (6.675 kN)**

10" diameter x 4" width
(254 mm diameter x 102 mm width)
Tread Type: molded urethane tread, maximum 1/16" (1.59 mm) crown

## Test Procedure:

1. Each mock-up assembly shall be subjected to the imposed caster rolling load traversing the center panel along a fixed path at a speed of 100 FPM (0.5 m/s) (+ - 10%), at a minimum stroke distance of 36" (914 mm) or panel dimension plus 12 inches (305 mm).
2. The fixed paths for the imposed caster rolling loads are defined as follows, with the center of the wheel width dimension being the locator of the path:
   **Path "1"**
   Fixed path traversing across mock-up panels at panel centers.
   **Path "2"**
   Fixed path traversing across all three mock-up panels, along a line inboard and parallel from the outer edge as determined by the "weakest point." The "weakest point" is to be determined by the certifying independent testing agency and is defined as the path which yields the greatest top surface deformation under rolling loads as determined by this section.
3. Wheel A (See box with Rolling Load Wheel Specifications) shall be applied to separate mock-ups for each fixed paths 1 & 2 for ten (10) passes with deformation measurements at start and upon completion.
   Wheel B and Wheel C shall be applied to separate mock-ups for each fixed paths 1 & 2 for 10,000 passes with deformation measurements at start and upon completion of 500, 5,000 and 10, 000 passes.
4. Measurement(s) and reference locations prior to test shall be taken as follows:
   a. The center panel, prior to start of test, shall be measured for overall flatness utilizing a 32" (813 mm) long straightedge. The straightedge shall be placed parallel with each panel edge, flush with the edge or not more than 12" (12.7 mm) inboard from the edge. The straightedge shall also be placed along the diagonal in each direction. Measurement shall be taken at each straightedge location (6 locations) at the maximum variation and recorded and located for reference. (Note: If the panel configuration has an upward "crown", it shall be so measured and reported.)
   b. Prior to the start of test, the center panel, at points along the proposed caster path, shall be measured for local variation utilizing a 6" (152 mm) long straightedge. The largest six (6) variations shall be measured, recorded and located for reference.
5. Measurement upon completion of test:
   a. The center panel, upon completion of test shall be measured in an identical manner as described in 4a above. The maximum beam deformation measurements (6 required) shall be recorded and located for reference.
   b. Upon completion of test, the center panel shall be measured in an identical manner as described in 4b above. The maximum local deformation measurements (6 required) shall be measured, recorded and located for reference.

6. Actual vertical wheel force shall be verified with a load cell or similar device before the start of each test.
7. A separate mock-up assembly shall be utilized for each wheel type and path tested.
8. Panels or understructure systems which are not structurally symmetrical, shall be tested in accordance with the above procedure and then re-tested with separate mock-up materials installed (rotated) 90° to the first test mock-up.

## Report:

1. Reference of testing procedures described herein by CISCA A/F section number shall be included in report.
2. All apparatus, equipment, instrumentation, accuracy ranges, etc. shall be described including equipment calibration/certification dates.
3. Materials tested, mock-up configuration(s), and restraining frames, if used, should be fully described in verbiage or referenced to manufacturer's drawings and/or part numbers, either containing the following information:

   **Panels:**
   - Material(s) of panel construction.
   - Weight, nominal dimensions and thickness.

   **Stringers and Pedestals:**
   - Material(s) of construction.
   - Weight, and nominal dimensions and thickness, including fasteners, gaskets, coatings, clips, etc.

   **Other:**
   - Fully describe gasketing, pads, or other items utilized in the system.
4. For the 10,000 Pass test, the results of the test with only one wheel shall be reported.
5. Panel deformation shall be reported for each test and each path in accordance with the attached report format. Each listing of data shall indicate the following:

   | | |
   |---|---|
   | Wheel # | (A, B or C) |
   | Imposed Load | (Lbs) (N) |
   | Fixed Path | (1 or 2) |
   | Number of Passes | |
   | *Deformation Reported | (To nearest .001" [0.025 mm]) |

   *Deformation reported shall be the maximum measurement for both beam deformation and local deformation.
6. Any visible structural damage to any mock-up component shall be reported.

**Section 3: Rolling Loads**

- Fixed Path 1 or 2
- Deformation Readings
- Beam & Local
- Or panel dimension plus 12″ (305 mm) to length of stroke

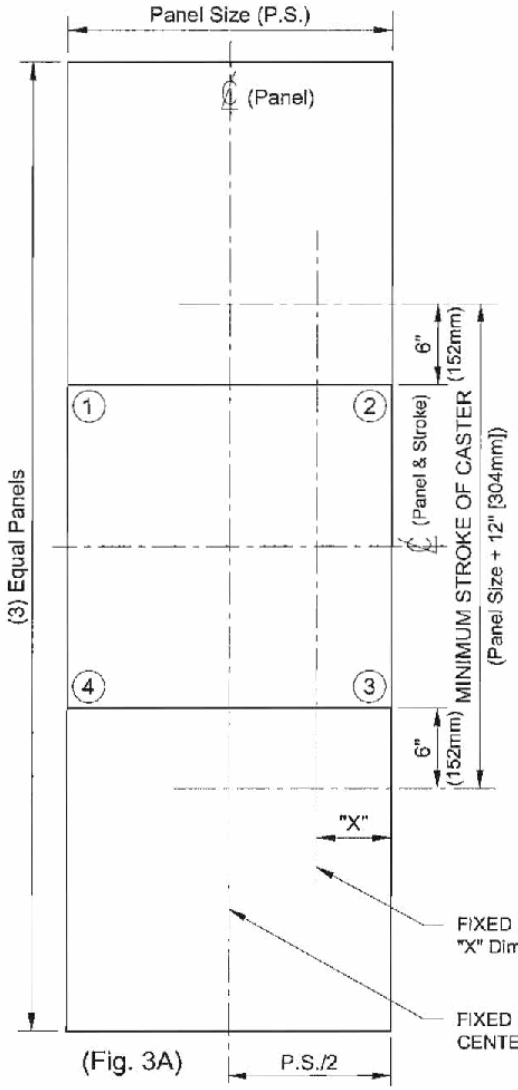


(Fig. 3A)

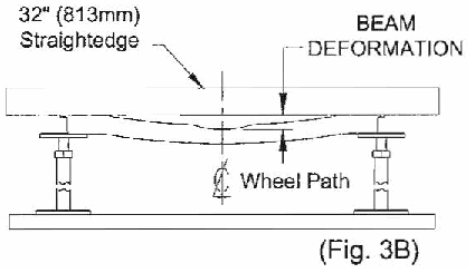


(Fig. 3B)

FIXED PATH "A"
BEAM DEFORMATION READING

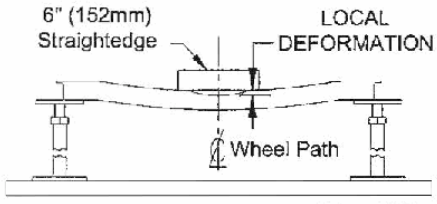


(Fig. 3C)

FIXED PATH "A"
LOCAL DEFORMATION READING

SETUP FOR ROLLING LOAD TEST
(Fig. 3)

**Rolling Load Drawings Section 3:** - Wheel A
- Wheel B
- Wheel C

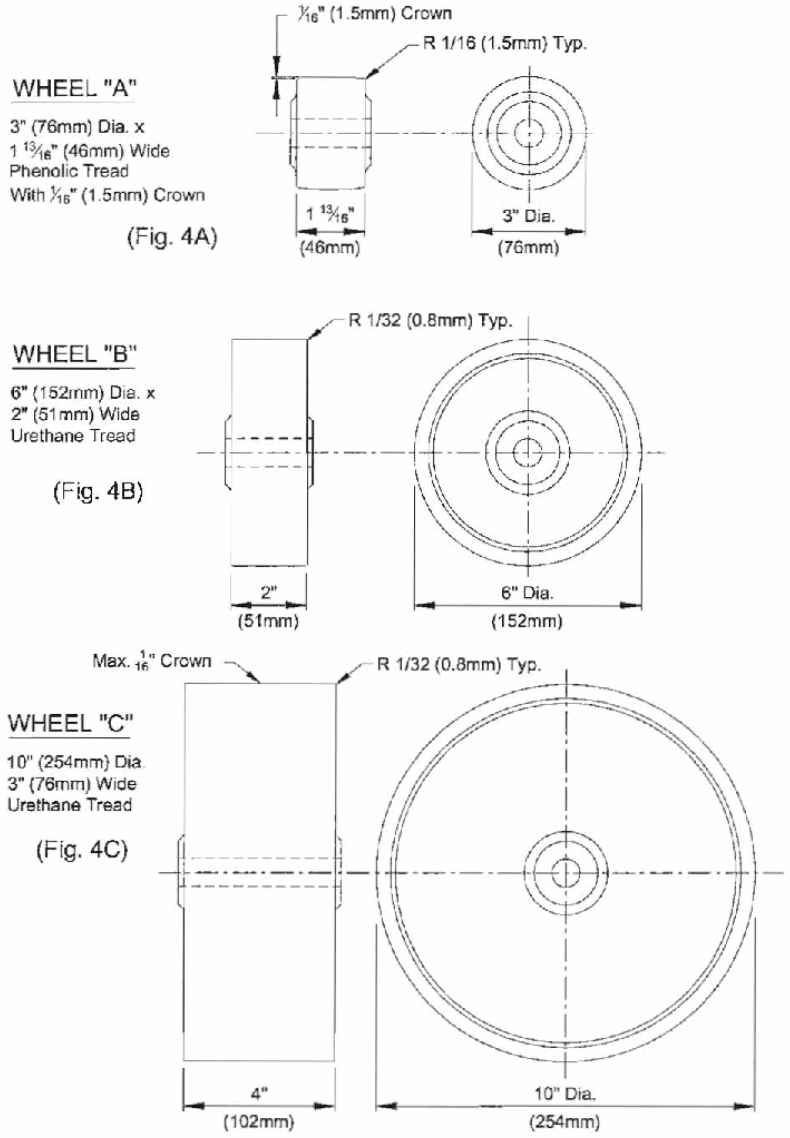


(Fig. 4)

**Report:** Wheel # (A,B, or C) Size _____
Imposed Load _____ Load
Fixed Path 1 or 2 Location _____
Number of Passes _____

## BEAM DEFORMATION: 32" STRAIGHTEDGE MEASUREMENT

EDGE 1 – 2: Beam Deformation (Perpendicular to Caster Path)
Prior: _____ inches. Location: *Example (8" [203 mm] Along Edge from Corner 1)*
After: _____ inches. Location: _____
Difference: _____inches (Report only if the start/finish locations are identical)

EDGE 3 – 4: Beam Deformation (Perpendicular to Caster Path)
Prior: _____inches. Location: _____
After: _____inches. Location: _____
Difference: _____inches (Report only if the start/finish locations are identical)

EDGE 2 – 3: Beam Deformation (Parallel w/Caster Path)
Prior: _____inches. Location: _____
After: _____inches. Location: _____
Difference: _____inches (Report only if the start/finish locations are identical)

EDGE 4 – 1: Beam Deformation (Parallel to Caster Path)
Prior: _____inches. Location: _____
After: _____inches. Location: _____
Difference: _____inches (Report only if the start/finish locations are identical)

DIAGONAL 1 - 3 Beam Deformation
Prior: _____inches. Location: *Example: (14" [356 mm] Along Diagonal from Corner 1)*
After: _____inches. Location: _____
Difference: _____inches (Report only if the start/finish locations are identical)

DIAGONAL 2 - 4 Beam Deformation
Prior: _____inches. Location: _____
After: _____inches. Location: _____
Difference: _____inches (Report only if the start/finish locations are identical)

---

Wheel # (A,B, or C) Size _____
Imposed Load _____ Load
Fixed Path 1 or 2 Location _____
Number of Passes _____

## LOCALIZED DEFORMATION: 6" STRAIGHTEDGE MEASUREMENT

Point 1 Location: *Example (8" [204 mm] Along Edge from Corner 1)*
Prior _____ inches.
After _____ inches.
Difference _____ inches.

Point 2 Location:_____
Prior _____ inches.
After _____ inches.
Difference _____ inches.

Point 3 Location:_____
Prior _____ inches.
After _____ inches.
Difference _____ inches.

Point 4 Location: _____
Prior _____ inches.
After _____ inches.
Difference _____ inches.

Point 5 Location: _____
Prior _____ inches.
After _____ inches.
Difference _____ inches.

Point 6 Location: _____
Prior _____ inches.
After _____ inches.
Difference _____ inches.

POINT MAXIMUM: "Report this Maximum Measurement of Localized Deformation." _____

---

# Section 4
# Stringer Load Testing

## Purpose:

To determine the amount of permanent set sustained by stringer when subjected to a concentrated load.

## Preparation:

1. Stringers shall be randomly selected and supported on two pedestal assemblies complete with all coatings, gaskets, clips, and fasteners, identical to that found in the installed floor system. Height shall be equivalent to that found in a 12" (305 mm) finished floor height or the maximum height of the system, whichever is less.
2. The loads shall be applied to the stringer through a steel indentor 1" (25.4 mm) square, imposed and measured through a properly calibrated and appropriately sized load sensor. A round indentor 1.128" (28.65 mm) diameter may be utilized in lieu of a square indentor provided the footprint contact area shall not exceed one square inch.

## Test Procedure:

1. Load shall be applied vertically at mid span of the stringer and held for a minimum of one-minute duration. The load shall then be relaxed and permanent set measured. Permanent set shall be measured at the top surface of the stringer at the point of load application. Rate of load application shall not exceed 500 pounds per minute (2.224 kN/min).

## Report:

1. Reference of testing procedure described herein by CISCA A/F section number shall be included in report.
2. Al apparatus, equipment, instrumentation, accuracy ranges, etc. shall be described including equipment calibration/certification dates.
3. Materials tested and mock-up configuration(s) should be fully described or referenced to manufacturers' drawings and part numbers containing the following:
   - Material(s) of construction, weight, nominal dimensions and thickness.
   - Span of stringer between pedestal center-lines
   - Height of system
   - Fasteners, gaskets, coatings, clips, etc.
   Record corresponding load(s) applied.
4. Description of any visual defects of any component.

# Section 5
# Pedestal Axial Load Test

## Purpose:

To verify the axial load an access floor pedestal assembly can withstand without structural failure or damage to components inclusive of threads, nuts, collars, etc.

## Preparation:

1. A minimum of three (3) randomly selected pedestal assemblies shall be tested for each floor height. Pedestals shall be identical to those used in normal installations for their corresponding floor heights, including thread engagements normally utilized in field conditions.
2. Pedestal assemblies shall be tested for maximum floor heights of each assembly design or configuration.
3. Loads shall be imposed and measured through a properly calibrated and appropriately sized load sensor over the center of the pedestal head. The load indentor or applicator may be machined to integrate with the pedestal head to simulate the loading of the four corners of the panels.

## Test Procedure:

1. Align the Pedestal assembly in the testing apparatus and apply an increasing load centered on the pedestal until the desired load is reached. Hold imposed load for minimum of one (1) minute duration. The load shall then be relaxed and the assembly visually inspected for damage. Adjusting devices, locking devices, threads shall be workable by hand. Rate of load application shall not exceed 10,000 pounds per minute (44.5 kN/min).

## Report:

1. Reference of testing procedure described herein by CISCA A/F section number shall be included in report.
2. All apparatus, equipment, instrumentation, accuracy ranges, etc. shall be described including equipment calibration/certification dates.
3. Materials tested shall be fully described or referenced to manufacturers' drawings and part numbers containing the following:
   - Materials of construction, weight, nominal dimensions and thicknesses.
4. Report load applied and relaxed for each pedestal and describe damage to components, if any.

**Section 5:** Pedestal Axial Load Test - Report Format

**FINISHED FLOOR HEIGHT:_____ INCHES (mm)**

**IMPOSED LOAD**

Pedestal Assembly 1 - _____ lbs. (N)

Pedestal Assembly 2 - _____ lbs. (N)

Pedestal Assembly 3 - _____ lbs. (N)

Average: _ _____ lbs. (N)

Description of Component Damage if any: _____

_____

# Section 6
# Pedestal Overturning Moment Test

## Purpose:

To determine the overturning moment an access floor pedestal assembly and its application to the sub-floor can resist.

## Preparation:

1. A minimum of five (5) pedestal assemblies shall be secured to a sound unsealed surface consistent with practice normally found in actual installations. Application methods shall be noted in report and may include adhesive and/or mechanical fasteners.
   Note: Where pedestals are not axisymmetric, additional sets of pedestals may need to be tested to verify the weakest direction of force application.
2. For adhesive application, follow manufacturers' adhesive application procedure and allow to cure for the minimum cure time recommended by the adhesive manufacturer.
3. For mechanical application, follow fastener manufacturers' recommended procedure.

## Test Procedure:

1. Lateral loads shall be applied slowly and continuously to the prescribed location of the assembly until any failure of the pedestal assembly or its methods of application to the sub-floor occurs. Where pedestals are not axisymmetric, loads shall be applied in the direction which will result in the least overturning resistance.

Pedestal Overturning Moment Test

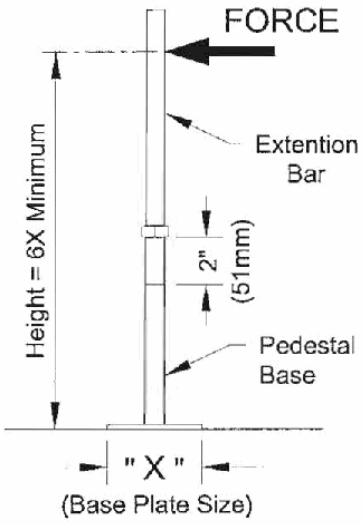


TEST SETUP FOR
PEDESTAL OVERTURNING MOMENT
(Fig. 5)

## Report:

1. Reference of testing procedure described herein by CISCA A/F section number shall be included in report.
2. All apparatus, equipment, instrumentation, accuracy ranges, etc. shall be described including equipment calibration/certification dates.
3. Materials tested and load application configuration shall be fully described and referenced to manufacturers' drawings and/or part numbers containing the following:
   - Materials of construction, weight, nominal dimensions and thicknesses.
   - Adhesive if used, designate the manufacturer, product description, and identifying commercial stock numbers, etc., curing time and conditions.
   - Mechanical fasteners, if used, shall be identified by manufacturer, type, catalog number, size, and depth of engagement.
4. If mechanical fasteners are used, state the number used, location of fasteners in base plates, and relationship dimensionally of fastener locations to applied loading direction. Also state method of application. The height measured from the sub-floor to the horizontal location of the applied load (moment arm) shall be reported along with the applied load for each loading.
5. Type of overturn failure and description thereof shall be reported for each test. Where forces have been applied in more than one direction, report worst-case (weakest) results in addition to any other results.

**Section 6:** - Data Report Format

Pedestal Description: _____ _____

*Fastening Method: _____ *(Adhesive, Mech., Etc.)*

Pedestal Height _____ for _____ Finished Floor Height.

Height of Applied Load _____

**Pedestal Assembly:**

1 Horizontal Load _____ lbs. (N) _____ inch pounds (Nm)

2 Horizontal Load _____ lbs. (N) _____ inch pounds (Nm)

3 Horizontal Load _____ lbs. (N) _____ inch pounds (Nm)

4 Horizontal Load _____ lbs. (N) _____ inch pounds (Nm)

5 Horizontal Load _____ lbs. (N) _____ inch pounds (Nm)

AVERAGE _____ inch pounds (Nm)

* FASTENING METHOD SHALL BE FULLY DESCRIBED: _____

_____

* DESCRIPTION OF FAILURE (IF ANY) FOR EACH PEDESTAL SHALL BE REPORTED:

_____

# Section 7
# Uniform Load Test

## Purpose:

To determine the maximum deflection(s) and permanent set(s) of an access floor under a uniformly distributed load.

## Preparation:

1. Test shall be performed on a randomly selected bare panel assembly. Panel shall be placed on steel blocks or supports configured to provide support identical to that provided by an installed system. Any coatings, gaskets, pads, clips, fasteners, floor covering, or other materials as required by manufacturer shall be identical to an installed system. Blocks or supports shall not reduce the unsupported edge span below that normally provided with a standard installed system.
2. Panel designed for stringer support shall have stringers spanning the blocks or supports with panel perimeter support and/or interface in an identical manner to the configuration of the installed floor systems. Stringers shall be identical to those of the installed floor system, attached or fitted to the support blocks in an identical manner to the installed floor system, and shall include any coatings, gaskets, pads, clips, fasteners, finishes or other materials as required by the manufacturer in the installed floor system.
3. Height of the test mock-up shall be sufficient to accommodate deflections of stringers and panels.
4. Load shall be applied as described in the air bag or vacuum methods prescribed in ASTM E2322 Standard Test Method for Conducting Transverse and Concentrated Load Tests on Panels Used in Floor and Roof Construction.
   Note: This ASTM test method is to be used in this section only for evaluation of uniform loading resistance, and is not appropriate for use as a concentrated load test method for access floors.
5. Any restraining frames or configurations utilized in the test procedure shall not interfere with vertical movement of the test specimen.

## Test Procedure:

1. Except as outlined in this procedure, the panel shall be loaded according to the air bag or vacuum methods prescribed in ASTM E2322. In the case of access flooring systems where panels are not contiguous, load shall also be applied to any connecting material (e.g. steel cap) between panels.
2. The panel shall be pre-loaded to the test load. A pre-load of 50 lbs/ft² (i.e. 200 lb in the case of a panel that is 4 ft² – 2′ x 2′) shall then be applied and the instrumentation measuring deflection and load shall be set at zero. (Reference zero = 50 lbs/ft² pre-load)
3. After the pre-load, the panel shall be tested by increments not exceeding 50 lbs/ft², with initial load no more than one-half test load. Rate of load application shall not exceed 375 lbs/ft² per minute.
4. Deflection and permanent set shall be measured at the panel's center, midspan of edge, and "weakest point" as defined by the manufacture and verified by the independent test agency.
   Note: For products with uneven bottom surfaces and where the deflection and set are measured on the bottom of the panel, the measurements shall be taken at the lowest adjacent horizontal surface.
5. Loads shall be applied for a minimum of one (1) minute and deflection readings taken at the end of that period. The load shall then be relaxed to reference zero (Reference zero = 50 lbs/ft² pre-load) for a minimum one (1) minute and deflection shall be recorded.

## Report:

1. Reference of testing procedure described herein by CISCA A/F section number shall be included in report.
2. All apparatus, equipment, instrumentation, accuracy ranges, etc. shall be described including equipment calibration/certification dates.
3. Materials tested and mock-up configuration(s) should be fully described in verbiage or referenced to manufacturers' drawings and/or part numbers, either containing the following information:
   **Panels:**
   - Material(s) of panel construction.
   - Weight, nominal dimensions and thicknesses.

   **Stringers:**
   - Material(s) of construction.
   - Weight, and nominal dimensions and thickness, including fasteners, gaskets, coatings, clips, etc.

   **Other:**
   - Fully describe gasketing, pads, other items utilized in the system.
4. Panel deflection measurements of the bottom surface shall be reported to the nearest .001" (0.025 mm) for each applied load.
5. Panel permanent set of the bottom surface shall be reported to the nearest .001" (0.025 mm) for each applied load.

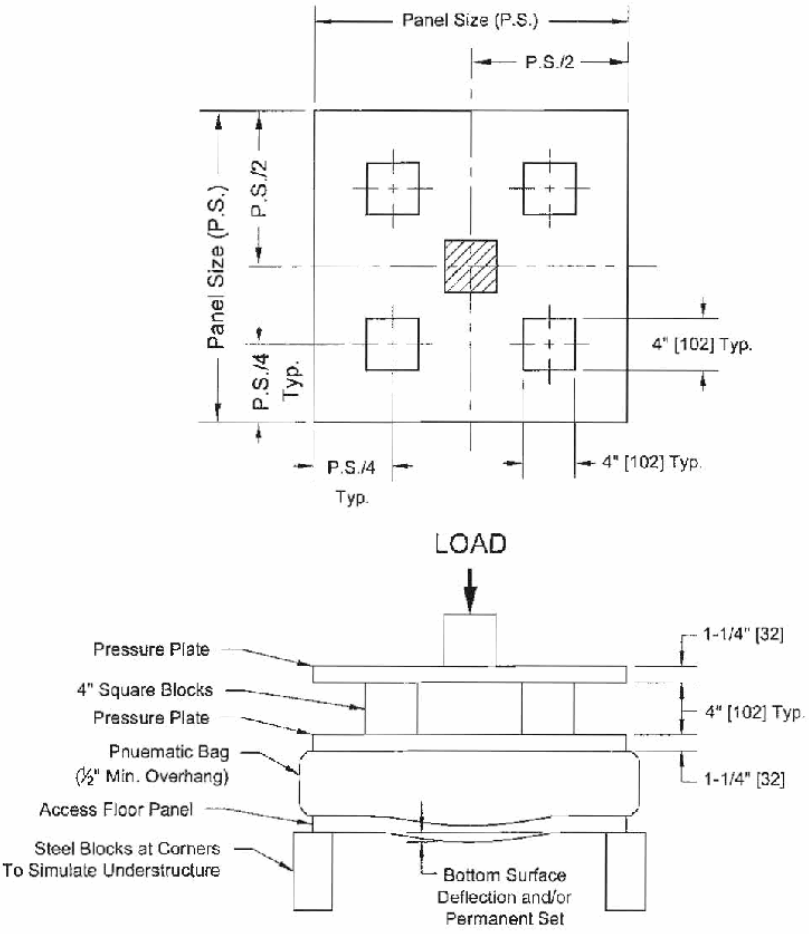


SETUP FOR UNIFORM LOAD

(Fig. 6)

**Report Format:**

| | Center Deflection | Midspan Edge Deflection | "Weakest Point" Deflection | Set |
|---|---|---|---|---|
| Panel 1: 50 lbs/ft² Pre-load | | | | |
| Uniform Load _____lbs/ft² | | | | |

LOADS AND DEFLECTION(S) MAY BE REPORTED AT ANY INCREMENT LESS THAN OR EQUAL TO 50 LBS/ft².

# Section 8
# Drop Impact Load Test

## Purpose:

The purpose of this test is to show the effect upon access floor panels and supporting understructure system(s) when subject to impact from heavy loads being accidentally dropped onto the floor panel.

## Preparation:

Test(s) shall be performed on three (3) randomly selected bare panels placed on an understructure support system that is configured identical to an installed system. Any stringers, coatings, gaskets, pads, clips, fasteners, locking devices or other materials normally used shall be configured identical to that provided in an installed system. The test mock-up configuration shall be at a finished floor height suitable for the system being tested. A safety-restraining device may be utilized for load constraint to prevent possible injuries, providing it does not restrict the purpose of the test. The load to be dropped shall be either a single hard object or objects placed inside a rigid container that will not flex or distort during the impact of the test. The load shall be dropped vertically from a given height onto the center of a steel "impact" plate of not less than one-half inch (1/2") [12.7 mm] thick x eight inches (8") [20.3 mm] square that is placed centrally on top of a one inch (1") [25.4 mm] square steel indentor not less than one-half inch (1/2") [12.7 mm] thick.

## Test Setup:

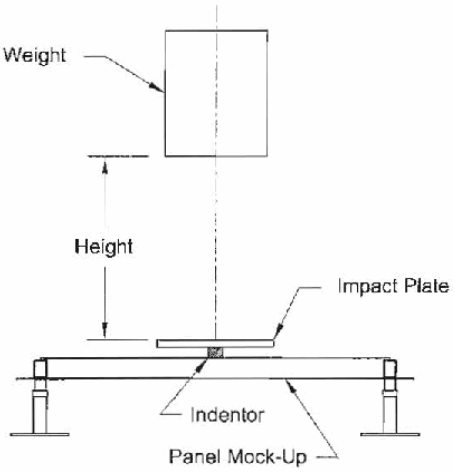


SETUP FOR DROP IMPACT LOAD TEST

(Fig. 7)

## Test Procedure:

1. The load shall be dropped, free fall from a height of 36" (914 mm) measured from the top of the steel "impact" plate to the underside of the weight being dropped.
2. Two one-panel mock-up assemblies shall each be tested with the load target directly in the center of each panel.
3. Two one-panel mock-up assemblies shall each be tested with the load target directly on the midpoint of the edge of each panel.
4. Two one-panel mock-up assemblies shall each be tested with the load target at the discretion of the testing lab to determine the weakest points.
5. After completion of the impact test on each panel, one panel shall be tested according to Section 1: Concentrated Loads at the point of impact, and the other shall be tested according to Section 2: Ultimate Load. (The weights dropped on panels for Concentrated and Ultimate Load testing may be different.)
   NOTE: Panels or understructure systems which are not symmetrical, shall be tested in accordance with the above procedure and then re-tested with separate mock-up materials installed (rotated) 90° to the first test mock-up.

## Report:

1. Reference of testing procedure described herein by CISCA A/F section number shall be included in report.
2. All apparatus, equipment, instrumentation etc. shall be described including equipment calibration/certification dates.
3. Materials tested and any load restraining device, if used, should be fully described in verbiage or referenced to manufacturer's drawings and part numbers, containing the following information:
   **a. Panels:**
   - Materials of the panel construction.
   - Weight, nominal dimensions and thickness.

   **b. Stringers and pedestals:**
   - Material(s) of construction.
   - Weight, and nominal dimensions and thickness, including fasteners, gaskets, coatings, clips, etc.

   **c. Other:**
   - Fully describe any gaskets, pads, or other items utilized in the system.
4. Amount of weight dropped onto system.
5. Height from which weight was dropped onto system.
6. For each panel subjected to testing under Section 1, report the impact weight, the concentrated load and deflection realized. For each panel tested according to Section 2, report the impact weight and ultimate load achieved.

# SECTION 9
# Fire Performance

This guidance is not all-inclusive of the fire test methods that may be applicable to access floors. The authority having jurisdiction (e.g. fire marshal, building inspector, etc.) makes the final determination of what test or other qualification methods may apply. Nor is it to be implied that CISCA requires any of the following be performed on access floors. CISCA has provided clarification for sample preparation for the following test methods:

## Surface Burning Characteristics of Building Materials

- ASTM E 84 Standard Test Method for Surface Burning Characteristics of Building Materials
- NFPA 255 Standard Method of Test of Surface Burning Characteristics of Building Materials
- UL 723 Test for Surface Burning Characteristics of Building Materials
- CAN/ULC S102 Method of Test for Surface Burning Characteristics of Building Materials and Assemblies
- UBC Standard 8-1 Test Method for Surface Burning Characteristics of Building Materials

## Non-Combustibility Assessment of Materials

- ASTM E 136 Standard Test Method for Behavior of Materials in a Vertical Tube Furnace and 750° C
- CAN/ULC S114 Standard Method of Test for Determination of Non-Combustibility in Building Materials
- UBC Standard 2-1 Noncombustible Material - Tests

## Purpose:

To provide a standard practice for specimen preparation and mounting of access floors for testing for Surface Burning Characteristics and Non-Combustibility of Building Materials.

The following practice describes specimen preparation and mounting procedures for such materials. All testing shall be conducted using the methodology described in the referenced test method.

## Test for Surface Burning Characteristics of Building Materials

This practice describes procedures for specimen preparation and mounting when testing access floors to assess flame spread and smoke development as surface burning characteristics using the tests methods listed above. This practice does not apply to discrete components such as diffusers, junction boxes, grommets, trim, etc. Discreet components may be tested per UL 2043.

Note: Under floor supports cannot be tested using these test methods.

This practice does not provide pass/fail criteria that can be used as a regulatory tool.

This practice does not purport to address all of the safety concerns, if any, associated with its use. It is the responsibility of the user of this practice to establish appropriate safety and health practices and determine the applicability of regulatory limitations prior to use.

## Test Specimen:

The test specimen sizes shall comply with those described in the test specimen section of the referenced test methods. The test specimens shall be butted against the vent end of the fire test chamber and shall consist of a continuous, unbroken length, or of sections joined or butted end-to-end. The test specimens shall have a width of 20 to 24 inches (510 to 610 mm), a length of 24 ft. (+12 in /–6 in) (7.32 m [+305 mm /–152 mm]) and a maximum thickness of 4 inches (101 mm).

## Preparation:

Access floor products shall be representative of the materials for which the test is intended to examine.

Access floors with sufficient structural integrity to support themselves within the test chamber without sagging more than 1/16 inch (1.5 mm) when measured at the center-line of the test chamber shall be sized to the width of the fire test chamber, butted end-to-end, and mounted on the ledges of the test chamber without using additional means of support.

Access floors without sufficient structural integrity to support themselves within the test chamber without sagging should be supported in accordance with the guidance provided in the respective test methods.

The sample shall be representative of the standard construction and application of the access floor. If raceways, channels, cover plates, etc. are an integral part of the access floor installation, then these products shall also be assembled in the test chamber in the same manner as intended in use. Two tests should be run: one test exposing the underside of the floor, the second test exposing the topside of the floor.

## Report:

1. Report a detailed description of the material(s) being tested.
2. Report a detailed description of the specimen preparation method used, including adhesives, if used, and its application method.
3. Report all information required in the reporting section of the referenced test method, including observations, graphical results and the values of the flame spread index and the smoke developed index in each test.

## Test for Non-Combustibility Assessment of Materials

This practice describes procedures for specimen preparation for tests for Non-Combustibility of Building Materials.

This practice does not purport to address all of the safety concerns, if any, associated with its use. It is the responsibility of the user of this practice to establish appropriate safety and health practices and determine the applicability of regulatory limitations prior to use.

## Test Specimen:

Test specimen should contain proportional amounts (by weight) of each material contained within the tested product. Panels and support structures are to be tested independently.

## Report:

- Report a detailed description of the material(s) being tested.
- Report a detailed description of the specimen preparation method used, including adhesives, if used, and its application method.
- Report all information as required in the referenced test method.

# SECTION 10
# Air Leakage Test (Through Panel Seams)

## Purpose:

To determine the rate at which air will pass through the cracks and gaps in an access floor panel assembly, at a specified and controlled differential static air pressure. This test applies only to floors used for underfloor air distribution.

## Preparation:

1. The test shall be performed on a specimen of panels in a relatively airtight box or chamber, as shown below. The gap between the perimeter of the floor panels and the chamber opening shall be sealed to minimize air leakage.

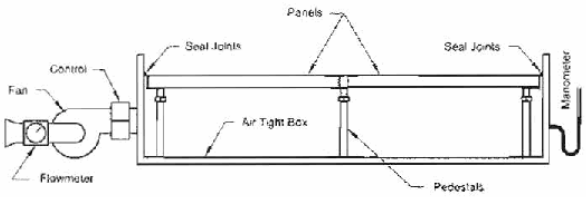


SETUP FOR AIR LEAKAGE TEST

(Fig. 8)

General arrangement of Air Leakage Test Apparatus

2. The dimensions of the panel assembly shall be at least 72 inches (1829 mm) square. Finished floor height shall be 12 inches (305 mm), or the maximum height of the system; whichever is less.
3. Any coatings, stringers, gaskets, pads, clips, fasteners, or other materials normally used shall be identical to that utilized in an installed system. The pedestals shall be anchored to the base of the chamber only if such anchorage will affect the air leakage rate in some way. If so, such anchorage shall be described in the report.
4. A controllable blower, fan, or air pump shall be fitted to the chamber to supply airflow to the chamber at a rate sufficient to maintain the positive air pressure required. The system should provide essentially constant airflow for a period of time sufficient to obtain readings of airflow rate and pressure.
5. A flowmeter or other suitable device to measure the rate of airflow into the test chamber shall be fitted.

A manometer or other suitable device to measure the differential test pressures shall be connected between the chamber and atmosphere.

Note: The referenced test method, ASTM E283, requires the device be capable of recording the pressure within ±2% of setpoint. The static air pressure differentials typically employed in under floor air distribution systems are much lower than in the referenced method, so care must be taken by the test agency to employ the appropriate pressure measuring device.

## Test Procedure:

1. Calibrate the air leakage test equipment in accordance with the calibration instructions in ASTM E283 *Standard Test Method for Determining Rate of Air Leakage Through Exterior Windows, Curtain Walls, and Doors Under Specified Pressure Differences Across the Specimen,* except that the calibration pressure shall be 0.10 inch of water column (25 Pa).
2. With the floor specimen installed as described above, adjust the total airflow into the chamber to provide the specified test pressure difference across the test specimen. When the test conditions have stabilized, record the airflow through the flowmeter, and the test pressure difference. This measured air flow is designated the total air flow, $Q_t(p)n$, where p is the pressure, and n is the number of the measurement. Measure the barometric pressure, *B*, and temperature of the air at the test specimen, *T*.
3. Repeat the measurement of the leakage at each pressure level at least 4 times. Calculate the arithmetic average of all leakage measurements at each pressure, $Q_t(p)$.
4. Seal all gaps and holes in the floor specimen.
5. With the floor specimen sealed, measure the amount of air leakage through the test chamber itself, at the same air pressure differentials as in step 2. Each measured air flow is designated the extraneous airflow, $Q_e(p)n$.
6. Repeat the measurement of the extraneous leakage at each pressure the same number of times as in step 3. Calculate the arithmetic average of all extraneous leakage measurements at each pressure, Qe(p).
7. Measure the total crack length between the access floor panels, l. Do not include any of the joints between the perimeter of the specimen and the chamber.

## The Calculation:

1. Calculate ratio $A_p/l_p$ , where:
   $A_p$ = *Area* of a floor panel, ft² (m²)
   $l_p$ = *Perimeter* of a single floor panel, ft² (m²)
   *Note: For some systems, where multiple panel sizes or shapes are employed together in one floor assembly, determination of lp may require more careful analysis. Generally, the perimeter of each panel should be measured only once in determining lp.*
2. Express the total average air flow at each pressure $Q_t(p)$, and the extraneous average air flow at each pressure $Q_e(p)$, in terms of flow at standard conditions, as outlined in ASTM E283.
   *Note: Ensure all units of measure referenced in the E283 calculation are observed, and that the correct equation is employed.*
3. Express the air leakage through the test specimen at each pressure, $Q_s(p)$, as
   $Q_s(p) = Q_t(p) - Q_e(p)$, ft³/min (L/s) (1)
4. Calculate the rate of air leakage per unit crack length at each pressure, $q_l(p)$, as
   $q_l(p) = Q_s(p)/l$, ft3/min-ft (L/s-m) (2)
5. Calculate the rate of air leakage per unit area at each pressure, $q_A(p)$, as
   $q_A(p) = q_l(p) /[2 (A_p/l_p)]$, ft3/min-ft2 (L/s-m²) (3)

## Report:

1. Reference of testing procedure described herein by CISCA A/F section number shall be included in the report.
2. All apparatus, equipment, instrumentation, accuracy ranges, etc., shall be described including equipment calibration/certification dates.
3. Materials tested, and specimen configuration(s) should be fully described in text and/or photograph and/or drawing, or by reference to manufacturer's drawings and/or part numbers, including the following:
   **Panels:**
   - Floor finishes
   - Materials of the panel construction
   - Weight, and nominal dimensions and thicknesses

   **Supporting structure:**
   - Height
   - Materials, sections, fasteners, adhesives or other anchors

   **Other:**
   - Fully describe other materials used in the mock-up
4. For each of test pressures, report the rate of air leakage per unit crack length, and per unit area, as noted. At a minimum, report the air leakage rate at the pressures noted in the table. Other pressures may also be reported, at the discretion of the proponent or authority.
5. Calculated accuracy of the measured air leakage, based on the precision of the air pressure measurement.

| Test Pressure inches h2o (Pa) | Air Leakage Rate | |
|---|---|---|
| | Per unit crack length ft³/min-ft (L/s-m) | Per unit area ft³/min-ft² (L/s-m²) |
| 0.05 (12.5) | | |
| 0.10 (25.0) | | |

# Section 11
# Sound Transmission

At the time of the release of this CISCA publication, the ASTM E33 committee was working on a new ASTM standard for airborne sound transmission loss through access floors and therefore, CISCA has yet to review this test method.

# Glossary of Terms

## Access Floor System

An access floor system is an elevated or "raised" floor area upon another floor (typically a concrete slab in a building) creating an interstitial space for service distribution. It consists of modular floor panels that are designed to be removable from their support so that "access" to services is quickly and easily achieved. These services may include but are not limited to electric power, data, plumbing, telecom, environmental control, air conditioning, fire detection suppression, security, etc.

## Air Leakage

As it pertains to access floors, air leakage is defined as the passage of air from an underfloor air cavity through elements other than the designed air outlet devices. Leakage typically falls into two categories: 1) leakage in the air cavity under the floor due to construction quality, and 2) leakage through floor panel seams and other non-air outlet devices.

## Axial Load

A vertical load (or force) whose line of action passes through the center of the member's cross sectional area and is perpendicular to the plane of the section such that no bending or torsion moments are produced. This is the load that is typically specified when referring to the axial load performance of an access floor pedestal support.

## Beam Deformation

Deformation is defined as the act of distorting or changing the shape or dimensions of a structural element or body resulting from forces or stresses. Beam deformation as related to access floors is generally the term used when referring to the permanent set of the entire span of the access floor panel after application of a rolling load and is determined by measuring the overall flatness of the access floor panel before and after the application of the load.

## Cable Management Access Floor Systems

An access floor system which incorporates an easy access, independent of panel removal, creating an interstitial pathway for routing cabling and other supportive services, excluding air distribution.

## Concentrated Load

A single load or force that has a small contact area as to be negligible compared with the entire surface area of the supporting member. Concentrated loads (sometimes referred to as static loads) are typically imposed by stationary furniture and equipment with legs. A concentrated load is applied to the surface of the panel (1"x 1" square or 1.128" diameter indentor) (25.4 mm x 25.4 mm square or 28.65 mm diameter) resulting in deflection and permanent set. Concentrated load rating is specified in pounds force applied over a one square inch (645 mm2 ) area.

## Deflection

Deflection is the vertical displacement of a structural member or system under load. This is generally referred to when discussing the vertical displacement a floor panel experiences upon application of a concentrated load or uniform load.

## Design Load

The load expected to be imposed on the floor system in service. The access floor concentrated load rating is not the safe working load or design load for the floor system.

## Dynamic Load

Loads that vary significantly with time as measurements are being made. Two dynamic loads are generally referred to: rolling loads and impact loads.

## Finished Floor Height

Finished floor height is defined as the height of the access floor system as measured from the top of the supporting sub-floor to the top of the access floor panel.

## Impact Load

Impact loads are caused by objects being accidentally dropped onto an access floor. These loads are defined by the weight of the load, height or distance dropped, impact area, and hardness/softness of the object. Impact loads generate severe shocks that can cause structural and panel damage. Impact loads most often occur during construction, move-in, and equipment / furniture rearrangements.

## Live Load

A live load is produced by the use or occupancy of the building. This does not include construction, environmental, seismic, or access floor dead loads. The live load should not be confused with the uniform load capacity of an access floor.

## Local Deformation

Local deformation is generally the term used when referring to the permanent set recorded along the wheel path after a rolling load test. It is determined by measuring the local flatness of the panel along the wheel path before and after the application of the load using a 6" (152 mm) spanner perpendicular to the wheel path. The difference between before and after measurements is defined as local deformation.

## Overturning Moment

Overturning moment is the term generally used to refer to the capability of the floor pedestal attached to a supporting floor to withstand tip over forces generated by the application of a lateral force applied to the top of a moment arm. Overturning moment capacity is calculated by multiplying the lateral force by the height at which the force is applied.

## Panel/Panel Assembly

Modular and removable structural floor element or elements designed to rest on separate or integral elevated supports that may be used as an interstitial space for distribution of building services (wire, cable, air, etc.).

## Pedestal (Adjustable Height)

An access floor pedestal with adjustable height option is defined as the structural element that supports the access floor panel and raises it off the floor slab to create an interstitial space for service distribution. The adjustable height or leveling feature of the pedestal allows the access floor panels to be installed level regardless of the changes in elevation of the floor slab.

## Pedestal (Fixed Height)

A fixed height floor pedestal is defined as the structural element that supports the access floor panel and raises it off the slab to create an interstitial space for service distribution. The fixed height floor pedestals and corresponding access floor panels are designed to lay on the floor slab and follow its contour and undulations.

## Permanent Set

A material that is deflected so far that its elastic properties have been exceeded and it does not return to its original condition upon release of load is said to have taken a "permanent set."

## Raised Floor System (See Access Floor System)

## Rolling Load

Rolling loads are dynamic loads typically imposed by equipment on wheels moving across the access floor.

## Stanchion

The term stanchion is sometimes used to describe an access floor pedestal.

## Static Load

Static load is defined as a force that does not undergo a change in magnitude or direction during a measurement procedure. Three static loads are generally referred to: concentrated, ultimate and uniform loads.

## Stringer

A stringer is a structural element used to connect access floor pedestals together, thus providing lateral stability to the system and floor supports.

## Uniform Load

Uniform load is a static force applied equally over the entire area of an access panel and is typically imposed by stationary furniture, equipment without legs, boxes, pallets, etc. The uniform load rating is specified in pounds per square foot or Newtons per square meter.

## Ultimate Load

The greatest applied vertical static force(s) beyond which additional deflection is achieved without additional load or resistance.

CISCA
Ceilings & Interior Systems Construction Association

**Ceilings and Interior Systems Construction Association**
1010 Jorie Blvd., Suite 30
Oak Brook, IL 60523
Ph. 630.584.1919
Fax 866.560.8537
Web cisca.org

# Design Guidelines for Roof Pavers against Wind Uplift

Maryam Asghari Mooneghi[1]; Peter Irwin[2]; and Arindam Gan Chowdhury[3]

[1]Ph.D. Candidate, Civil and Environmental Engineering/ International Hurricane Research Center, Florida International University, Miami, FL. E-mail: masgh002@fiu.edu
[2]Professor of Practice, Civil and Environmental Engineering/ International Hurricane Research Center, Florida International University, Miami, FL. E-mail: peairwi@fiu.edu
[3]Associate Professor, Civil and Environmental Engineering/ International Hurricane Research Center, Florida International University, Miami, FL. E-mail: chowdhur@fiu.edu

## Abstract

The objective of this paper is to develop guidance for design of loose laid roof pavers against wind uplift. Large-scale experiments were performed on concrete roof pavers installed on the flat roof of a low-rise building using the Wall of Wind (WOW) facility at Florida International University (FIU). Both wind blow-off tests and pressure measurements on the top and bottom surfaces of the pavers were performed. The results are used to develop specific guidelines for design of loose-laid roof pavers. Account is taken of pressure equalization, the gaps between the pavers, and the space beneath the pavers. These guidelines are intended to be simple enough to be used by designers in parallel with the usual code provisions for exterior suctions on roofs.

## INTRODUCTION

Roofing systems are one of the most commonly damaged portions of the building envelope during high wind events. The ability to withstand wind-induced uplift forces across the building roofs is one of the critical design aspects. Suction forces on the roof can loosen and lift both roof sheathing and roof coverings, such as tiles, shingles, and roof pavers which might become wind born debris impacting other structures downwind causing extensive damage. Also, water leaking through failed roofing systems during hurricanes can result in considerable interior damage.

Flat roofs are commonly used in many residential and commercial buildings. Loose-laid concrete roof pavers are usually used on flat roofs. Concrete pavers are placed on the roof with gaps in between them and with spacing from the surface underneath the pavers (Figure 1).The gaps between the edges of adjacent pavers allow communication of top surface pressures to the underneath which results in a pressure equalization effect that reduces the net uplift (Asghari Mooneghi et al, 2014; Bienkiewicz and Sun, 1992, 1997; Kind and Wardlaw, 1982; Kramer et al, 1979). However, vortices emanating from roof corners can cause localized suctions on the top surface which cannot be fully countered by pressure equalization. These are the main cause of pavers being lifted off under strong winds. The pressure equalization

effect is subject to a number of influencing variables such as location relative to a corner, paver size, parapet height, building height, size of the gaps between pavers, and the stand-off distance of the pavers above the underlying roof surface.

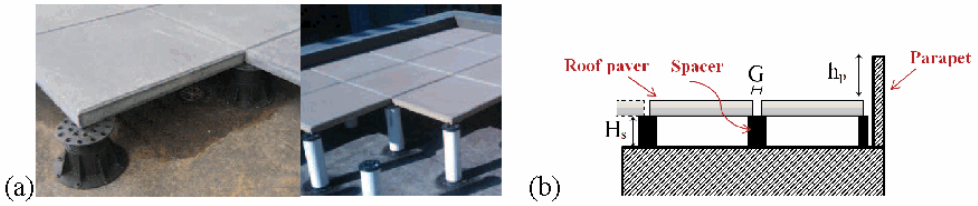


**Figure 1. a) Roof pavers on flat roofs; b) Geometrical parameter definition**

A number of experimental as well as theoretical research studies have been published in the literature concerning the wind loading mechanism of loose-laid roof pavers and the pressure equalization phenomenon. Researchers such as Cheung and Melbourne (1988), Bienkiewicz and Sun (1992), O'Brien et al (2004) and Asghari Mooneghi et al (2014) showed that the degree of pressure equalization depends on ratio of the size of the gap between the pavers to the spacer height, in such a way that the lower the ratio, the lower the pressure equalization.

Currently little guidance is supplied in most wind codes for the pressures underneath roof pavers. In addition, wind tunnel testing to measure them can be demanding considering both time and cost. With this in mind, some researchers have developed analytical models which are mainly concerned with simulating time-varying pressure distributions underneath roof pavers (i.e., interior pressure in the cavity between the inner and outer layers) given the external pressure data (Amano et al, 1988; Bofah et al, 1996; Gerhardt et al, 1990; Kind, 1994; Lou et al, 2012; Oh and Kopp, 2014; Sun and Bienkiewicz, 1993; Trung et al, 2010). The complexity of the current numerical methods makes it desirable to develop a simplified method that can be used in codes and standards for calculating the net uplift force of roofing systems from the available external pressure data on roofs.

A large-scale experimental study is presented that investigated the wind loading mechanism for concrete roof pavers on the flat roof of a low rise building. Half-scale roof pavers were installed on a square portion of the flat roof of a low-rise building. Results of wind lift-off tests and pressure measurements were used for accurate investigation of the net pressure distributions and the effect of the pavers' edge-gap/spacer height ratio on the wind performance of roof paving systems. Design guidelines are developed for roof pavers against wind uplift.

## EXPERIMENTS

The experiments were performed in the Wall of Wind open jet facility at FIU. It can generate up to a Category 5 Saffir–Simpson Scale hurricane wind speed and replicate the mean wind speed profile and turbulence characteristics of hurricane

winds. A set of triangular spires and floor roughness elements were used that generate turbulence and boundary layer characteristics (Figure 2). It is to be noted that WOW flow for large-scale wind testing is representative of a flow with partial turbulence simulation. In partial turbulence simulation, only the high frequency part of the wind spectrum is simulated and the low frequencies are missing mainly because of the limited size of the facility. So, the turbulence intensity is lower than that for the ABL flow containing all the low frequency fluctuations. However, using the method proposed by Katsuchi and Yamada (2011), the adequacy of the current turbulence intensity was shown. The size of the test section is 6.1 m wide and 4.3 m. high.

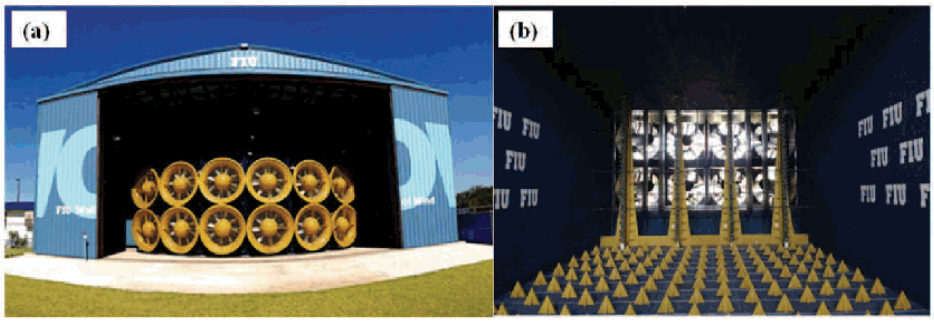


**Figure 2. a) Wall of Wind, Florida International University; b) Spires and floor roughness elements**

Tests were performed in suburban terrain with the target power law coefficient of $\alpha$=1/4. The size of the 1:2 test building model was 3.35 m by 3.35 m in plan by 1.524 m high representing a low-rise prototype building with height of 3.48 m. The windward parapet was interchangeable to allow the study of the effects of relative parapet height on the wind loading mechanism of roof pavers (relative parapet heights tested were $h_p/H$=0, 0.03, 0.05, 0.1, 0.15). In this paper, results are given for the case that the windward parapet height was $h_p$ =7.62 cm above the paver surface (Figure 1.b) resulting in a relative parapet height of $h_p/H$=0.05. There were no parapets on the leeward side of the building so that the roof can be representative of the windward corner of a bigger roof structure (Asghari Mooneghi et al, 2014; Lin and Surry, 1998; Lin et al, 1995).

Wind blow-off tests and pressure measurements were performed for three different edge-gap to spacer height ratios ($G/H_s$=0.28, 0.083 and 0.028). Adjustable height pedestals were used to change the space between the paver and the roof deck ($H_s$, Figure 1.b). A constant G=3.175 mm space between the pavers (Figure 1.b) was maintained. Only one wind angle of attack was tested which was 45° which is the most critical orientation for generating high uplifts under conical vortices on flat rectangular roofs (Holmes, 2007).

Wind blow-off tests were performed first. Concrete pavers with a dimension of 0.305 m by 0.305 m by 2.54cm thickness with weight per unit area of 535 N/m$^2$ were installed on the roof which can be considered as modeling typical 0.61 m square pavers at half-scale (Figure 3.a). The aim of these tests was to provide guidance on

the location where the failure first occurred. This could then be used to decide on the pressure tap layout. The tests were performed by gradually increasing the wind speed in WOW and visually observing the behavior of the roofing system. The most critical pavers which dislodged first were identified. Wind speeds were measured at the roof height of the test model (1.524 m height) using a turbulent flow Cobra probe.

For pressure measurements, the original pavers were replaced by pavers made from Plexiglas with the exact dimension as actual concrete roof pavers (Figure 3.b). Pressure measurements were carried out at wind speed of 18.5 m/s which was below the failure wind speed of concrete pavers (but required some special measures to hold the Plexiglas pavers in place). A total of 447 pressure taps were installed on the external and underneath surfaces of roof pavers on the whole roof. Nine critical pavers, identified during wind lift-off tests were fitted with total of 256 pressure taps to allow detailed measurements of the pressure distribution above and underneath the pavers (Figure 3.c).

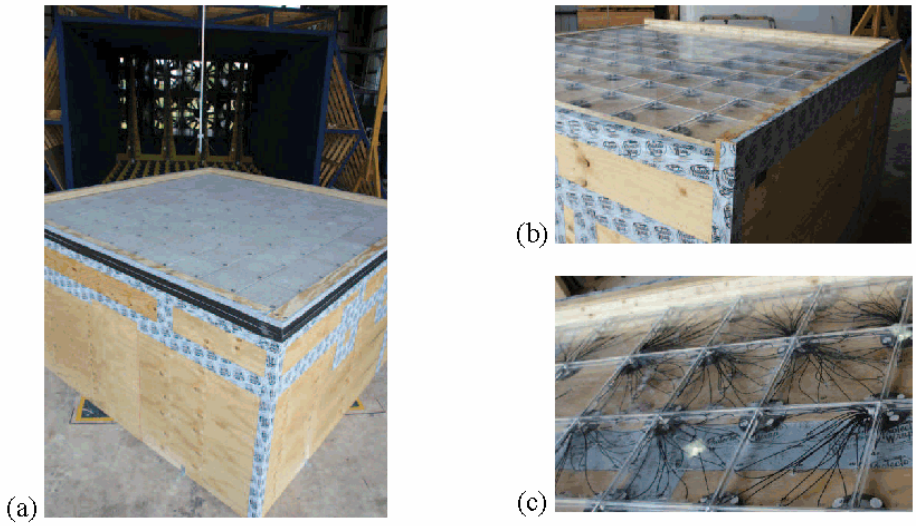


**Figure 3. a) Test building for wind blow-off tests; b) Test building for pressure measurements; c) Critical pavers instrumented with pressure taps**

Figure 4 shows the numbering of the pavers and the location of the 9 critical pavers. A 512 channel Scanivalve Corporation pressure scanning system was used for pressure measurements. Pressure data were acquired at sampling frequency of 512 Hz for a period of two minutes. A transfer function designed for the tubing (Irwin et al, 1979) was used to correct for tubing effects.

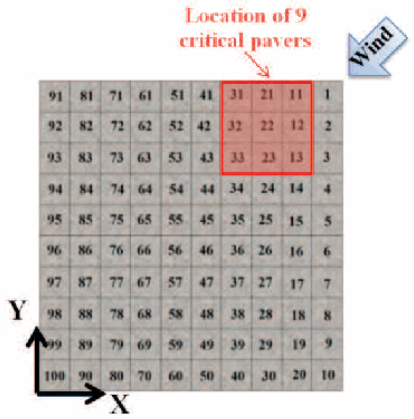


**Figure 4. Roof pavers numbering**

## DATA ANALYSIS

The mean pressure coefficient at any location was obtained from:

$$Cp_{mean} = \frac{P_{mean}}{\frac{1}{2}\rho U_{mean}^2} \quad (1)$$

where $P_{mean}$ is the mean pressure, $\rho$ is the air density at the time of the test (1.225 kg/m$^3$) and $U$ is the mean wind speed measured at the building height of the test model (1.524 m). The peak pressure coefficient was obtained from:

$$Cp_{peak} = \frac{P_{peak}}{\frac{1}{2}\rho U_{3s}^2} \quad (2)$$

where $P_{peak}$ is the peak pressure. Data were low-pass filtered at 30 Hz (equivalent to 21 Hz at full scale).The Sadek and Simiu (2002) method was used to obtain statistics of pressure peaks from observed pressure time histories. Because estimates obtained from this approach are based on the entire information contained in the time series, they are more stable than estimates based on single observed peaks. For the evaluation of these estimated values 95% confidence was considered. $U_{3s}$ is the peak 3-s gust at the reference height. The peak value of the $U_{3s}$ was obtained by performing moving averages. The net total pressure coefficient defined as the instantaneous difference between the external and the corresponding underneath pressure coefficient at the same location are:

$$Cp_{net} = Cp_{ext} - Cp_{int} \quad (3)$$

The overall wind lift load, $L$, acting on any single paver is obtained as:

$$L = \frac{1}{2}\rho U^2 \iint_{A_{paver}} Cp_{net}(x,y)dA \quad (4)$$

$$C_L = \frac{L}{\frac{1}{2}\rho U^2 A} \quad (5)$$

where A is the surface area of the paver. The reduction in the net wind uplift can be expressed as:

$$r = \frac{C_{L_{net}}}{C_{L_{ext}}} \quad (6)$$

The blow-off takes place when the uplift force is equal to the paver's weight, W. Therefore, the critical wind velocity $U_{CRIT}$ at which blow-off occurs is:

$$U_{CRIT} = \sqrt{\frac{W}{\frac{1}{2}\rho C_L A}} \quad (7)$$

## RESULTS AND DISCUSSION

Results from wind lift-off tests and pressure measurements showed that in all cases Paver 21 (Figure 4) was the most critical paver experiencing the highest uplift force. So, results presented in the following are based on the results calculated for this most critical paver (unless otherwise mentioned). Figure 5 shows a comparison between the failure wind speeds when wobbling of pavers was observed, the critical wind speeds calculated using net lift coefficient obtained for Paver 21 from pressure measurement tests using Eq. (7), and a practice based on ASCE 7-10 pressure coefficients for components and claddings using Eq. (7). It should be noted that ASCE 7-10 does not provide any recommendations for the pressure coefficient in the underneath cavity of multi-layered roofing systems. So, the net uplift coefficient cannot be calculated directly from ASCE 7-10. Consequently, a common practice mainly proposed for roof tiles (FPHLM, 2005, Volume II, p. 55) is to consider the external pressure coefficient as the net pressure coefficient. For gable roofs with slope $\theta \leq 7°$ the largest external pressure coefficient for edge Zone 2 and corner Zone 3 for tributary areas less than 0.9 $m^2$ is given as -1.8 and -2.8 respectively in Figure 30.4-2A (ASCE 7-10). Results presented in Figure 5, demonstrate the effect of pressure equalization for air permeable roofing systems in increasing the critical wind speed at which failure occurs and shows that the values based on ASCE 7-10 external pressure coefficients are conservative. This was in agreement with past studies in the literature which showed that for double-layer roof systems (e.g. roof pavers), estimates of wind loads obtained in most of regions of the roof can be considerably conservative by ignoring the effects of pressure equalization through application of the building codes to the design of the exterior roof layer (Bienkiewicz and Endo, 2009; Bienkiewicz and Sun, 1992, 1997; Chino et al, 1991; Kind and Wardlaw, 1982; Kramer and Gerhardt, 1983; O'Brien et al, 2004). Results in Figure 5 also showed that by increasing the gap to spacer height ratio ($G/H_s$), the failure wind speed increases. This is in agreement with studies of Bienkiewicz and Endo (2009). Also, tests on the effects of relative parapet height ($h_p/H$) showed that generally parapets reduce the net uplift force on the roof pavers. However, a certain relative parapet height in the range $h_p/H$=0.10 exists in which the uplift loads reach the worst case values.

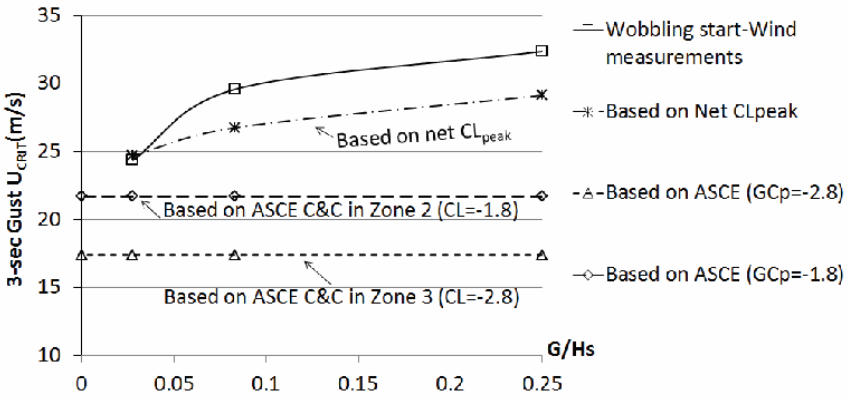


**Figure 5. Critical lift-off speed**

Figure 6 shows the variation of the net uplift force coefficient and the reduction factor ($r = \frac{C_{L_{net}}}{C_{L_{ext}}}$) with $G/H_s$ on Paver 21. The results show that increasing the $G/H_s$ ratio reduces the net uplift force coefficient on the paver.

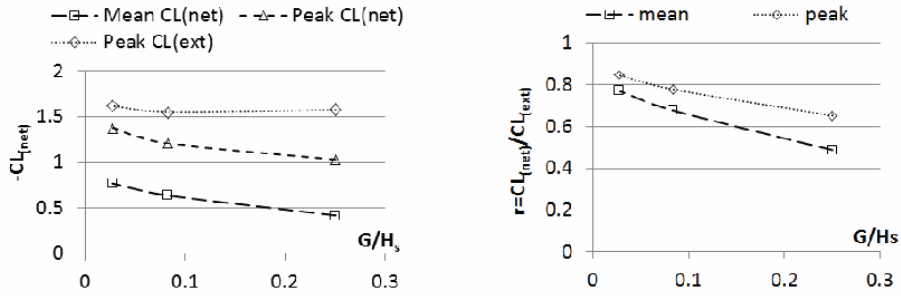


**Figure 6. Variations of $CL_{net}$ and $r = \frac{C_{L_{net}}}{C_{L_{ext}}}$ with $G/H_s$**

As explained previously, pressure equalization is dependent on the geometric parameters of the roof pavers (Bienkiewicz and Endo, 2009; Bienkiewicz and Sun, 1992, 1997). These include the gap (G) between panels, the spacer height ($H_s$) between the pavers and the roof, and the panel size. This research has focused on characterizing the pressure equalization on roof pavers and the effect of the gap to spacer height ratio ($G/H_s$) and relative parapet height ($h_p/H$) for developing simple design guidelines for loos-laid roof pavers. A journal paper is in preparation which includes these design guidelines which will be presented during the conference. The guidelines have been formatted so that the existing information in codes and standards such as ASCE 7-10 on exterior pressures on components and cladding can be utilized. The effects of the paver's edge-gap to spacer height ratio and parapet height as a fraction of building height will be included in the guidelines as adjustment

factors. These guidelines incorporate appropriate factors of safety in order to achieve the normal levels of reliability used in the design of building envelopes.

## CONCLUSIONS AND FUTURE WORK

The objective of this paper was to investigate the wind loading mechanism of concrete roof pavers with the ultimate goal of developing simple design guidelines in code format for design of commonly used loose-laid roof pavers. The experiments were performed in the Wall of Wind, a large-scale hurricane testing facility at Florida International University. Experiments included both wind blow-off tests and detailed pressure measurements on the top and bottom surfaces of the pavers. Large-scale concrete roof pavers were installed on a square portion of a flat roof. The effects of changing the pavers' edge-gap to spacer height ratio were investigated. Based on the information gathered in the current tests and review of literature, guidelines suitable for codes and standards are being developed for the design of roof pavers and will be presented. The guidelines will be formatted so that use can be made of the existing information in codes and standards such as ASCE 7-10 pressures coefficients. Limitations and applications of the guidelines will be addressed.

## ACKNOWLEDGEMENT

This research was supported by the Florida Division of Emergency Management (DEM) and the National Science Foundation (NSF) (NSF Award No. CMMI-1151003) through the Wall of Wind flow simulation and large-scale testing of roof pavers. We would like to acknowledge with thanks the Tile Tech Company for providing us with concrete roof pavers and the pedestal system for the wind blow-off tests. The help offered by the Wall of Wind manager, Walter Conklin and research scientists, Roy Liu Marquis and James Erwin is greatly acknowledged. The help offered by graduate research assistant, Ramtin Kargarmoakhar is also greatly appreciated.

## REFERENCES

(FPHLPM), F.P.H.L.P.M., 2005. Predicting the Vulnerability of Typical Residential Buildings to Hurricane Damage.

Amano, T., Fujii, K., Tazaki, S., 1988. Wind loads on permeable roof-blocks in roof insulation systems. Journal of Wind Engineering & Industrial Aerodynamics 29, 39-48.

ASCE 7-10, 2010. Minimum Design Loads for Buildings and Other Structures, American Society of Civil Engineers, ASCE, Virginia.

Asghari Mooneghi, M., Irwin, P., Gan Chowdhury, A., 2014. Large-scale testing on wind uplift of roof pavers. Journal of wind engineering and industrial aerodynamics 128, 22-36.

Bienkiewicz, B., Endo, M., 2009. Wind considerations for loose-laid and photovoltaic roofing systems, Structures Congress, Austin, Texas, pp. 2578-2587.

Bienkiewicz, B., Sun, Y., 1992. Wind-tunnel study of wind loading on loose-laid roofing system. Journal of wind engineering and industrial aerodynamics 43, 1817-1828.
Bienkiewicz, B., Sun, Y., 1997. Wind loading and resistance of loose-laid roof paver systems. Journal of wind engineering and industrial aerodynamics 72, 401-410.
Bofah, K.K., Gerhardt, H.J., Kramer, C., 1996. Calculations of pressure equilibration underneath loose-laid, flow permeable roof insulation boards. Journal of wind engineering and industrial aerodynamics 59, 23-37.
Cheung, J.C.K., Melbourne, W.H., 1988. Wind Loading on a Porous Roof. Journal of wind engineering and industrial aerodynamics 29, 19-28.
Chino, N., Iwasa, Y., Mataki, Y., Hagiwara, T., Sato, H., 1991. Internal pressure of double composite exteriors. Journal of wind engineering and industrial aerodynamics 38, 381-391.
Gerhardt, H.J., Kramer, C., Bofah, K.K., 1990. Wind loading on loosely laid pavers and insulation boards for flat roofs. Journal of wind engineering and industrial aerodynamics 36, Part 1, 309-318.
Holmes, J.D., 2007. Wind Loading of Structures. Taylor & Francis.
Irwin, P., Cooper, K., Girard, R., 1979. Correction of distortion effects caused by tubing systems in measurements of fluctuating pressures. Journal of Wind Engineering and Industrial Aerodynamics 5, 93-107.
Katsuchi, H., Yamada, H., 2011. Study on turbulence partial simulation for wind-tunnel testing if bridge deck, 12th International Conference on Web Engineering ICWE 2012, Amsterdam, Netherlands.
Kind, R.J., 1994. Predicting pressure distribution underneath loose laid roof cladding systems. Journal of Wind Engineering and Industrial Aerodynamics 51, 371-379.
Kind, R.J., Wardlaw, R.L., 1982. Failure mechanisms of loose laid roof insulation systems. Journal of wind engineering and industrial aerodynamics 9, 325-341.
Kramer, C., Gerhardt, H.J., 1983. Wind loads on permeable roofing systems. Journal of Wind Engineering and Industrial Aerodynamics 13, 347-358.
Kramer, C., Gerhardt, H.J., Scherer, S., 1979. Wind pressure on block-type buildings. Journal of Wind Engineering and Industrial Aerodynamics 4, 229-242.
Lin, J.X., Surry, D., 1998. The variation of peak loads with tributary area near corners on flat low building roofs. Journal of wind engineering and industrial aerodynamics 77–78, 185-196.
Lin, J.X., Surry, D., Tieleman, H.W., 1995. The distribution of pressure near roof corners of flat roof low buildings. Journal of wind engineering and industrial aerodynamics 56, 235-265.
Lou, W., Huang, M., Zhang, M., Lin, N., 2012. Experimental and zonal modeling for wind pressures on double-skin facades of a tall building. Energy and Buildings 54, 179-191.
O'Brien, C., Neff, D.E., Bienkiewicz, B., Dinwoodie, T., 2004. Optimization of wind resistance of photovoltaic roofing system, Proceedings of the 2004 Structures Congress, Nashville, Tennessee, pp. 1-8.
Oh, J.H., Kopp, G.A., 2014. Modelling of spatially and temporally-varying cavity pressures in air-permeable, double-layer roof systems. Building and Environment 82, 135-150.

Sadek, F., Simiu, E., 2002. Peak non-Gaussian wind effects for database-assisted lowrise building design. Journal of engineering Mechanics 128, 530-539.

Sun, Y., Bienkiewicz, B., 1993. Numerical simulation of pressure distributions underneath roofing paver systems. Journal of wind engineering and industrial aerodynamics 46–47, 517-526.

Trung, V., Tamura, Y., Yoshida, A., 2010. Numerical computation for lower surface pressures on a porous sunshade roof cover sheet, Fifth International Symposium on Computational Wind Engineering (CWE2010), Chapel Hill, North Carolina, USA.

**Wind and Structures**, *Vol. 22, No. 2 (2016) 133-160*
DOI: http://dx.doi.org/10.12989/was.2016.22.2.133 

# Towards guidelines for design of loose-laid roof pavers for wind uplift

Maryam Asghari Mooneghi[1a], Peter Irwin[2b] and Arindam Gan Chowdhury[*2]

[1]*Advanced Technology and Research, Arup, San Francisco, CA, USA*
[2]*Department of Civil and Environmental Engineering/International Hurricane Research Center, Florida International University, Miami, FL, USA*

*(Received June 3, 2014, Revised October 28, 2015, Accepted November 2, 2015)*

**Abstract.** Hurricanes are among the most costly natural hazards to impact buildings in coastal regions. Building roofs are designed using the wind load provisions of building codes and standards and, in the case of large buildings, wind tunnel tests. Wind permeable roof claddings like roof pavers are not well dealt with in many existing building codes and standards. The objective of this paper is to develop simple guidance in code format for design of loose-laid roof pavers. Large-scale experiments were performed to investigate the wind loading on concrete roof pavers on the flat roof of a low-rise building in Wall of Wind, a large-scale hurricane testing facility at Florida International University. They included wind blow-off tests and pressure measurements on the top and bottom surfaces of pavers. Based on the experimental results simplified guidelines are developed for design of loose-laid roof pavers against wind uplift. The guidelines are formatted so that use can be made of the existing information in codes and standards such as American Society of Civil Engineering (ASCE) 7-10 standard's pressure coefficients for components and cladding. The effects of the pavers' edge-gap to spacer height ratio and parapet height to building height ratio are included in the guidelines as adjustment factors.

**Keywords:** design guidelines; roof pavers; large-scale testing; wind uplift

## 1. Introduction

It is clearly important that roofing materials be designed so that they can withstand the uplift forces that occur in strong winds. Some of the major losses that have occurred in hurricanes have been due to loss of roofing materials (Huang *et al.* 2009). Experience indicates that hurricane winds are well capable of ripping off materials such as tiles, shingles, roof pavers and gravel ballast (Smith 1994, Huang *et al.* 2009). The building itself then becomes vulnerable to considerable additional damage through water infiltration and changes in internal pressure (Bitsuamlak *et al.* 2009, Chowdhury *et al.* 2012). As well, the wind-borne debris coming from the damaged roof often causes extensive additional damage to buildings downwind as it impacts them with high momentum (Fernandez *et al.* 2010, Masters *et al.* 2010).

*Corresponding author, Associate Professor, E-mail: chowdhur@fiu.edu
[a] Ph.D., E-mail: maryam.asghari@arup.com
[b] Professor of Practice, E-mail: peairwi@fiu.edu


http://www.techno-press.org/?journal=was&subpage=8 ISSN: 1226-6116 (Print), 1598-6225 (Online)

Wind uplift of roof pavers is not only the result of the suction on their top surface, but also of the pressure on their underside for which no guidance is currently supplied in most wind codes. Therefore, for lack of better information, building designers often make the simplifying assumption that the net uplift acting on air permeable roofing elements is the same as the exterior pressure specified in the building code (Florida Public Hurricane Loss Projection Model (FPHLPM) 2005). In reality a significant amount of pressure equalization occurs which tends to make this assumption quite conservative in many instances for roof pavers (Banks *et al.* 2000). On the other hand, the pressure equalization effect is subject to a number of influencing variables such as paver's location relative to a corner, paver size and geometry, parapet height, building height, gaps between pavers, and the stand-off distance of the pavers above the underlying roof surface (Bienkiewicz and Sun 1997, Banks *et al.* 2000). This has deterred the development of more specific guidance in codes. Interlocking and strapping systems are often used to improve the resistance of roof pavers, and they can be very effective (Irwin *et al.* 2012). However failures do still occur and it will help in the design of such systems if better knowledge of the aerodynamic forces working on the pavers can be obtained. The aerodynamic mechanisms that cause uplift are quite complex but in this paper guidance is developed in the form of relatively simple rules for the design of loose-laid roof pavers against uplift wind forces, rules that are amenable to use alongside or within building codes.

A set of large-scale experiments was performed to study the wind loading mechanism of concrete roof pavers using the Wall of Wind (WOW) facility at Florida International University (FIU). Concrete pavers were installed on a square portion of a flat roof of a low-rise building. Both wind blow-off testing and pressure measurements were performed. Experiments included the wind lift-off tests and detailed pressure measurements on the external and underneath surfaces of roof pavers. The effects of the pavers' edge gap to spacer height ratio, relative parapet height and the effects of connecting pavers were studied. The results from the pressure measurements were compared with estimates obtained from American Society of Civil Engineering (ASCE) 7-10 pressure coefficients. Finally, guidelines were proposed for design of loose-laid roof pavers using ACSE 7-10 components and cladding exterior pressure coefficients taking into account the effects of pavers' edge-gap to spacer height ratio, relative parapet height, and pressure equalization.

## 2. Background

Solid pavers are frequently used as ballast and walking surfaces on flat roofs and as decorative elements on terraces. It is necessary that they be capable of resisting uplift forces due to wind. A number of experimental and analytical studies are reported on wind loading and performance of loose-laid roofing systems. Wind tunnel experiments on small scale models have been performed by researchers to investigate the wind loading and failure mechanism of loose-laid roof paving system (Kind and Wardlaw 1979, Kind and Wardlaw 1982, Bienkiewicz and Sun 1992, Bienkiewicz and Sun 1997, Irwin *et al.* 2012, Oh and Kopp 2015). Large-scale testing is preferred for small structures and building appurtenances for maintaining modeling accuracy and minimizing Reynolds number effects (Kargarmoakhar *et al.* 2015). However, studies using full- and large-scale models (Aly *et al.* 2012, Asghari Mooneghi *et al.* 2014) have been limited. As explained by Geurts (2000), small scale wind tunnel experiments are not normally suitable for investigating the pressure equalization over air permeable roof covering materials and its effects on the net loading. This is because when the batten space and permeability are scaled, their sizes

get too small to simulate the realistic mechanisms in the flow due to Reynolds number effects. Therefore, large scale test data or full scale field measurements are necessary for proposing calculation models and design guidelines for these materials.

The complex nature of the flows above and beneath air permeable roofing systems has also been explored using numerical simulations. Amano *et al*. (1988) proposed a simplified numerical model based on the unsteady Bernoulli equation with one value of pressure at each paver edge for obtaining the internal wind pressure distribution of roof pavers under a known external pressure field. Correction terms were employed to take into account the effects of viscosity. The effect of the gap between the pavers was also investigated. Kind *et al*. (1988) proposed a correlation for predicting wind lift-off speeds of loose-laid insulation boards based on extensive wind tunnel testing results. The correlation accounts for the effects of building characteristics (low, intermediate or high–rise building), parapet height, element weight per unit area and interlock effects. The tests of Kind *et al*. (1988) were primarily for pavers laid directly on the roof with no spacers underneath. Gerhardt *et al*. (1990) performed a set of experiments and calculations and developed an equation for calculating the failure wind speed based on the external pressure, the element size relative to smaller plan dimension of the building and the weight of the elements. Diagrams were provided to help choose the best possible solution when using these roofing systems. Sun and Bienkiewicz (1993) stated that the flows between and beneath the loose-laid pavers are very slow because of the boundary effects of the flow field, and should be treated as viscous. They employed Darcy's law to develop a numerical model for calculating the pressure distribution underneath roof pavers. In their model, the pressure distribution along paver edges was assumed piecewise linear. The experimental data and their numerical results show similar trends. This model was refined later to allow arbitrary pressure distribution along paver edges, and to take into account the interlock effects between pavers. This flow model was limited to steady flow and was sufficient to estimate the mean pressure distribution for small stand-off distances between the roof surface and pavers and for low speeds of the flow, which means low Reynolds number. However, it may not be so applicable for a relatively high flow speed with high turbulence (Oh and Kopp 2012). Kind (1994) proposed a numerical method based on Laplace's equation for predicting the underneath pressure distribution for loose laid roof pavers. It was assumed that inertia effects are negligible in the under-element flow and it was thought to be viscosity dominated. Also, the flow resistance in the element/roof deck interface plane was considered as uniform. With these assumptions the flow continuity equation reduces to the Laplace equation. The results were in reasonable agreement with measured pressure distributions in cases where the roof deck and the undersides of the elements were reasonably flat with uniform surface texture. The results are more likely to be applicable for pavers lying directly on the roof surface. Bofah et al. (1996) proposed a theory for calculating the pressure distribution underneath roof pavers based on approximating the underneath flow by a two-dimensional laminar flow in a very shallow channel with a porous upper roof. Sinusoidal and uniform outer pressure distributions were investigated which were consistent with experimental results. Trung *et al*. (2010) applied a method based on the Multiple Discharge Equations (MDE) as described in Oh *et al*. (2007) to predict the underneath pressures of a porous sunshade roof cover from a known external pressure distribution. Computational results were compared with experiments performed on a 1:50 scale model of a low-rise building. The results of the computations were in good agreement with the experiments for 5% and 10% porosity ratios (ratio between the areas of orifices to the area of the sheet) and 4.7 mm height from the roof deck to the cover used in the experiments. Oh and Kopp (2014) developed a one-dimensional analytical model for simulating cavity pressures within multi-layer

roofing systems from a known external pressure distribution using the unsteady Bernoulli equation and Couette flow assuming laminar flow in the cavity. The model was verified by comparing its predictions with results obtained from wind tunnel testing.

Previous experimental and numerical studies on the wind loading mechanism of loose-laid roofing systems like roof pavers, gravel ballast, green roofs, etc. can assist in developing code specific models for design of such systems. However, many unanswered questions still remain in the current state of knowledge on this issue. In research aimed at codification of wind loading on porous claddings and covers over roofs which have a similar wind loading mechanism as roof pavers, Cheung and Melbourne (1986) and Cheung and Melbourne (1988) investigated the effect of porosity on wind loading on such systems. Reduction factors were proposed as a function of distance from the roof leading edge for different porosities and different internal volumes for a typical low-pitch roof cladding, and adopted by AS/NZS 1170.2. Design wind loads could then be estimated from external pressure coefficients given in the existing building codes. Bienkiewicz and Meroney (1988) developed a rough design guideline for loose-laid ballast pavers. The system failure condition was considered in terms of the failure wind speed and the wind loading parameters specified by the building code parameters (UBC, ANSI or ASCE 7-05 (Bienkiewicz and Endo 2009). This theory is limited to low buildings with rectangular flat roofs. The allowable building heights are given in the design guidelines for a range of design wind speeds and wind exposures.

Some codes and standards do address the design of roof paver systems. In the Netherlands code, NEN EN 1991-1-4/NA, a set of values for net pressure coefficients (difference between the external and underneath pressure coefficients; $Cp_{net}=Cp_e-Cp_i$) is proposed for design of roofing tiles and pavers. These values were based on a number of experiments and full-scale studies on roof tiles on pitched roofs and roof pavers on flat roofs including those of Geurts (2000), who proposed equalization factors defined as $C_{eq}=Cp_{net}/Cp_e$ from full-scale measurements on roof tiles and roof pavers. The equalization factors are to be applied to the external pressure coefficients given in the Netherlands wind loading code. The proposed value of $C_{eq}$ for roof pavers with and without interlock were 0.25 and 0.6, respectively. In the German Wind Code (DEUTSCHE NORM 2001-03) design pressure coefficients are provided for building envelopes with permeable facades based on a study by Gerhardt and Janser (1995). In the Australian Standard for wind loads (AS 1170.2 2011) reduction factors are given for estimating design wind loads on porous claddings. These factors depend on the cladding porosity and the horizontal distance from windward building edge, and are based on the work of Cheung and Melbourne (1988).

Major international codes and standards for wind loads in USA and Canada (NBCC; ASCE 7-10) specify roof wind pressures for typical roof geometries but there are no specific provisions on how to apply such pressures to roofing elements such as tiles, shingles, and pavers. Using the available numerical methods proposed in literature for designers and suppliers of roof pavers is quite complex, and performing project specific wind tunnel testing is not practical, except for very large projects. This paper proposes a simplified yet reasonably accurate method for calculating the net uplift force on roof paver systems from the existing external pressure coefficients in the current ASCE 7-10 standard and takes into account the effect of pavers' edge gap to spacer height ratio, relative parapet height, and pressure equalization.

## 3. Pressure gradient effects

Multi-layer building envelopes, e.g. roof pavers are particularly sensitive not just to pressures but to spatial pressure gradients. Concrete roof pavers are usually placed on the roof with spacing above the roof deck and with gaps between the pavers. The pressure distribution produced by the wind flow over the outer surface of the roof produces secondary flows through the spaces between and underneath the paver elements. The so called pressure equalization occurs very quickly, provided the space between the pavers and the roof deck below is not too large, typically in a small fraction of a second, because very small volumes of air exchange are needed to bring the underside pressure into equilibrium with the pressures around the paver perimeter. This phenomenon is controlled by the same physics as the internal pressure. However, in pressure equalization, much smaller volumes of air through many openings are involved. The pressure equalization effect greatly reduces the net uplift force on pavers in most areas of a roof. However, in areas of very high spatial gradients of pressure, such as those which occur under vortices near roof corners, significant net uplift pressures can still occur. Figure 1 illustrates the typical path of the vortices over a flat roof for cornering winds.

Along with the high suctions from the vortices there are also high velocities passing over the surface as the flow rotates rapidly about the vortex center. The vortex is analogous to a small tornado with axis approximately horizontal and with very high velocities near the vortex core. Thus, not only are there high suctions tending to lift roofing material, but also high tangential air speeds immediately adjacent to the roof surface, which are prone to penetrating under the edges of roofing elements and lifting them. It is very important to generate these vortices as part of the test to fully replicate these wind effects on a roof. The bell-shaped curves in Fig. 1 have greatest central suction near the roof corner but as distance from the roof corner increases, the suction reduces and the width of the bell-shape grows larger (Banks *et al.* 2000). The effect of these suction distributions on the roof will depend on the type of roof system being used and is clearly very different from a simple uniform pressure distribution. The diagram in Fig. 2 illustrates schematically the general mechanism of uplift on roof pavers. The aerodynamic uplift force is the difference between the pressure on the lower surface of the paver, $P_L$ and the pressure on the upper surface, $P_U$ (Fig. 2). The pressure on the upper surface due to the presence of a conical vortex (solid curve) is negative (when measured relative to the static pressure in the surrounding air stream) and has a concentrated peak.

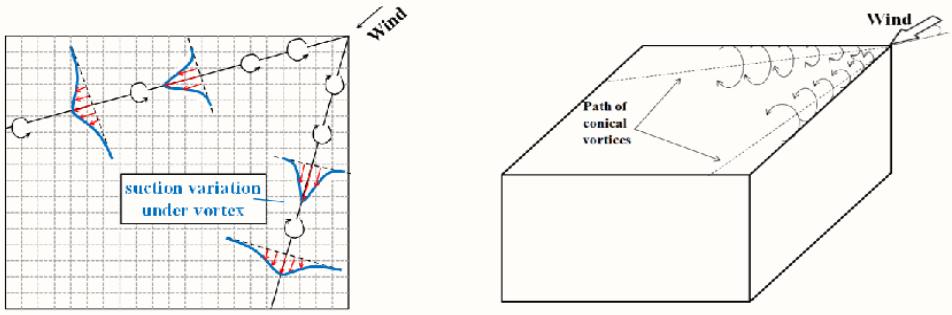


Fig. 1 Conical vortices; Suction variation on roof under corner vortices

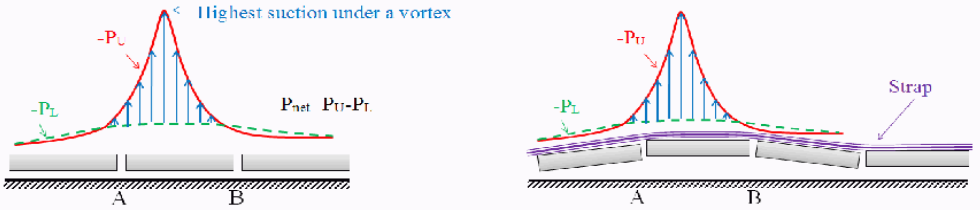


(a) Pressure distributions on upper and lower surfaces of a roof paver (b) Straps running transverse to the axis of the vortex

Fig. 2 General mechanism of uplift on roof pavers

The pressure on the lower surface is depicted by the broken curve and at the paver edge it is shown as being equal to that on the top surface. In practice, the top and bottom edge pressures do not always match exactly. The underneath pressure is dictated by the outer pressure distribution and the relative magnitude of the joint resistances compared to the under-element resistance which prevents a complete pressure equilibration between upper and lower surfaces of the element (Bofah *et al*. 1996, Gerhardt *et al.* 1990, Kind 1994). Detailed measurements done by Kind and Wardlaw (1982) showed that the underneath pressure does tend to vary roughly linearly between the pressures at the paver edges as depicted in Fig. 2 (also discussed in Bofah *et al.* (1996)). It is only due to the sharp peak of the upper pressure under a vortex (between points A and B) that a net uplift might occur, signified by the large difference between the solid and broken curves. If the upper surface pressure does not have the peak (e.g., the pavers are not sitting directly under a vortex) then pressure equalization caused by flow around the edges of the paver results in much smaller net uplift as shown by the small differences between the solid and dashed curves on the pavers outside of the zone between points A and B. The impact of pressure equalization depends on the size of the paver relative to the width of the conical vortex. If the paver is much larger than the width of the vortex then the impact is reduced since only a small fraction of the paver area is affected by the high suction. Also, if the paver is much smaller than the width of the vortex then, even if it is sitting in a high suction zone, the pressure equalization effect of the gaps at its edges substantially reduces the difference in pressure between top and bottom surfaces. If the paver and vortex widths are similar the net uplift will tend to be maximized.

At sufficient wind speed the aerodynamic uplift force and/or the overturning moment on the element may become higher than the weight and/or the resisting moment due to gravity or other restraints, such as strapping, and lift off will occur.

Interlocking and strapping systems are commonly used to improve the wind performance of roof pavers. In this case, the uplift force tends to be shared across several pavers. Fig. 2(b) shows a strapping system running transverse to the axis of the vortex which connects to the center of each paver. The lift on the paver AB is now restrained not only by the weight of the paver AB but also by at least part of the weight of the adjacent pavers, on which there is little if any lift. The lift on the paver AB that is needed to both lift paver AB and also cause the adjacent pavers to rotate so that their edges at A and B become airborne, but not the farther edges, is about double that needed to lift the unconnected paver (Irwin *et al*. 2012). The lift required to cause the farther edges also to become airborne is about 3 times that for the unconnected paver. These considerations, along with

the assumption that lift on real pavers varies approximately as wind velocity squared, lead to the expectation that strapping in the direction transverse to the line of the vortex will increase the lift off speed by a factor of approximately $\sqrt{2} = 1.4$ to $\sqrt{3} = 1.7$ (Irwin *et al.* 2012). Aly *et al.* (2012) also showed that locking a group of pavers together can be very effective for preventing lift-off of pavers located in critical regions on the roof. They recommended using a locking system able to hold a group of at least 4x4 or 5x5 pavers together.

## 4. Experimental setup and testing protocol

A number of large-scale experiments were performed by the authors, and described in an earlier paper (Asghari Mooneghi *et al.* 2014, Mooneghi *et al.* 2014). In the work discussed in this paper, the same experimental setup was used for additional tests to facilitate the development of design guidelines. The experiments were performed in the 12-fan Wall of Wind (WOW) open jet facility at FIU which is able to generate hurricane winds up to Category 5 Saffir–Simpson Scale that replicate a representative mean wind speed profile and the high frequency end of the turbulence spectrum. A set of triangular spires and floor roughness elements was used to generate appropriate turbulence and boundary layer characteristics (Fig. 3).

Fig. 4 shows the comparison of longitudinal WOW spectrum and the Von Karman longitudinal spectrum at full scale using $L_u$=12 m and $I_u$=0.3 at 3.048 m height in suburban terrain (z0=0.2). It can be seen that there is a good match between the two spectra at high frequencies which has been noted by a number of previous researchers as necessary for correct simulation of local flow aerodynamics on low-rise buildings (Melbourne 1980, Saathoff and Melbourne 1997, Kumar and Stathopoulos 1998, Tieleman 2003, Richards *et al.* 2007, Yamada and Katsuchi 2008, Irwin 2009, Banks 2011, Kopp and Banks 2013). However, at low frequencies turbulence energy is missing. This is a common limitation when testing at large model scales, due to the limited size of wind tunnel working sections, but it can be largely overcome in post-test analysis using Partial Turbulence Simulation (PTS) theory based on quasi-steady assumptions as described by Asghari Mooneghi (2014) and Asghari Mooneghi *et al.* (2015).

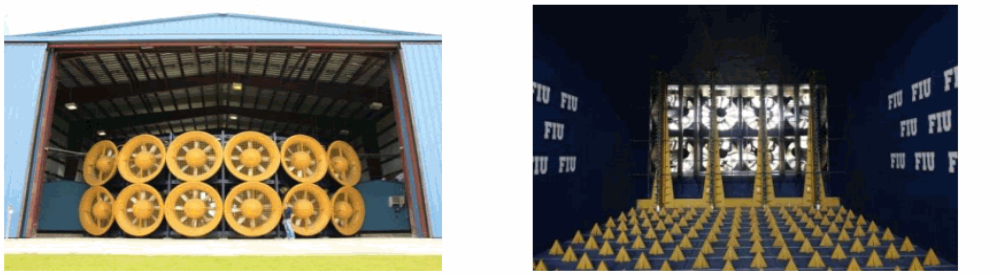


(a) Inlet view (b) Outlet view, Spires and floor roughness elements

Fig. 3 Wall of Wind, Florida International University

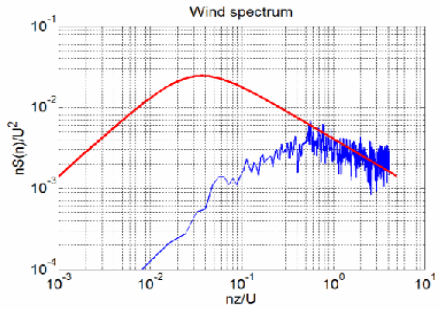


Fig. 4 Comparison of WOW Partial Spectrum and the Von Karman Spectrum at Full Scale

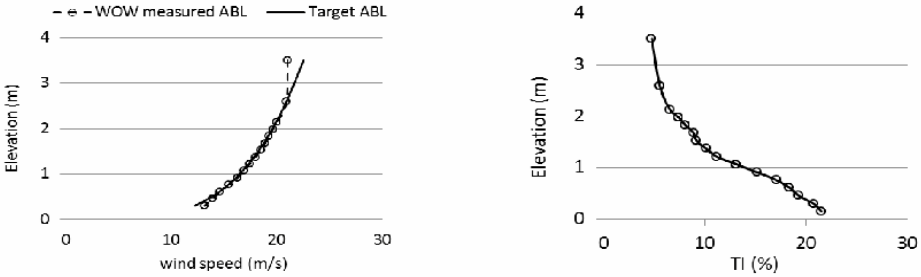


(a) Atmospheric Boundary Layer (ABL) profile (b) Turbulence intensity profile

Fig. 5 Simulated Suburban Terrain

The mean wind speed and turbulence intensity profiles for suburban terrain are shown in Fig. 5 for 20.1 m/s wind speed (target power law coefficient was $\alpha$=1/4).

The dynamic similarity requirements for the tests and how they were satisfied have been described by Asghari Mooneghi *et al.* (2014). The size of the 1:2 test building model was 3.35 m by 3.35 m in plan by 1.524 m high, representing at half scale a low-rise prototype building with height of 3.048 m. The size of the test section was 6.1 m wide and 4.3 m. high.

The test model height was around 35% of the wind field height generated by the WOW. This was within the 33% to 50% of the wind field height recommended by Aly *et al.* (2011) for obtaining roof pressure measurements with insignificant blockage effects in open jet facilities (Habte *et al.* 2015). The test model was located at a distance of around 13.70 m from the WOW fans, thus abiding by the minimum proximity requirement recommended by Bitsuamlak *et al.* (2010).

The roof deck was made from plywood and was completely sealed and rigid. The rectangular sharp edged parapets on the building model were interchangeable which allowed the parapet height to be adjusted. There were no parapets on the leeward side of the building. This was done with the intent that the model roof could be representative of the windward corner of a bigger roof

structure on which the downwind parapets would not significantly influence flow over the upwind portions of the roof. Lin and Surry (1998) and Lin *et al.* (1995) showed that, for low buildings which are large enough to have reattached flows on the roof, the distribution of pressure coefficients in the corner region is mainly dependent on the eave height, *H*, and not so much on the building plan dimensions for similar terrain conditions. Moreover, external pressure coefficients measured in the wind tunnel by Kopp *et al.* (2005) on roof corners of a nearly flat building model were consistent with those measured on roof corners of flat roof low-rise building models with the same height but with different plan aspect ratios (Stathopoulos 1982, Stathopoulos and Baskaran 1988, Ho *et al.* 2005, Pierre *et al.* 2005).

Both wind blow-off testing (i.e., blowing at sufficient speed to dislodge pavers) and pressure measurements were performed. For the wind blow-off tests, concrete pavers with dimensions of 0.305 m by 0.305 m by 2.54 cm thickness with weight per unit area of 535 N/m$^2$ were installed on the roof which can be considered as modeling typical 0.61 m square pavers at half-scale (Fig. 6(a)). The pavers were numbered from 1 to 100 (Fig. 7(a)). For the pressure measurements, pavers with exactly the same dimensions as the concrete pavers (0.305 m × 0.305 m × 2.54 cm thickness) were made from Plexiglas which made it more convenient to install pressure taps on both upper and lower surfaces.

In order to study the effects of the pavers' edge gap to spacer height ratio, adjustable height pedestals were used to change the space between the pavers and the roof deck ($H_s$, Fig. 6(c)). A constant gap of G=3.175 mm at model scale (6.35 mm at full scale) between adjacent pavers (Fig. 6(c)) was maintained. Bienkiewicz and Endo (2009) carried out a wind tunnel study for studying the effects of the gap (G) between pavers, and the space ($H_s$) beneath the pavers on the pressures underside the loose-laid roof pavers. Results from these experiments showed that G reduced the underside pressure significantly but $H_s$ did not show clear tendencies. Instead, they introduced a parameter of the gap to spacer height ratio ($G/H_s$) and showed that this parameter controls the underside pressures, in a way that the higher the ratio, the less the net pressure on the pavers. Here the authors have adopted the same approach of using the $G/H_s$ ratio as the governing parameter. For very small gap sizes, Reynolds number effects could eventually make this assumption questionable but for the size of gap tested here (which is typical for most current paver systems) Reynolds number effects were expected to be minor.

A total of 13 experiments were carried out, including three wind blow-off tests and 10 pressure measurement tests. A summary of the parameters for each test is given in Table 1.

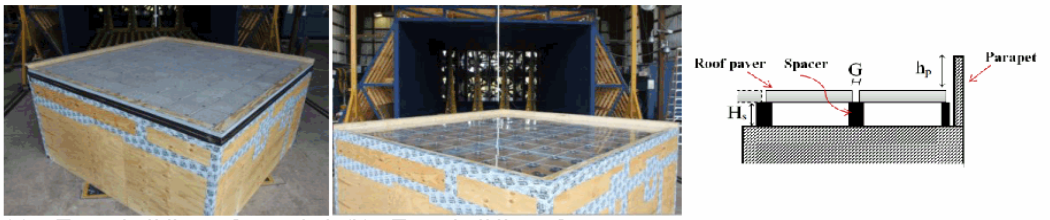


(a) Test building for wind blow-off tests (b) Test building for pressure measurements (c) Geometrical parameter definition

Fig. 6 Test setup configuration

Table 1 Test number and characteristics

| Test Number | $G/H_s$* | $(h_p/H)_{windward}$** |
|---|---|---|
| Wind Uplift 1 | 0.25 | 0.05 |
| Wind Uplift 2 | 0.083 | 0.05 |
| Wind Uplift 3 | 0.028 | 0.05 |
| Pressure 1-1 | 0.25 | 0.05 |
| Pressure 1-2 | 0.25 | 0.067 |
| Pressure 1-3 | 0.25 | 0.1 |
| Pressure 2-1 | 0.083 | 0.033 |
| Pressure 2-2 | 0.083 | 0.05 |
| Pressure 2-3 | 0.083 | 0.1 |
| Pressure 2-4 | 0.083 | 0.15 |
| Pressure 3-1 | 0.028 | 0 |
| Pressure 3-2 | 0.028 | 0.05 |
| Pressure 3-3 | 0.028 | 0.1 |

*Constant G=3.175 mm (at model scale) for all tests

** Parapet height was measured from top of the pavers. Leeward building sides did not have any parapet.

Table 2 Failure wind speed

| Test Number | Failure wind speed when wobbling of pavers started (m/s) | Failure wind speed when a couple of pavers lifted off from roof (m/s) |
|---|---|---|
| Wind Uplift 1 | 50 | 53.7 |
| Wind Uplift 2 | 45.7 | 50.1 |
| Wind Uplift 3 | 37.6 | 41.3 |

The test procedure consisted of first conducting wind lift-off tests to find out the location where paver lift-off first occurred so that the pressure tap layout for the pressure measurements could be concentrated on the most critical pavers. Only one wind direction was tested, a quartering direction of 45° relative to the roof edge. Based on past studies this wind direction was assessed to be the critical orientation for generating high paver uplift under conical vortices on flat rectangular roofs (Holmes 2015). Also, extensive experiments on roof pavers by Kind (1981) showed that, even though higher local roof suctions may occur for other directions, 45° is still the most critical direction for paver lift-off. Presumably this is due to the shape of the pressure distribution being less effective in lifting the pavers for other directions. The failure wind speeds measured at the

roof height of the test model (1.524 m height) are reported in Table 2. These values are converted to full-scale values using Froude number scaling, i.e. full scale velocity $=\sqrt{2}\times$model velocity. The values reported in Table 2 are equivalent to 3s gust speeds at full scale. A summary of the method to calculate the equivalent 3s gust speeds is given in Appendix A.

The failure mechanism for the wind lift-off tests is explained in detail in the previous paper by the authors (Asghari Mooneghi *et al.* 2014). For pressure measurements, the original concrete pavers were replaced by the Plexiglas pavers with installed pressure taps (total of 447 pressure taps were used). The pressure tap layout is given in Fig. 7(b) for the exterior surface. The pressure tap layout for the underneath surface was about the same as the one given on the exterior surface with some minimal difference in the locations of pavers on the pedestals (Asghari Mooneghi *et al.* 2014). Nine critical pavers were fitted with a total of 256 pressure taps allowing accurate measurements to be made of the pressure distribution on the top and bottom surfaces.

Pressure measurements were carried out at a wind speed of 18.5 m/s which was below the failure speed of concrete pavers. A 512 channel Scanivalve Corporation pressure scanning system was used for pressure measurements. Pressure data were acquired at a sampling frequency of 512 Hz for a period of three minutes. Data were low-pass filtered at 30 Hz (equivalent to 21 Hz at full scale). A transfer function was used to correct for tubing effects in the post-test analysis (Irwin *et al.* 1979).

## 5. Experimental results and discussion

### *5.1 Aerodynamic pressure results*

In this section the results from the pressure measurement experiments are discussed. The mean pressure coefficient at any location was obtained from

$$Cp_{mean} = \frac{(P-P_0)_{mean}}{\frac{1}{2}\rho U^2} \quad (1)$$

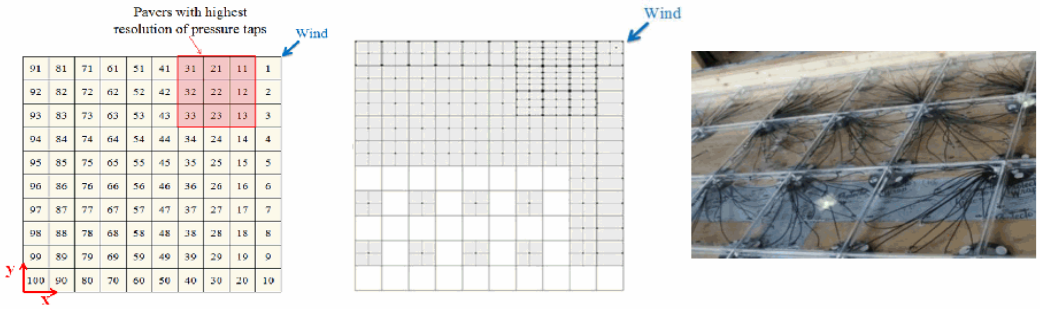


(a) Pavers numbering (b) External pressure tap layout (c) Critical pavers instrumented with pressure taps

Fig. 7 Details of the Experimental Setup

where $P_{mean}$ is the mean pressure, $P_0$ is the static reference pressure, ρ is the air density at the time of the test (1.225 kg/m$^3$) and $U$ is the mean wind speed measured at the building height of the test model (1.524 m). The peak pressure coefficient was obtained from:

$$Cp_{peak} = \frac{(P-P_0)_{peak}}{\frac{1}{2}\rho U_{3s}^2} \quad (2)$$

where $P_{peak}$ is the peak pressure, and $U_{3s}$ is the peak 3-s gust speed at the reference height. The tests were performed in partial turbulence simulation, hence the turbulence intensity at roof height was lower than that of atmospheric boundary layer (ABL) which contains full spectrum of turbulence. In order to calculate the peak pressure, $P_{peak}$, a method called "Partial Turbulence Simulation" (PTS) was used. In this method, the turbulence is divided into two distinct statistical processes, one at high frequencies which can be simulated correctly in WOW, and one at low frequencies which can be treated in a quasi-steady manner. The joint probability of load from the two processes is derived, with one part coming from the WOW data and the remainder from the Gaussian behavior of the missing low frequency component. The PTS method is discussed in details in Asghari Mooneghi (2014). It should be noted that in this method, the $Cp_{peak}$ is first calculated based on mean hourly dynamic pressure, that would have been obtained had the full spectrum been present which can then be converted to $Cp_{peak}$ based on gust pressure corresponding to any selected gust duration, e.g., 3 seconds. For the current test configuration, $U_{3600sec}/U_{3sec}$ = 1.8 was used. This factor was calculated for suburban terrain at z=3.048 m. The procedure for converting the wind speed averaging time was based on Harris and Deaves (1981) model taken from ESDU (1985). For the evaluation of these estimated values, the peak value with 85% probability of not being exceeded in one hour of full spectrum wind was selected (Asghari Mooneghi 2014). The choice of the 85% probability of non-exceedance for obtaining the peak pressure coefficients is not materially very different from the 80% recommendation of the ISO 4354 standard (International Standard 2009).

The net total pressure coefficient, defined as the instantaneous difference between the external and the corresponding underneath pressure coefficient at the same location, is

$$Cp_{net}(t) = Cp_{ext}(t) - Cp_{int}(t) \quad (3)$$

Mean and peak external pressure coefficients, mean underneath pressure coefficient and net mean pressure coefficients contours for the case of $G/H_s$=0.028 and $h_p/H$=0 (i.e., no parapet case) are given in Fig. 8.

The results of the tests show that pavers close to the edges and corners of the roof are subjected to the highest local negative pressures. These areas are under the conical vortices. As compared to external pressures the underneath pressures are lower in magnitude and show more uniformity. Pressure equalization reduces the net uplift force on the pavers. It should be noted that the peak values correspond to the estimated peak values for each tap during the test and do not happen simultaneously on all taps. In all tests, paver 21 was shown to be the most critical paver. So, in the rest of the paper, results are calculated for this paver.

The overall wind lift load, $L(t)$, acting on any single paver and the lift coefficient $C_L(t)$ are obtained as

$$L(t) = \frac{1}{2}\rho U^2 \iint_{A_{paver}} Cp_{net}(t)dA \quad (4)$$

$$C_L(t) = \frac{L(t)}{\frac{1}{2}\rho U^2 A} \tag{5}$$

where $A$ is the surface area of the paver. It should be noted that the highest suction on the paver does not necessarily occur at the center of the paver. This means that even for cases where the total uplift force is less than the weight of the paver, the weight of the paver might not overcome the corresponding overturning moment from the wind suction forces. The overturning moment about a selected axis and the moment coefficient $C_M(t)$ can be obtained from

$$M(t) = \frac{1}{2}\rho U^2 \iint_{A_{paver}} Cp_{net}(t) \times d \times dA \tag{6}$$

$$C_M(t) = \frac{M(t)}{\frac{1}{2}\rho U^2 Aa} \tag{7}$$

where $d$ is the moment arm defined as the distance from a selected axis to each point on the paver (Fig. 9).

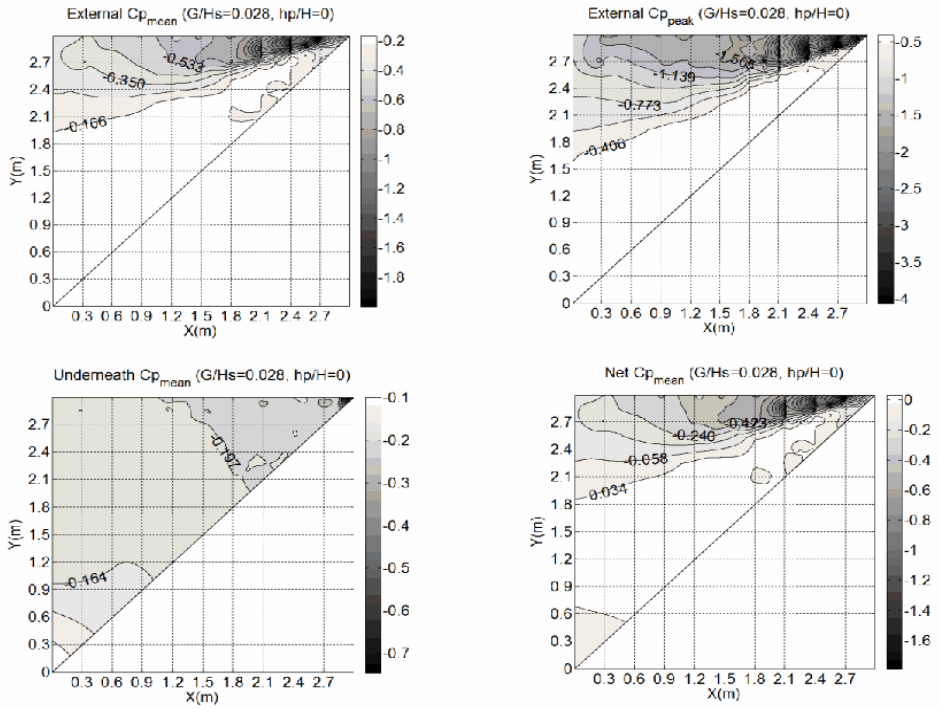


Fig. 8 Pressure coefficient contours ($G/H_s$=0.028 and $h_p/H$=0)

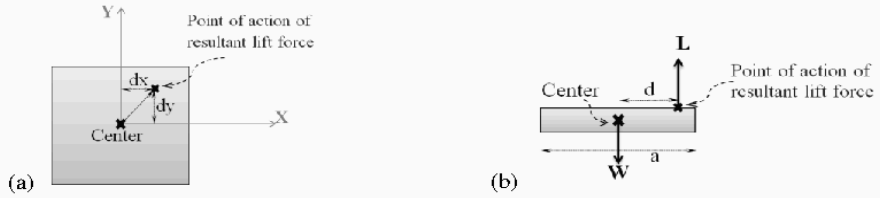


Fig. 9 Definition of the point of action of the resultant lift force: (a) plan view and (b) side view

Table 3 shows the variations of the most negative mean and peak local $C_{p,ext}$ values, $C_{Lext}$, $C_{Lnet}$, $C_{Mx,net}$ and $C_{My,net}$ on paver 21. Fig. 10 shows highest local suction coefficients for various $G/H_s$ and $h_p/H$ ratios. The $G/H_s$ ratio affects the underside pressures such that the higher the ratio, the less the net pressure on the pavers.

The highest external single tap pressure coefficients and the external area averaged pressure coefficient ($C_{Lext}$) observed on the most critical paver (paver 21) obtained for different cases (Table 3) were compared to component and cladding external pressure coefficients for roofs as given in ASCE 7-10. For gable roofs with slope $\theta \leq 7°$ the largest external pressure coefficient for corner Zone 3 for tributary areas less than 0.9 $m^2$ is given as -2.8 in Fig. 30.4-2A (ASCE 7-10).

Table 3 $C_{p,ext}$, $C_{Lext}$, $C_{Lnet}$, $C_{Mx,net}$ and $C_{My,net}$ on paver 21

| Test case | | Highest $C_{p,ext}$ read on a tap (paver 21) | | $C_{Lext}$ | | $C_{Lnet}$ | | $C_{Mx,net}$ | | $C_{My,net}$ | |
|---|---|---|---|---|---|---|---|---|---|---|---|
| **$G/H_s$** | **$h_p/H$** | **Mean** | **Peak** | **Mean** | **Peak** | **Mean** | **Peak** | **Mean** | **Peak** | **Mean** | **Peak** |
| **0.25** | 0.05 | -1.70 | -3.14 | -0.89 | -1.38 | -0.44 | -0.80 | -0.02 | -0.10 | -0.02 | -0.08 |
| **0.25** | 0.067 | -1.44 | -2.92 | -0.90 | -1.41 | -0.44 | -0.80 | 0.00 | -0.10 | -0.03 | -0.08 |
| **0.25** | 0.1 | -1.45 | -2.43 | -0.96 | -1.39 | -0.39 | -0.77 | 0.01 | -0.06 | -0.02 | -0.08 |
| **0.083** | 0.033 | -1.68 | -2.88 | -0.86 | -1.30 | -0.57 | -0.96 | -0.02 | -0.10 | -0.03 | -0.08 |
| **0.083** | 0.05 | -1.71 | -2.71 | -0.89 | -1.35 | -0.60 | -1.01 | -0.01 | -0.09 | -0.03 | -0.09 |
| **0.083** | 0.1 | -1.60 | -2.44 | -0.98 | -1.43 | -0.59 | -0.99 | 0.02 | -0.07 | -0.03 | -0.09 |
| **0.083** | 0.15 | -1.31 | -2.05 | -0.91 | -1.26 | -0.47 | -0.81 | 0.01 | -0.02 | -0.02 | -0.07 |
| **0.028** | 0 | -1.20 | -4.10 | -0.70 | -1.19 | -0.52 | -0.98 | -0.06 | -0.15 | -0.01 | -0.10 |
| **0.028** | 0.05 | -1.86 | -2.85 | -0.97 | -1.44 | -0.75 | -1.20 | -0.01 | -0.09 | -0.03 | -0.10 |
| **0.028** | 0.1 | -1.53 | -2.50 | -0.99 | -1.40 | -0.74 | -1.14 | 0.02 | -0.06 | -0.04 | -0.09 |

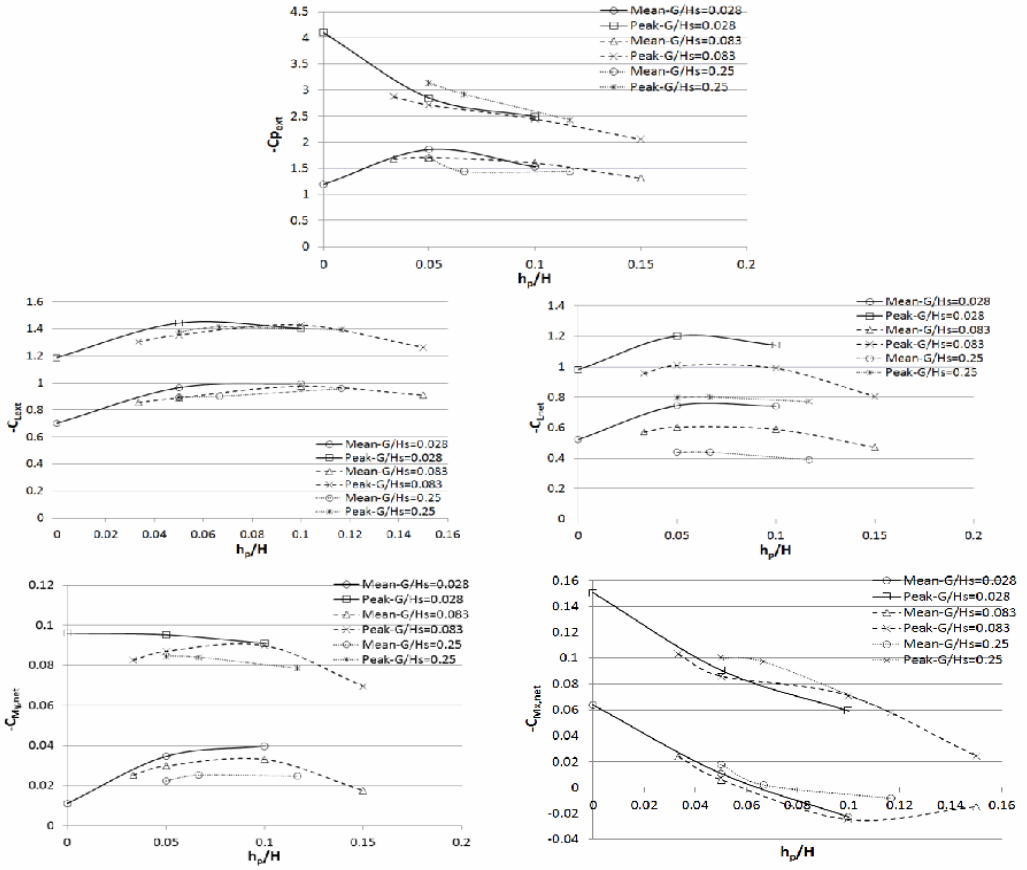


Fig. 10 Highest local suction coefficients on the roof $C_{Lext}$, $C_{Lnet}$, $C_{Mx,net}$ and $C_{My,net}$ on paver 21

The highest single tap peak suction coefficients observed in the present tests for all cases ranged from -4.1 for $h_p/H$=0 and $G/H_s$=0.028 to -2.05 for $h_p/H$=0.15 and $G/H_s$=0.083 in the critical paver zone. The highest peak external lift coefficients ranged from -1.44 for $h_p/H$=0.05 and $G/H_s$=0.028 to -1.19 for $h_p/H$=0 and $G/H_s$=0.028. The underneath pressure coefficients required for calculating the net pressure coefficients are not dealt with in ASCE 7-10.

The reduction in the net wind uplift can be expressed as

$$r = \frac{C_{Lnet}}{C_{Lext}} \tag{8}$$

The reduction factor defined as the ratio of the net lift coefficient to the external lift coefficient is plotted as a function of relative parapet height ($h_p/H$) for different $G/H_s$ for paver 21 (Fig. 11).

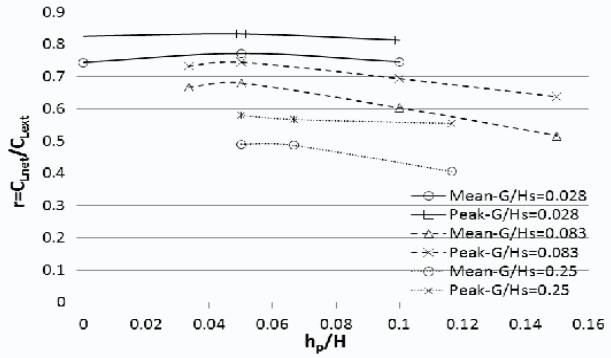


Fig. 11 Reduction factor $r = C_{L_{net}}/C_{L_{ext}}$

The results show that increasing the $G/H_s$ ratio decreases the reduction factor. This means that the correlation between upper and lower surface pressures decreases with decreasing the $G/H_s$ ratio. Thus, increasing the ratio of the pavers' edge-gap to spacer height can reduce the net wind-induced uplift loading on the pavers and improve the performance of the pavers. The reduction factor is not very sensitive to parapet height for $h_p/H$ less than about 0.1. For $h_p/H$ ratios beyond 0.1 the reduction factor reduces gradually, i.e., improved performance of the pavers can be expected.

### *5.2 Effect of connecting pavers*

There are various types of interlocking and strapping systems available to improve the wind performance of roof paving systems. The effect of a specific system has not been dealt with during the experiments in this study. However, guidance on the effectiveness of these systems can be obtained by evaluating the net uplift on groups of pavers rather than only one. The $C_{L_{net}}$ value is calculated for 6 different cases shown in Fig. 12 and compared to the highest $C_{L_{net}}$ value observed during the experiments on Paver 21 (Fig. 13). In Fig. 12, the highlighted pavers were assumed to act as a single unit for the case of $G/H_s$=0.083 and $h_p/H$=0.05. The most critical paver is shown with an X mark.

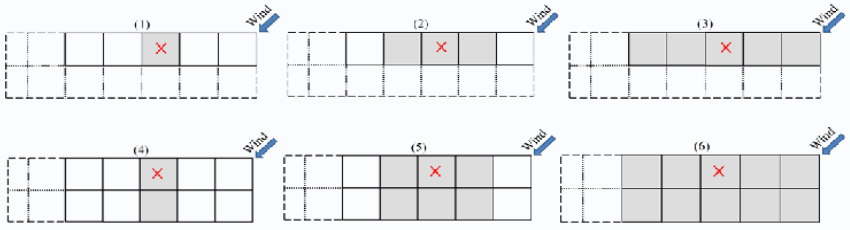


Fig. 12 Interlocked pavers in different configurations

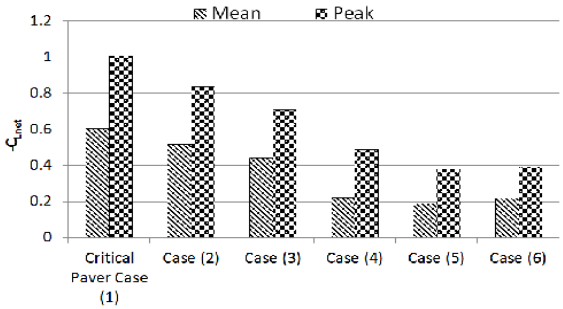


Fig. 13 Comparison between $C_{L_{net}}$ values for different configurations defined in Fig. 12

The results illustrate the effect of connecting pavers together in reducing the net uplift force on the linked pavers as a unit. Based on the characteristics of the strapping or interlocking system in hand, different degrees of improvement can be expected. It should be noted that the surface pressure variation along the axis of the vortex varies much more slowly than in the transverse direction. So, strapping in the direction roughly parallel to the axis of the vortex is not expected to be as effective in restraining pavers from lift off as strapping in the transverse direction. If there is a high uplift on one paver the adjacent pavers in the direction along the vortex axis are likely to also experience significant uplift. Real strapping systems rarely align directly with the vortex axis or transverse to it. Therefore strapping in both orthogonal directions of a paving system is preferable.

### *5.3 Comparison of the results from pressure measurement experiments with wind lift-off tests*

In this section the critical wind velocities for pavers' lift-off are calculated from the pressure measurement results and are compared to the results obtained from the wind lift-off tests. This is done to verify that the wind lift-off speeds that were calculated from the pressure measurements were in accord with the blow off tests. Lift-off takes place when the moment caused by the uplift force equals (or just exceeds) the resisting moment from the paver weight, $W$. Therefore, the critical wind velocity $U_{CRIT}$ at which lift-off occurs is calculated from Eq. (10) in which the moment is taken about the edge of the paver.

$$\frac{1}{2}\rho {U_{CRIT}}^2 C_L A\left(d+\frac{a}{2}\right) = W \times \frac{a}{2} \tag{9}$$

$$U_{CRIT} = \sqrt{\frac{a}{2\left(d+\frac{a}{2}\right)} \times \frac{W}{\frac{1}{2}\rho C_L A}} \tag{10}$$

where $C_L$ is the lift coefficient obtained from the pressure measurement results and $a$ and $d$ are defined in Fig. 9. Fig.14 shows the critical wind lift-off speeds obtained from wind lift-off tests (Table 2) as compared to the critical wind lift-off speeds calculated from Eq. (10) using the pressure measurement results. The wind speeds presented in Fig. 14 are the equivalent 3-sec gust

speed.

For the limiting case of $G/H_s$ ~ zero (meaning a very large spacer height for a specific edge-gap between the pavers) one can assume that the underneath pressure needed would be similar to the internal pressure inside a building with a porous roof. The underneath pressure coefficient for this case is calculated as the average of external pressure coefficients recorded at the center of all pavers using

$$C_{p_{int}}(t) = \frac{1}{N}\left(\sum_{i=1}^{n=N} C_p(t)_{ext\,|_{center\ of\ paver\ i}}\right) \tag{11}$$

where N is the total number of pavers. The net lift coefficient was then calculated using

$$C_{L_{net}}(t) = C_{L_{ext,on\ paver\ 21}}(t) - C_{L_{int}}(t) \tag{12}$$

It is not known in advance what averaging time for wind load the pavers react to except by hypothesizing various values and seeing what lines up best with the lift-off test results. Therefore the lift-off speeds from pressure measurements presented in Fig. 14 were calculated once based on the mean $C_{Lnet}$ and once based on peak $C_{Lnet}$. The results showed that wobbling of the pavers started at slightly lower speed than would be predicted purely on the basis of the mean $C_{Lnet}$ value combined with 3 second gust speed. This implies that some of the high frequency gust action occurring at shorter duration than 3 seconds was also necessary to initiate wobbling. However, assuming that the full gust speed is required to start wobbling of the pavers would be on the conservative side. The results show that beyond a certain value of Hs (i.e., for small $G/H_s$ values) the pressures on the underneath can communicate very rapidly with other parts of the roof and further increases in $H_s$ do not make much difference. Once this point is reached there are no further decreases in lift-off velocity. The point where this situation is reached is around $G/H_s$ ~ 0.03 ($H_s/G$ ~ 30).

### *5.4 Comparison of the critical wind lift-off speeds from experiments with those obtained from studies based on ASCE 7-10 pressure coefficients*

The design wind pressures on buildings in the United States are determined using the ASCE 7-10 standard. It provides wind loads for the design of the Main Wind Force Resisting System (MWFRS), as well as Components and Cladding. These provisions cover buildings with common shapes, such as those with Flat, Gable, Hip, and Mono-slope roofs, under simple surrounding conditions. For the design of roof components and cladding, the roof is divided into rectangular shaped zones within which a constant pressure coefficient is specified. For permeable roof claddings such as loose-laid roof pavers, the ASCE standard currently does not provide specific guidance for estimating net wind uplift loads. Two methods were examined in this paper for estimating the critical wind lift-off speeds from the exterior pressure coefficients given in ASCE 7-10 as follows

Case I: A practice proposed for roof tiles (Florida Public Hurricane Loss Projection Model (FPHLPM), 2005, Volume II, p. 55) is to assume a zero underneath pressure coefficient and consider the exterior pressure coefficient as the net pressure coefficient. The critical lift of speed can then be calculated using

$$U_{CRIT} = \sqrt{\frac{W}{\frac{1}{2}\rho C_{p_{ext}} A}} \tag{13}$$

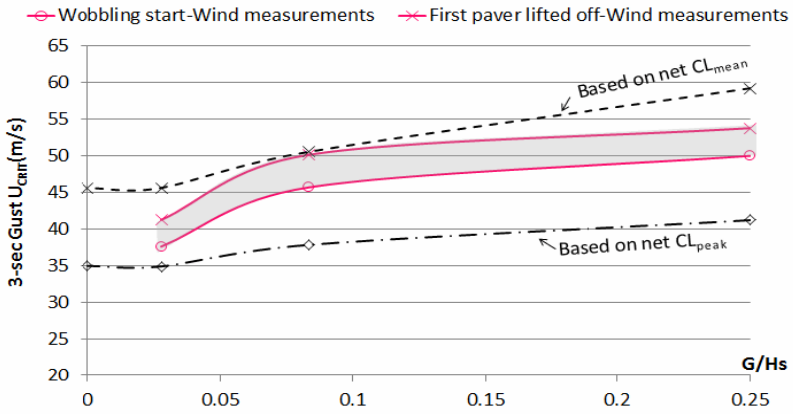


Fig. 14 Comparison between wind lift-off speeds from wind blow-off tests and those obtained from pressure measurements

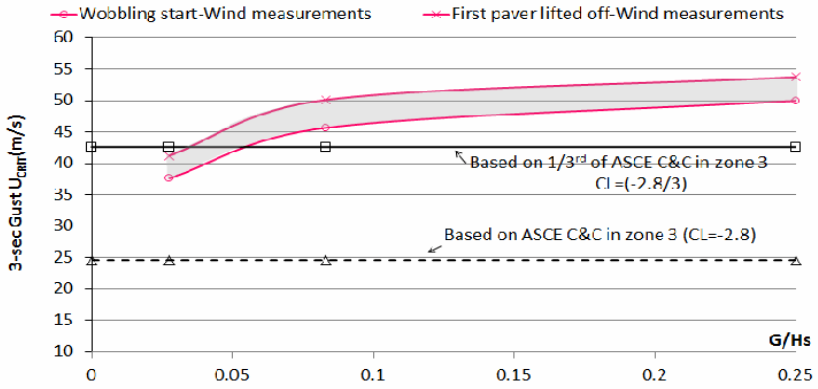


Fig. 15 Comparison between wind lift-off speeds from wind blow-off tests and those obtained from a typical practice based on ASCE 7-10 exterior pressures on C&C and 1/3rd Rule

Fig. 15 shows a comparison of this approach with the lift off speeds from the current experiments. For the estimates based on ASCE 7-10 exterior pressures, the wind blow-off speeds were calculated using GCp=-2.8 (external pressure coefficient in Zone 3 for $A_{eff}$=0.09 $m^2 \leq 0.93$ $m^2$). In Fig. 15 the critical wind blow-off speed calculated based on this approach is clearly very conservative. This emphasizes the need for better guidelines.

Case II: In Building Research Establishment (1985) it is stated that the magnitude of the net uplift coefficient was found empirically to be generally less than 1/3rd of the magnitude of the peak negative external pressure coefficient on the upper surface of the paver. In other words as a rule of

thumb, $C_L \leq -\frac{1}{3} Cp_{peak}$. This is broadly in line with earlier findings of Kind and Wardlaw (1982). Therefore, 1/3rd of the ASCE 7-10 exterior pressure coefficients for components and claddings was used to estimate the critical wind lift-off speed (Eq. (13)) and results are also shown in Fig. 15. This approach, called here the 1/3rd Rule, can be seen from Fig. 15 to over predict the wind lift-off speeds for lower G/$H_s$ ratios and under predict them at higher G/$H_s$ ratios. The design guidelines presented in Section 6 of this paper do take into account the effects of different G/$H_s$ ratios, thereby improving on the simple 1/3rd rule.

## 6. Design guidelines for roof pavers

Based on the results presented in the previous sections, the following equation is proposed for the design of loose-laid roof pavers

$$C_{L_{net}} = R_1 \times R_2 \times C_{p_{ASCE\,7-10,exterior,C\&C,Zone\,3}} \tag{14}$$

where $R_1$ is a reduction factor for different gap ratios and $R_2$ is a reduction factor for different parapet heights. These are to be applied to the ASCE 7-10 exterior pressure coefficients for components and claddings in Zone 3. Here, Zone 3 in ASCE 7-10 is chosen as the worst case scenario for design of roof pavers. However, $R_1$ in Eq. (14) can be modified to take into account the effects of location on the roof. Failure is defined here as the start of wobbling. $R_1$ and $R_2$ are to be calculated from the diagrams proposed in the following. The equivalent uplift force can then be calculated by multiplying Eq. (14) by the dynamic pressure at roof height.

### *6.1 $R_1$ reduction factor: Effect of G/$H_s$ ratio*

The $R_1$ reduction factor is defined as $C_{L_{net}}/C_{p_{ext}}$ in which $C_{p_{ext}}$ is the ASCE 7-10 exterior pressure coefficient for components and cladding in Zone 3 and $C_{L_{net}}$ values were calculated using the following formula in which failure is assumed to occur with the start of wobbling.

$$U = \sqrt{\frac{W}{\frac{1}{2}\rho C_L A}} \rightarrow C_{L_{estimated}} = \frac{(W/A)}{\frac{1}{2}\rho U^2_{CRIT(wobbling\ start\ from\ wind\ tests)}} \tag{15}$$

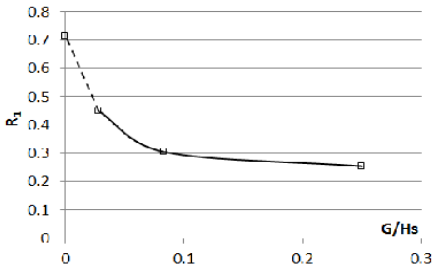


Fig. 16 $R_1$ reduction factor for different G/$H_s$ ratios

The proposed reduction factor $R_1$ based on G/$H_s$ ratio is plotted in Fig. 16. The value at G/$H_s$ ~ 0 comes from assuming $C_{L_{net}} = -2$ in which $C_{L_{ext}}$ is assumed to be -2.8 and $C_{L_{int}} = -0.8$ which is approximately calculated from averaging the external peak pressure coefficients on pavers 11, 12, 21, 22, 31, and 32. The $R_1$ factor changes an exterior local peak pressure coefficient into a net lift coefficient taking into account the pressure distribution over the paver and the effect of G/$H_s$ on pressure equalization.

### *6.2 $R_2$ reduction factor: Effect of parapet height*

$R_2$ reduction factor is proposed based on results presented in Fig. 11. For relative parapet height ratios less than 0.1 no reduction in the $C_L$ value is proposed (i.e., $R_2 = 1$). In ASCE 7-10 Figure 30.4-2A it is stated that the external pressure coefficients for Zone 3 can be reduced to the values in Zone 2 for parapets higher that 0.9144 m. (3 ft.). This means about 36% reduction for $h_p/H$ ratio of 0.3 and higher for the current experimental setup. This value is considered as the upper limit of the proposed reduction proposed in Fig. 17 (i.e., $h_p/H$=0.3). Kind *et al.* (1987) proposed $h_p/H$ =0.1, $h_p/H$ =0.02 and $h_p/H$ =0.03 for low, mid and high-rise buildings respectively, above which a somewhat rapid reduction in the worst suction values due to the parapet was observed. This would imply that application of the reduction factor in Fig. 17 to mid and high-rise buildings would be conservative.

In Fig. 18 the proposed curve in Fig. 17 for $R_2$ reduction factor is compared to the experimental results presented previously in Fig. 11. The solid and dashed lines are plotted by applying respectively the $R_2$ factor to the maximum of peak and mean reduction factor $r = C_{L_{net}}/C_{L_{ext}}$ obtained from experiments (given in Fig. 11). This was done to make comparisons possible between the curves since due to pressure equalization effects, the experimental reduction factor $r = C_{L_{net}}/C_{L_{ext}}$ curves do not start at one as is the case for proposed $R_2$ reduction factor. The results show a good degree of agreement. In some cases (e.g. left graph in Fig. 18) the reduction due to parapet height from experiments ($r = C_{L_{net}}/C_{L_{ext}}$) might start at $h_p/H$ ratios lower that the assumed $h_p/H$=0.1.

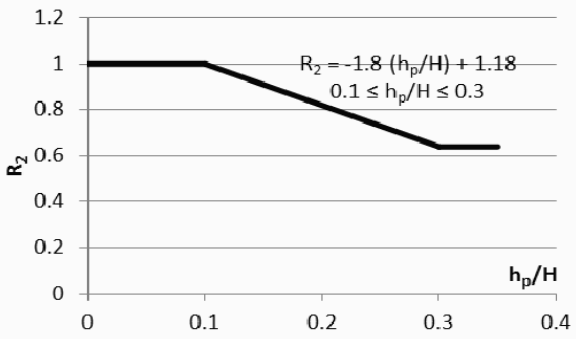


Fig. 17 $R_2$ reduction factor for different $h_p/H$ ratios

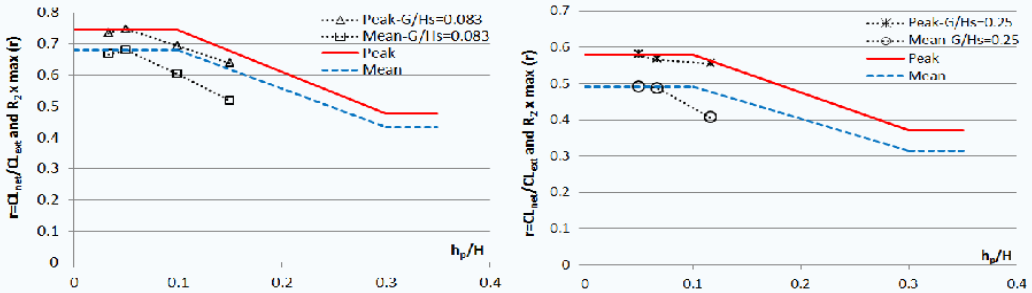


(a) $G/H_s$=0.083 (b) $G/H_s$=0.25

Fig. 18 Comparison of proposed $R_2$ curve with r as a function of $h_p/H$

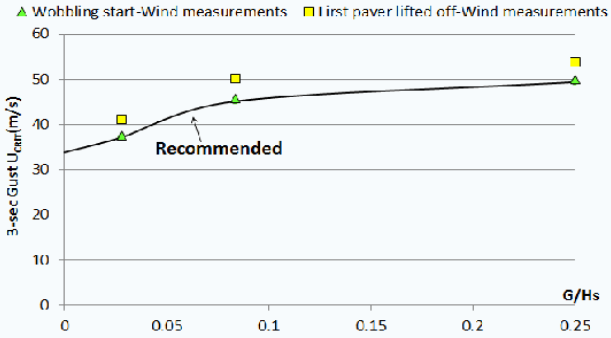


Fig. 19 Critical wind speed vs. $G/H_s$ ($h_p/H$=0.05 for wind measurements)

However, $h_p/H$=0.1 and the corresponding curve proposed in Fig. 18 are based on results obtained from multiple experiments in order to have a universal curve. The $h_p/H$=0.1 value is also obtained from the experiments of Kind et al. (1987). It should be noted that the rate of decrease of reduction factor $r = C_{L_{net}}/C_{L_{ext}}$ versus $h_p/H$ (slope of the diagram between $h_p/H$=0.1 to $h_p/H$=0.3) obtained from experiments is in good agreement with that of proposed $R_2$ curve (Fig. 18).

Fig. 19 shows the critical lift-off speeds from the measurements compared to values from the proposed guideline.

### *6.3 Applications and special notes*

1. The proposed guidelines were derived assuming a full scale paver size of 0.61 m by 0.61 m by 5.05 cm thickness. This particular size was selected as it represents a very common paver size on typical flat roof low-rise buildings used in the United States. The guidelines will work best for pavers that have sizes close to the size tested. Future experiments are

needed to investigate the applicability of the proposed guidelines for pavers with sizes and aspect ratios very different from the ones tested for the current work.

2. The effect of building height has not been examined in this paper. The building in the current experiments was a representative of a low-rise building. Based on the wind lift-off experiments performed by Kind *et al.* (1987) on the failure wind speeds for roof pavers on low-rise, mid-rise and high-rise buildings, the results presented in this paper are expected to be conservative when applied to mid and high-rise buildings provided the increase in roof height wind speed with building height is accounted for. However, further experiments are needed to fully quantify the effects of building height for mid and high-rise buildings.
3. The effect of paver size and geometry has not been evaluated in this paper. It is to be noted that the element size have an effect on the failure of non-interlocking roof pavers (Kind *et al.* 1987). Previous studies by Bienkiewicz and Sun (1997) indicated that square pavers are more wind-resistant than rectangular pavers.
4. The general effect of interlocking and strapping systems was investigated in this paper through the effect of load sharing mechanism between pavers. These systems are usually effective and improve the wind performance of roof pavers. The application of the proposed guidelines is primarily for loose-laid roof pavers without any interlocking or strapping system. However, some guidance of the effective reduction in lift-off forces can be drawn from the results in Figs. 12 and 13. For more precise results it is recommended to perform wind tunnel testing at large scale or full scale to find out the characteristics and wind performance of a specific interlocking or strapping system.
5. The experiments were performed in a simulated suburban terrain. The effect of wind turbulence was not examined in this paper but provided the 3 second gust speed is used to estimate lift-off the effects of different turbulence levels should be reasonably well accounted for.
6. The effect of thickness of the pavers on resistance to flow through the gaps between pavers was not examined in this paper. Increased thickness for the same gap might be expected to increase resistance to flow, thereby having a similar effect to reducing the gap. This is an area for further research.
7. It should be noted that the developed design guidelines are intended for use with the external pressure coefficients given in ASCE7-10 for components and claddings in zone 3. Caution should be exercised in using the proposed reduction factors in conjunction with external pressure coefficients given in other codes and standards.

## 7. Conclusions

The objective of this paper was to develop simple guidance in code format for design of commonly used loose-laid roof pavers. A set of 1:2 scale experiments was performed to investigate the wind loading on concrete roof pavers on the flat roof of a low-rise building. The experiments were performed in the Wall of Wind (WOW) hurricane testing facility at Florida International University (FIU). Experiments included both wind blow-off tests and detailed pressure measurements on the top and bottom surfaces of the pavers. Several conclusions were drawn:

- The paver's edge-gap to spacer height ratio affects the underside pressures such that the higher the ratio, the less the net uplift pressure on the paver. This may be regarded as increasing the failure wind speed.
- The relative parapet height, defined as the ratio of the parapet height to the building height, affects the failure wind speed. For very low-height parapets (~$h_p$/H<0.1), a small reduction in the failure wind speed was observed as compared to zero-height parapet. However, for taller parapets, increasing the parapet height results in an increased failure wind speed.
- The general effect of interlocking and strapping systems was studied through the effect of the load sharing mechanism between pavers. Interlocking and strapping systems improve the wind performance of the roof pavers since the uplift loads tend to be shared across several pavers.

Based on the experimental results and review of literature, guidelines are proposed for designing loose-laid roof pavers against wind uplift. The guidelines have been formatted so that use can be made of the existing information in codes and standards such as ASCE 7-10 on exterior pressures on components and cladding. The effects of pressure equalization, the paver's edge-gap to spacer height ratio and parapet height as a fraction of building height on the wind performance of roof pavers were investigated and are included in the guidelines as adjustment factors. The applications and limitations of the guidelines are discussed.

## Acknowledgments

We would like to greatly thank the Tile Tech Company for providing us with concrete roof pavers and the pedestal system required for the wind destructive tests. This research was supported by the National Science Foundation (NSF) (NSF Award No. CMMI-1151003) and the Florida Division of Emergency Management (DEM). The instrumentation was supported by NSF MRI Award (No. 0923365). The help received from our research assistant, Ramtin Kargarmoakhar is gratefully acknowledged. The help offered by the Wall of Wind manager, Walter Conklin and the Research scientists, Roy Liu Marquis and James Erwin is also greatly appreciated.

## References

Aly, A., Gan Chowdhury, A. and Bitsuamlak, G. (2011), "Wind profile management and blockage assessment for a new 12-fan Wall of Wind facility at FIU", *Wind Struct.*, **14**(4), 285-300.

Aly, A.M., Bitsuamlak, G.T. and Chowdhury, A.G. (2012), "Full-scale aerodynamic testing of a loose concrete roof paver system", *Eng. Struct.*, **44**, 260-270.

Amano, T., Fujii, K. and Tazaki, S. (1988), "Wind loads on permeable roof-blocks in roof insulation systems", *J. Wind Eng. Ind. Aerod.*, **29**, 39-48.

AS 1170.2 (2011), *Australian/New Zealand standard: structural design actions*, Standards Australia/Standards New Zealand, Sydney, Australia.

ASCE 7-10 (2010), *Minimum Design Loads for Buildings and Other Structures*, American Society of Civil Engineers, ASCE, Virginia.

Asghari Mooneghi, M. (2014), *Experimental and Analytical Methodologies for Predicting Peak Loads on Building Envelopes and Roofing Systems*, FIU Electronic Theses and Dissertations, Paper 1846. http://digitalcommons.fiu.edu/etd/1846.

Asghari Mooneghi, M., Irwin, P. and Gan Chowdhury, A. (2014), "Large-scale testing on wind uplift of roof pavers", *J. Wind Eng. Ind. Aerod.*, **128**, 22-36.
Asghari Mooneghi, M., Irwin, P. and Gan Chowdhury, A. (2015), "Partial Turbulence Simulation Method for Small Structures", *Proceedings of the14th International Conference on Wind Engineering*, Porto Alegre, Brazil, June.
Banks, D. (2011), "Measuring peak wind loads on solar power assemblies", *Proceedings of the 13th International Conference on Wind Engineering*, Amsterdam, Netherlands, July.
Banks, D., Meroney, R.N., Sarkar, P.P., Zhao, Z. and Wu, F. (2000), "Flow visualization of conical vortices on flat roofs with simultaneous surface pressure measurement", *J. Wind Eng. Ind. Aerod.*, **84**(1), 65-85.
Bienkiewicz, B. and Endo, M. (2009), "Wind considerations for loose-laid and photovoltaic roofing systems", *Proceedings of the Structures Congress*, Austin, Texas, April-May.
Bienkiewicz, B. and Meroney, R.N. (1988), "Wind effects on roof ballast pavers", *Eng. Struct.*, **114**(6), 1250-1267.
Bienkiewicz, B. and Sun, Y. (1992), "Wind-tunnel study of wind loading on loose-laid roofing system", *J. Wind Eng. Ind. Aerod.*, **43**(1-3), 1817-1828.
Bienkiewicz, B. and Sun, Y. (1997), "Wind loading and resistance of loose-laid roof paver systems", *J. Wind Eng. Ind. Aerod.*, **72**, 401-410.
Bitsuamlak, G., Dagnew, A. and Gan Chowdhury, A. (2010), "Computational assessment of blockage and wind simulator proximity effects for a new full-scale testing facilit", *Wind Struct.*, **13**, 21-36.
Bitsuamlak, G.T., Gan Chowdhury, A. and Sambare, D. (2009), "Application of a full-scale testing facility for assessing wind-driven-rain intrusion", *Build. Environ.*, **44**(12), 2430-2441.
Bofah, K.K., Gerhardt, H.J. and Kramer, C. (1996), "Calculations of pressure equilibration underneath loose-laid, flow permeable roof insulation boards", *J. Wind Eng. Ind. Aerod.*, **59**(1), 23-37.
Building Research Establishment (1985), *Digest 295: Stability under wind load of loose-laid external roof insulation boards*, Building Research Station, Garston, Watford, UK.
Cheung, J.C.K. and Melbourne, W.H. (1986), "Wind loads on porous cladding", *Proceedings of the 9th Australasian Fluid Mechanics conference*, Auckland, New Zealand, December.
Cheung, J.C.K. and Melbourne, W.H. (1988), "Wind loading on a porous roof", *J. Wind Eng. Ind. Aerod.*, **29**(1-3), 19-28.
Chowdhury, A.G., Bitsuamlak, G., Fu, T.C. and Kawade, P. (2012), "A study on roof vents subjected to simulated hurricane effects", *Nat. Hazards*, **12**, 158-165.
DEUTSCHE NORM (2001-03), *DIN 1055-4: Einwirkungen auf Tragwerke, Teil 4: Windlasten*.
ESDU (1985), *Characteristics of Atmospheric Turbulence Near the Ground, Part II: Single Point Data for Strong Winds (Neutral Atmosphere)*, London UK.
Fernandez, G., Masters, F.J. and Gurley, K.R. (2010), "Performance of hurricane shutters under impact by roof tiles", *Eng. Struct.*, **32**(10), 3384-3393.
Florida Public Hurricane Loss Projection Model (FPHLPM) (2005), *Predicting the Vulnerability of Typical Residential Buildings to Hurricane Damage: Vol. II*, International Hurricane Research Center, Florida International University.
Gerhardt, H.J. and Janser, F. (1995), "Windbelastung belufteter Fassadensysteme", *Bauingenieur*, **70**, 193-201.
Gerhardt, H.J., Kramer, C. and Bofah, K.K. (1990), "Wind loading on loosely laid pavers and insulation boards for flat roofs", *J. Wind Eng. Ind. Aerod.*, **36**, 309-318.
Geurts, C.P.W. (2000), "Wind loads on permeable roof covering products", *Fourth Colloquium on Bluff Body Aerodynamics and Applications*, Ruhr Universität Bochum, September.
Habte, F., Asghari Mooneghi, M., Gan Chowdhury, A. and Irwin, P. (2015), "Full-scale testing to evaluate the performance of standing seam metal roofs under simulated wind loading", *Eng. Struct.*, **105**, 231-248.
Harris, R.I. and Deaves, D.M. (1981), *The Structure of Strong Winds*, London, UK.
Ho, T.C.E., Surry, D., Morrish, D. and Kopp, G.A. (2005), "The UWO contribution to the NIST aerodynamic database for wind loads on low buildings: Part 1. Archiving format and basic aerodynamic data", *J. Wind Eng. Ind. Aerod.*, **93**(1), 1-30.

Holmes, J.D. (2015), *Wind Loading of Structures*, 3rd Ed., CRC Press, Boca Raton, Florida.
Huang, P., Mirmiran, A., Chowdhury, A.G., Abishdid, C. and Wang, T.L. (2009), "Performance of Roof Tiles under Simulated Hurricane Impact", *J. Architect. Eng.*, **15**(1), 26-34.
International Standard (2009), *ISO 4354*, Wind actions on structures.
Irwin, P. (2009), "Wind engineering research needs, building codes and project specific studies", *Proceedings of the 11th Americas Conference on Wind Engineering*, San Juan, Puerto Rico, June.
Irwin, P., Cooper, K. and Girard, R. (1979), "Correction of distortion effects caused by tubing systems in measurements of fluctuating pressures", *J. Wind Eng. Ind. Aerod.*, **5**(1-2), 93-107.
Irwin, P., Dragoiescu, C., Cicci, M. and Thompson, G. (2012), "Wind tunnel model studies of aerodynamic lifting of roof pavers", *Proceedings of the Advances in Hurricane Engineering Conference*, Miami, Florida, October.
Kargarmoakhar, R., Gan Chowdhury, A. and Irwin, P. (2015), "Reynolds number effects on twin box girder long span bridge aerodynamics", *Wind Struct.*, **20**(2), 327-347.
Kind, R.J. (1994), "Predicting pressure distribution underneath loose laid roof cladding systems", *J. Wind Eng. Ind. Aerod.*, **51**(3), 371-379.
Kind, R.J., Savage, M.G. and Wardlaw, R.L. (1987), *Further wind tunnel tests of loose-laid roofing systems*, National Research Council of Canada, Report LTR-LA-294.
Kind, R.J., Savage, M.G. and Wardlaw, R.L. (1988), "Prediction of wind-induced failure of loose laid roof cladding systems", *J. Wind Eng. Ind. Aerod.*, **29**(1-3), 29-37.
Kind, R.J. and Wardlaw, R.L. (1979), *Model studies of the wind resistance of two loose-laid roof-insulation systems*, National Research Council Canada, Report LTR-LA-234.
Kind, R.J. and Wardlaw, R.L. (1982), "Failure mechanisms of loose laid roof insulation systems", *J. Wind Eng. Ind. Aerod.*, **9**(3), 325-341.
Kopp, G.A. and Banks, D. (2013), "Use of the wind tunnel test method for obtaining design wind loads on roof-mounted solar arrays", *J. Struct. Eng. - ASCE*, **139**, 284-287.
Kopp, G.A., Surry, D. and Mans, C. (2005), "Wind effects of parapets on low buildings: Part 1. Basic aerodynamics and local loads", *J. Wind Eng. Ind. Aerod.*, **93**(11), 817-841.
Kumar, K.S. and Stathopoulos, T. (1998), "Spectral density functions of wind pressures on various low building roof geometries", *Wind Struct.*, **1**, 203-223.
Lin, J.X. and Surry, D. (1998), "The variation of peak loads with tributary area near corners on flat low building roofs", *J. Wind Eng. Ind. Aerod.*, **77-78**, 185-196.
Lin, J.X., Surry, D. and Tieleman, H.W. (1995), "The distribution of pressure near roof corners of flat roof low buildings", *J. Wind Eng. Ind. Aerod.*, **56**(2-3), 235-265.
Masters, F.J., Gurley, K.R., Shah, N. and Fernandez, G. (2010), "The vulnerability of residential window glass to lightweight windborne debris", *Eng. Struct.*, **32**(4), 911-921.
Melbourne, W.H. (1980), "Turbulence effects on maximum surface pressures – a mechanism and possibility of reduction", *Wind Eng.*, **1**, 541-551.
Mooneghi, M., Irwin, P. and Chowdhury, A. (2014), "Wind uplift of concrete roof pavers", *Proceedings of the Structures Congress 2014*, April.
NBCC (1995), *User's Guide-NBC 1995*, National Research Council of Canada, Ottawa, Canada.
NEN EN 1991-1-4/NA *Eurocode: Actions on structures – General actions – Part 1.4: Wind actions*.
Oh, J.H. and Kopp, G.A. (2012), "Pressure equalization and analytical solutions for pressures between double-layer envelopes", *Proceedings of the 3rd American Association for Wind Engineering Workshop*, Hyannis, Massachusetts, USA, August.
Oh, J.H. and Kopp, G.A. (2014), "Modelling of spatially and temporally-varying cavity pressures in air-permeable, double-layer roof systems", *Build. Environ.*, **82**, 135-150.
Oh, J.H. and Kopp, G.A. (2015), "An experimental study of pressure distributions within an air-permeable, double-layer roof system in regions of separated flow", *J. Wind Eng. Ind. Aerod.*, **138**, 1-12.
Oh, J.H., Kopp, G.A. and Inculet, D.R. (2007), "The UWO contribution to the NIST aerodynamic database for wind loads on low buildings: Part 3. Internal pressures", *J. Wind Eng. Ind. Aerod.*, **95**(8), 755-779.
Pierre, L.M.S., Kopp, G.A., Surry, D. and Ho, T.C.E. (2005), "The UWO contribution to the NIST

aerodynamic database for wind loads on low buildings: Part 2. Comparison of data with wind load provisions", *J. Wind Eng. Ind. Aerod.*, **93**(1), 31-59.
Richards, P.J., Hoxey, R.P., Connell, B.D. and Lander, D.P. (2007), "Wind-tunnel modelling of the Silsoe Cube", *J. Wind Eng. Ind. Aerod.*, **95**(9-11), 1384-1399.
Saathoff, P.J. and Melbourne, W.H. (1997), "Effects of free-stream turbulence on surface pressure fluctuation in a separation bubble", *J. Fluid Mech.*, **337**, 1-24.
Smith, T.L. (1994), *Hurricane Andrew provides insights on roof damage*, National Roofing Contractors Association, Professional Roofing, 36-44.
Stathopoulos, T. (1982), "Wind pressure on low buildings with parapets", *J. Struct. Division*, **108**(12), 2723-2736.
Stathopoulos, T. and Baskaran, A. (1988), "Turbulent wind loading on roofs with parapet configurations", *Can. J. Civil Eng.*, **29**, 570-578.
Sun, Y. and Bienkiewicz, B. (1993), "Numerical simulation of pressure distributions underneath roofing paver systems", *J. Wind Eng. Ind. Aerod.*, **46-47**, 517-526.
Tieleman, H.W. (2003), "Wind tunnel simulation of wind loading on low-rise structures: a review", *J. Wind Eng. Ind. Aerod.*, **91**(12-15), 1627-1649.
Trung, V., Tamura, Y. and Yoshida, A. (2010). "Numerical computation for lower surface pressures on a porous sunshade roof cover sheet", *Proceedings of the 5th International Symposium on Computational Wind Engineering (CWE2010)*, Chapel Hill, North Carolina, USA, January.
Yamada, H. and Katsuchi, H. (2008). "Wind-tunnel study on effects of small-scale turbulence on flow patterns around rectangular cylinder", *Proceedings of the 6th International Colloquium on Bluff Bodies Aerodynamics & Applications*, Italy, July.

*AD*

## Appendix: Method for obtaining 3-second gust speed from wind blow-off tests

In large-sale testing there are challenges in simulating the full wind turbulence spectrum of the natural wind mainly due to the limited size of the wind tunnels. As a result, just the high frequency part of the turbulence spectrum can be simulated adequately and low frequencies are missing as shown in Fig. 4 in the paper. A test procedure and analysis technique called Partial Turbulence Simulation (PTS) methodology was developed by Asghari Mooneghi (2014) and Asghari Mooneghi *et al.* (2015) in order to produce aerodynamic data for low-rise buildings by using large-scale models in wind tunnels and open-jet wind testing facilities like the Wall of Wind at FIU. Asghari Mooneghi (2014) showed that Eq. (A1) can be used for approximately calculating a cut-off frequency between the high frequency and the low-frequency turbulence.

$$n_c = 0.0716 \frac{U}{{}^{x}L_u} \left( \frac{I_u}{I_{uH}} \right)^3 \tag{A1}$$

where the ${}^{x}L_u$ and $U$ are the full spectrum values of longitudinal integral scale and the mean velocity respectively. $I_{uH}$ is the turbulence intensity in a partial turbulence simulation and $I_u$ is the full-spectrum longitudinal turbulence intensity. For the current problem representative values of $U = 30$ m/s, ${}^{x}L_u = 12$ m, $I_u = 0.3$ and $I_{uH} = 0.07$ were used, implying $n_c = 14$ Hz.

The cut-off frequency as calculated from the above Eq. (A1) can be used to estimate the equivalent gust-duration at full scale using (Asghari Mooneghi 2014)

$$t_{gust} = 0.45/n_c \tag{A2}$$

The derivation of the above equations is a separate topic by itself and has been described in detail in Asghari Mooneghi (2014) and Asghari Mooneghi *et al.* (2015). Using the above methodology, the equivalent gust duration at full scale for the current test is equal to 0.032 s. A moving average was performed to calculate the peak 0.03 s gust from wind speed measurements during the wind lift-off tests. In order to convert the wind lift-off speeds to a 3-second gust speed a conversion factor equal to $U_{3sec}/U_{0.03\,sec} = 0.83$ was calculated for suburban terrain at z=3.048 m (building height at full scale). The procedure for converting the wind speeds averaging time was based on Harris and Deaves (1981) model taken from ESDU (1985).

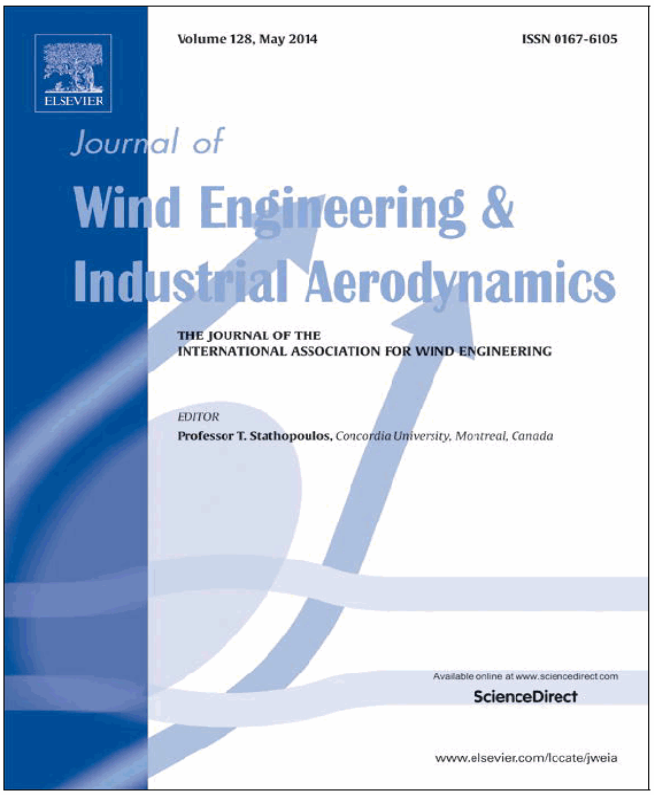

J. Wind Eng. Ind. Aerodyn. 128 (2014) 22–36

Contents lists available at ScienceDirect

Journal of Wind Engineering and Industrial Aerodynamics

journal homepage: www.elsevier.com/locate/jweia

# Large-scale testing on wind uplift of roof pavers

Maryam Asghari Mooneghi [a], Peter Irwin [b], Arindam Gan Chowdhury [b,*]

[a] Department of Civil and Environmental Engineering and International Hurricane Research Center, Florida International University, Miami, FL, USA
[b] Department of Civil and Environmental Engineering, Florida International University, Miami, FL, USA

ARTICLE INFO

*Article history:*
Received 15 November 2013
Received in revised form
3 March 2014
Accepted 4 March 2014
Available online 29 March 2014

*Keywords:*
Wind uplift
Roof pavers
Conical vortices
Pressure taps resolution
Low-rise building

ABSTRACT

This paper presents a large-scale experimental study to investigate the wind loading on concrete roof pavers on the flat roof of a low rise building. The experiments were performed in Wall of Wind, a large-scale hurricane testing facility at Florida International University. Experiments included both wind blow-off tests and pressure measurements on the top and bottom surfaces of the pavers. The effects of the pavers' edge-gap to spacer height ratio and the relative parapet height on the wind performance of roof pavers were also investigated. The results showed that increasing the edge-gap to spacer height ratio parameter decreases the net pressures by enhancing pressure equalization between top and bottom surfaces. Also, increasing the relative parapet height reduces the worst suctions for the parapet heights considered in this study. The resolution of the pressure taps was found to have significant influence on the test results. Too few taps can result in underestimation of the net uplift and overturning moments that can cause failure under strong winds. Guidelines on the resolution and location of pressure taps were provided for better capturing the effects of conical vortices on wind loads on pavers. Results of the wind blow-off tests are compared with those obtained from pressure measurements and a typical practice based on ASCE 7-10 exterior pressures.



## 1. Introduction

Due to the rising loss of life and economic losses associated with the frequent occurrence of severe wind storms, wind induced loads are one of the most critical design parameters for coastal construction. Roof systems are exposed to higher loading than any other building element (Smith and McDonnald, 1991). Suction forces on the roof can loose and lift both roof sheathing and roof coverings, such as tiles, shingles, and roof pavers. Dislodged roofing elements may become wind-borne debris impacting other structures downwind. Internal pressure generated when windows, doors, or sections of the roof are breached can lift and separate the roof from the rest of the structure. This may result in total failure of the building or increased losses because of water infiltration and interior damage.

Loose-laid roof pavers are commonly used on flat roofs and as decorative elements on terraces. Wind uplift of roof pavers is not only the result of the suction on their top surface, but also of the pressure on their underside. Designers of these materials often rely on a significant amount of pressure equalization between top and bottom to help keep them in place. Interlocking and strapping systems are used to improve the resistance of pavers but these typically are not based on true knowledge of the forces involved and failures still occur despite such systems.

Many studies are reported on wind loading and performance of loose laid roofing systems. The failure mechanisms have been extensively studied (Kind, 1988; Kind and Wardlaw, 1982). Bienkiewicz and Sun (1992) performed wind tunnel experiments to investigate the wind loading of loose-laid roof paving systems on a low-rise building with flat roof. The effects of space under the paver and the parapet height on the pressure correlation were investigated. Kramer and Gerhardt (1983) investigated the critical loading on permeable roofing elements including tiles and paving slabs and presented typical test results for roof tiles and flat roof elements. Bienkiewicz and Endo (2009) carried out a wind tunnel study on wind loads on loose-laid roof pavers and photovoltaic roofing systems. Effects of the edge-gap between pavers, and the space beneath the pavers on the pressures underside the pavers were discussed. Trung et al. (2009) conducted wind tunnel tests in order to investigate the effects of parapet height and underside volume on wind loading of porous roof cover sheets. They concluded that the correlation between upper and lower surface pressures decreased with increasing the underside volume. This means that increasing the underside volume increases the net pressure on porous roofs. Studies of wind effects on full- and large-scale building models have been limited. Aly et al. (2012) performed an experimental study to assess wind induced pressures on full-scale loose concrete roof pavers using the 6-fan Wall

* Corresponding author.

http://dx.doi.org/10.1016/j.jweia.2014.03.001
0167-6105/

of Wind, at Florida International University (FIU). A limited number of numerical simulations of wind loading on roof paver systems have been proposed in the literature (Amano et al., 1988; Bofah et al., 1996; Gerhardt et al., 1990; Kind, 1994; Sun and Bienkiewicz, 1993; Trung et al., 2010). Results from some of the preceding studies have been used for the development of models for design of loose-laid roofing systems e.g. roof pavers (Bienkiewicz and Endo, 2009; Cheung and Melbourne, 1986; Cheung and Melbourne, 1988). Some codes and standards address the design of these systems. In the Netherlands code, NEN EN 1991-1-4/NA, 1991, a set of values for net pressure coefficients (difference between the external and underneath pressure coefficients; $Cp_{net}=Cp_e-Cp_i$) is proposed for design of roofing tiles and pavers. These values were based on a number of experiments and full-scale studies on roof tiles on pitched roofs and roof pavers on flat roofs including those of Geurts (2000), who proposed equalization factors defined as $C_{eq}=Cp_{net}/Cp_e$ from full-scale measurements on roof tiles and roof pavers to be applied to the external pressure coefficients given in the Netherlands wind loading code. The proposed values for roof pavers with and without interlock were 0.25 and 0.6, respectively. In the German Wind Code (DEUTSCHE NORM, 2001-03) design pressure coefficients are provided for building envelopes with permeable facades based on a study by Gerhardt and Janser (1995). In the Australian Standard for wind loads (AS 1170.2, 2011) reduction factors are given for estimating design wind loads on porous claddings. These factors depend on the cladding porosity and the horizontal distance from windward building edge. Other major international codes and standards for wind loads in Canada and USA (ASCE 7-10; NBCC, 1995) specify roof wind pressures for typical roof geometries but there are no specific provisions on how to apply such pressures to roofing elements such as tiles, shingles, and pavers.

To better understand the effects of conical vortices on roof pavers under cornering winds, the present work focused on a large-scale experimental study on the wind loading mechanism of concrete roof pavers using the 12-fan Wall of Wind (WOW) facility at FIU. Half-scale concrete pavers were installed on a square portion of a flat roof of a low-rise building. Tests in which pavers were actually lifted off by the wind were conducted and pressure measurements were performed. The aim of the study was to investigate the external and underneath pressure distributions over loose-laid roof pavers in order to develop more effective protections against wind damage. In the course of the work guidelines were developed for the resolution and location of pressure taps on critical pavers to better resolve the effects of conical vortices. The effects of paver's edge-gap to spacer height ratio and the relative parapet height were also explored. Wind blow-off speeds were compared to those calculated using a typical informal practice based on ASCE 7-10 external pressures and also with the current net-pressure measurements.

## 2. Wind loading mechanism on permeable roofing elements

Solid pavers are frequently used as ballast and walking surfaces on roofs and it is necessary that they be capable of resisting uplift forces due to wind. Usually concrete pavers are placed on the roof with gaps in between them and with spaces between their under sides and the roof deck. This is necessary to allow for water drainage and for vapor diffusion when using an "inverse roof" in which the principal thermal insulation material is applied on top of the waterproof covering. Since air can readily leak around the edges of pavers, the pressure distribution produced by the wind flow over the outer surface of the roof produces secondary flows through the spaces between and underneath the paver elements. A pressure distribution is generated under the roof pavers which is related to, but different from, that on the outer surface. The pressure equalization occurs very quickly, typically in less than 0.1 of a second, because very small volumes of air exchange are needed to bring the underside pressure into equilibrium with the pressures around the paver perimeter. The pressure equalization effect greatly reduces the net uplift force on pavers in most areas of roofs. However, in areas of very high spatial gradients of pressure, such as those which occur under vortices near roof corners, significant net uplift pressures can still occur. Fig. 1 illustrates the typical path of the vortices over a flat roof for cornering winds.

The diagram in Fig. 2 illustrates the general mechanism of uplift on roof pavers. The aerodynamic uplift force is the difference between the pressure on the lower surface of the paver, $P_L$ and the pressure on the upper surface, $P_U$ (Fig. 2). The pressure on the upper surface due to the presence of a corner vortex (solid curve) is negative (when measured relative to a non-zero baseline, e.g. the static pressure in the surrounding air stream) and has a

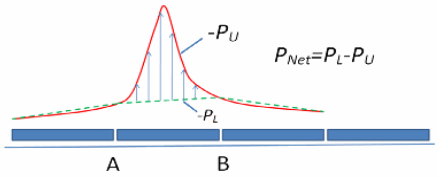


**Fig. 2.** General mechanism of pressure distributions on upper and lower surfaces of a roof paver.

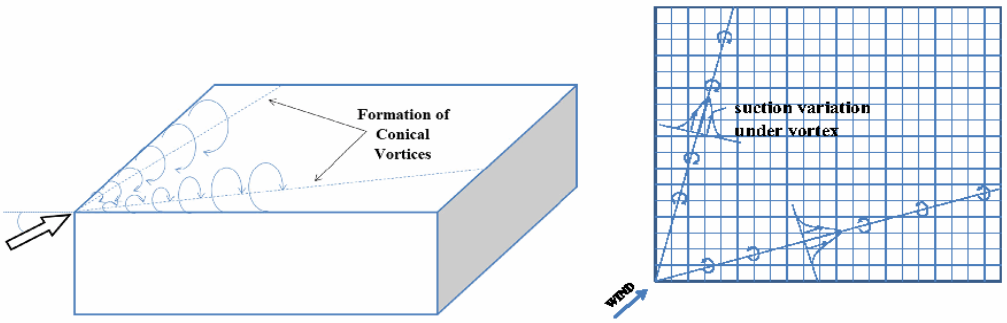


**Fig. 1.** Paths of corner vortices and resulting suction variations on roof.

concentrated peak. The pressure on the lower surface is depicted by the broken curve and it is shown as being equal to that on the top surface at the paver edges. In practice the top and bottom edge pressures do not always match exactly. The underneath pressure depends on the outer pressure distribution and the relative magnitude of the joint resistances compared to the under-element resistance which prevents a complete pressure equilibration between upper and lower surfaces of the element (Bofah et al., 1996; Gerhardt et al., 1990; Kind, 1994). Detailed measurements done by Kind and Wardlaw (1982) showed that the underneath pressure does tend to vary roughly linearly between the pressures at the paver edges as depicted in Fig. 2 (this is also discussed in Bofah et al. (1996)). More precisely, it should satisfy the Laplace equation as explained by Kind (1994). It is only due to the sharp peak of the negative pressure under a vortex (between points A and B) that a net uplift occurs, signified by the large difference between the solid and broken curves. If the upper surface pressure does not have the peak then pressure equalization caused by flow around the edges of the paver results in smaller net uplift as shown by the small differences between the solid and dashed curves on the pavers outside the zone between points A and B.

The aerodynamic uplift force and/or the overturning moment on the element may become higher than the weight and/or the resisting moment. Parameters influencing the wind loading mechanism of roof pavers in terms of the nonlinear net (i.e., external minus internal) pressure distribution over the paver due to conical vortices include: paver size, paver edge-gap to spacer height ratio, distance of the paver from the roof corner, and height of parapets. Roof external pressures are a function of building height, exposure, building orientation, parapet height, and other roof top features such as elevator housings, stairwell cover, and cooling towers (Kramer and Gerhardt, 1983). The internal pressure (i.e. pressure underneath the pavers) depends on the external pressure distribution, the edge-gap to spacer height ratio, and the flow resistance underneath the pavers. A large gap between the pavers has a considerable effect on the reduction of the wind force because it makes the internal pressure approach the external one (Kramer and Gerhardt, 1983).

## 3. Description of the experimental set up and testing procedure

### 3.1. 12-Fan Wall of Wind facility

The full-scale 12-fan Wall of Wind (WOW) open jet facility at FIU was used to generate the wind field for the present study. It can generate up to a Category 5 Saffir–Simpson Scale hurricane wind speed that reasonably replicates mean wind speed and partial turbulence characteristics of real hurricane winds. Fig. 3 shows the comparison between the atmospheric boundary layer (ABL) full spectrum for suburban terrain as simulated in a boundary layer wind tunnel by Fu (2013) and the WOW partial spectrum. The dimensionalized Kaimal spectrum is also shown. Note that the high frequency portions of the WOW and wind tunnel spectra match satisfactorily and show good agreement with the −5/3 slope corresponding to the inertial subrange of the dimensionalized Kaimal spectrum. As noted by several researchers (Banks, 2011; Irwin, 2009; Kopp and Banks, 2013; Kumar and Stathopoulos, 1998; Melbourne, 1980; Richards et al., 2007; Saathoff and Melbourne, 1997; Tieleman, 2003; Yamada and Katsuchi, 2008), accurate simulation of high frequency turbulence is necessary for an adequate simulation of the separated flows on local aerodynamic effects on low-rise structures. A set of triangular spires and floor roughness elements were used to generate the turbulence and the boundary layer characteristics (Fig. 4).

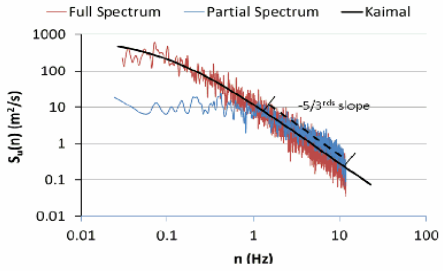


**Fig. 3.** Comparison of ABL full spectrum for suburban terrain simulated in wind tunnel by Fu (2013), WOW partial spectrum and the dimensionalized Kaimal spectrum.

The mean wind speed and turbulence intensity profiles for suburban terrain are shown in Fig. 5 for 20.1 m/s wind speed at $z=2.6$ m elevation (target power law coefficient was $\alpha=1/4$). It should be noted that the tests were performed in a partial turbulence simulation in which the turbulence intensity was lower than that for the ABL flow containing the full spectrum of turbulence. However, using the method proposed by Katsuchi and Yamada (2011), the adequacy of the current turbulence intensity was shown.

### 3.2. Test condition

If the tests results are to be meaningful, conditions must be such that the test model behavior is dynamically similar to that of the prototype. The wind approaching the model should satisfactorily simulate the natural wind, and the Reynolds number ($UL/\vartheta$), the Froude number ($U^2/Lg$), and the density ratio ($\rho_s/\rho$) should have the same numerical values between the model and the prototype. $U$

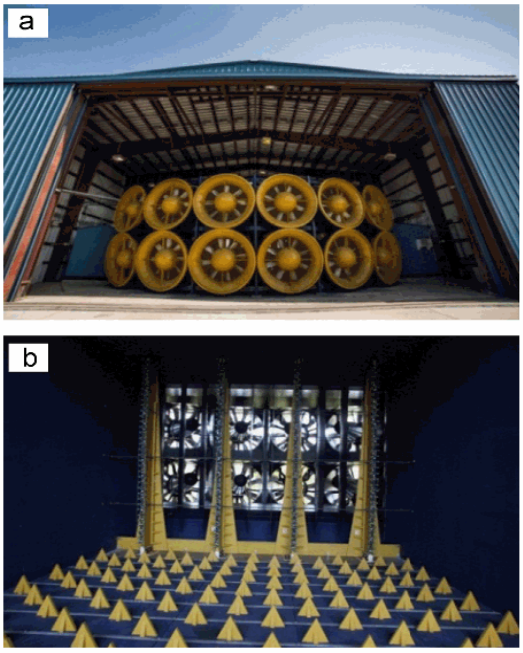


**Fig. 4.** (a) Wall of Wind, Florida International University and (b) spires and floor roughness elements.

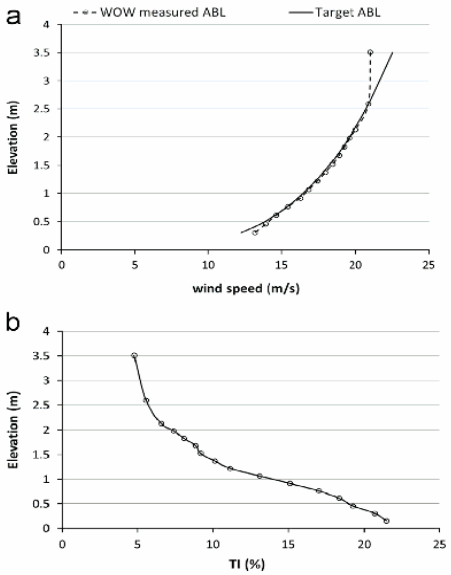


**Fig. 5.** Suburban terrain: (a) ABL profile and (b) turbulence intensity profile.

is the speed of approaching wind at roof height, $L$ is a reference length, $\vartheta$ is the kinematic viscosity of air, $g$ is the gravitational acceleration, $\rho$ is the density of air, and $\rho_s$ is the density of the solid paver. In the case of thin objects, the requirement that the density ratios be matched between the model and the prototype can be relaxed, if the weight per unit area of the model is correctly scaled meaning that $(\rho_s t)_M/(\rho_s t)_P = L_M/L_P$ in which symbol $t$ denotes the thickness of the pavers and subscripts M and P denote the model and the prototype, respectively. Except at a scale of 1:1, Froude number and Reynolds number similarity cannot be satisfied simultaneously. The flow underneath and through the joints might be somewhat dependent on Reynolds number but it was assumed in the present experiments that being out by a factor of 2 in Reynolds number would have very minor effect on the results. Kind and Wardlaw (1982) discuss Re effects and accepted a larger mismatch in their experiments. The complete simulation of the atmospheric boundary layer is not possible at ½ scale in most wind testing facilities due to their limited size. Typically, the large scale turbulence present at full scale cannot be generated and only the high-frequency part of the power spectrum can be simulated (Fu et al., 2012; Yeo and Chowdhury, 2013). However, previous experiments have shown that the flow pattern over the upwind corner of the building roof is mainly dependent on the correct simulation of high frequency turbulence, as was done in the present tests, and achieving a Reynolds number of approximately the right order.

### 3.3. Test building

A test building was constructed to install the roof pavers (a total of 100) in a similar way to real roof pavement systems. The size of the 1:2 test building model was 3.35 m by 3.35 m in plan by 1.524 m high; thus it represented a low-rise prototype building with height of 3.48 m. The model was engulfed completely in the 6.1 m wide and 4.3 m high wind field generated by the WOW. The roof deck was made from plywood and was completely sealed and rigid. The rectangular sharped edge parapets on the building model were interchangeable which allowed evaluation of the effect of parapet height on the wind effects on pavers. The parapet height

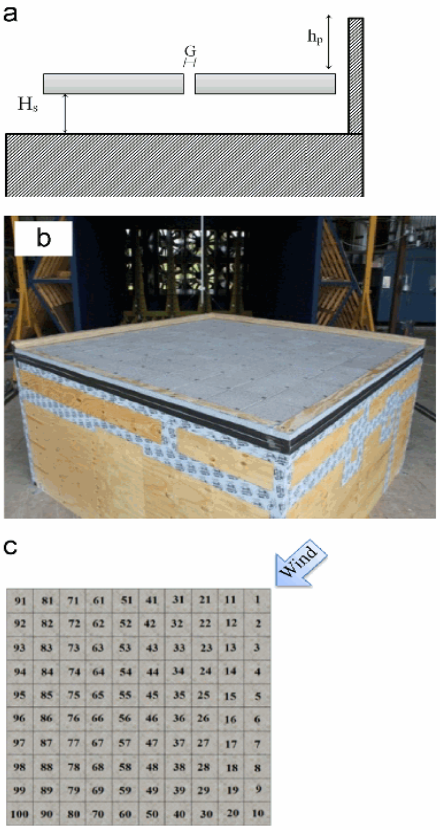


**Fig. 6.** (a) Geometrical parameter definition, (b) test building for wind blow-off tests, and (c) roof pavers numbering.

was measured from the top of the pavers (Fig. 6a). There were no parapets on the leeward side of the building so that the roof could be representative of the windward corner of a bigger roof structure. The justification of this comes from the studies of Lin and Surry (1998) and Lin et al. (1995) who found that for low buildings which are large enough to have reattached flows on the roof, the distribution of pressure coefficients in the corner region is mainly dependent on the eave height, $H$, and not so much on the building plan dimensions as long as terrain conditions are similar. Also, external pressure coefficients measured in wind tunnel by Kopp et al. (2005) on roof corners of a nearly flat building model were consistent with those measured on roof corners of flat roof low-rise building models with different plan aspect ratios as reported by Stathopoulos (1982), Stathopoulos and Baskaran (1988), Ho et al. (2005), and Pierre et al. (2005). The experiments included both the wind blow-off testing (i.e. blowing at sufficient speed to dislodge pavers) and pressure measurements. For the wind blow-off tests, concrete pavers with a dimension of 0.305 m by 0.305 m by 2.54 cm thickness and having weight per unit area of 532 N/m$^2$ were installed on the roof which can be considered as modeling typical 0.61 m square pavers at half-scale. Fig. 6b shows the test building for the wind blow-off tests with the concrete roof pavers installed. For pressure measurements, pavers with exactly the same dimensions as the actual concrete pavers were made from Plexiglas. This made it more convenient to install pressure taps on both upper and lower surfaces of the pavers. Adjustable height pedestals were

used to change the space between the paver and the roof deck ($H_s$, Fig. 6a). Pedestals had top caps which created a constant $G=3.175$ mm space between the pavers (Fig. 6a). Pavers were numbered from 1 to 100 (Fig. 6c). Pressure taps were installed on Plexiglas roof pavers for simultaneous measurement of the external and the underneath pressures. Fig. 7 shows the external and underneath pressures tap layout (total of 447).

### 3.4. Test procedure

A total of 9 experiments were carried out, including three wind blow-off tests and 6 pressure measurement tests. A summary of each test characteristics is shown in Table 1. Only one wind direction was tested which was 45°. Based on past studies this wind direction was selected as the most critical orientation for generating high uplifts under conical vortices on flat rectangular roofs (Holmes, 2007).

The basic test procedure consisted of first conducting wind blow-off tests. The aim of these tests was to provide guidance on the location where paver blow-off, i.e. failure, first occurs, which

**Table 1**
Test number and characteristics.

| Wind test number | Spacer height ($H_s$) (cm) | Windward parapet height (cm) | *$G/H_s$ | $h_p/H$ |
|---|---|---|---|---|
| **Wind Uplift 1** | 1.27 | 7.62 | 0.25 | 0.05 |
| **Wind Uplift 2** | 3.81 | 7.62 | 0.083 | 0.05 |
| **Wind Uplift 3** | 11.43 | 7.62 | 0.028 | 0.05 |
| **Pressure 1-1** | 1.27 | 7.62 | 0.25 | 0.05 |
| **Pressure 2-1** | 3.81 | 5.08 | 0.083 | 0.033 |
| **Pressure 2-2** | 3.81 | 7.62 | 0.083 | 0.05 |
| **Pressure 2-3** | 3.81 | 15.24 | 0.083 | 0.1 |
| **Pressure 2-4** | 3.81 | 22.86 | 0.083 | 0.15 |
| **Pressure 3-2** | 11.43 | 7.62 | 0.028 | 0.05 |

* Constant $G=3.175$ mm for all tests.

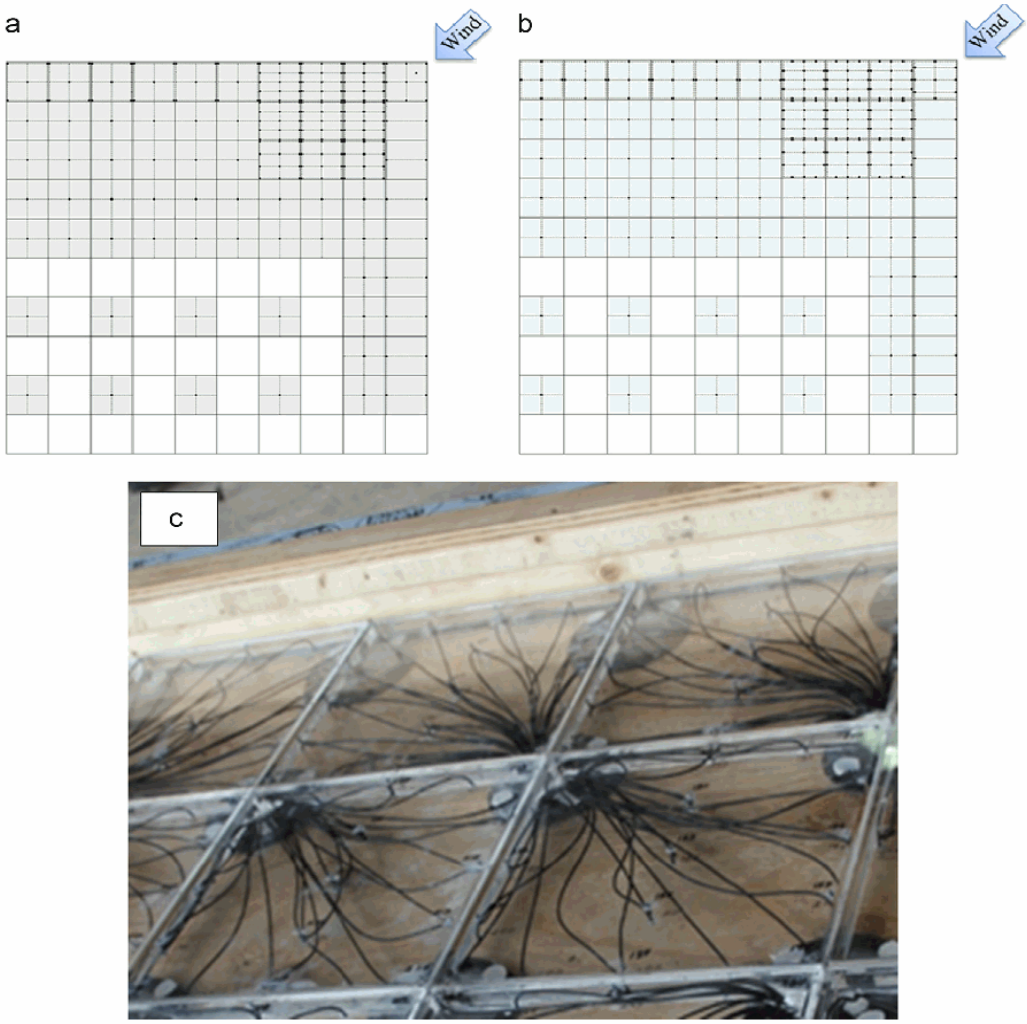


**Fig. 7.** (a) External pressure tap layout, (b) underneath pressure tap layout, and (c) plexiglas pavers with pressure taps.

could then be used to decide on the pressure tap layout. The test was done by gradually increasing the wind speed in WOW and visually observing the behavior of the roofing system. The most critical pavers which dislodged first were identified. Wind speeds were measured at the roof height of the test model (1.524 m height) using a turbulent flow Cobra probe. After identifying the critical pavers and deciding on the pressure tap layout, the original pavers were replaced by the Plexiglas pavers with pressure taps. Pressure measurements were carried out at wind speed = 18.5 m/s which was below the failure speed of concrete pavers (but required some special measures to hold the Plexiglas pavers in place). Nine critical pavers were fitted with total of 256 pressure taps to allow accurate measurements of the pressure distribution above and underneath the pavers. A 512 channel Scanivalve Corporation pressure scanning system was used for pressure measurements. Pressure data were acquired at sampling frequency of 512 Hz for a period of two minutes. Each pressure measurement test was repeated for three times to assure repeatability of the data. A transfer function designed for the tubing (Irwin et al., 1979) was used to correct for tubing effects.

### 3.5. Data analysis

The mean pressure coefficient at any location was obtained from

$$Cp_{mean} = \frac{P_{mean}}{\frac{1}{2}\rho U_{mean}^2} \quad (1)$$

where $P_{mean}$ is the mean pressure, $\rho$ is the air density at the time of the test (1.225 kg/m$^3$) and $U$ is the mean wind speed measured at the building height of the test model (1.524 m).

For the proper securing of individual pavers, measured values of $Cp_{peak}$ should be considered. Due to the highly fluctuating nature of wind pressures, significant differences might be expected in the peak values of pressure time series obtained from several different tests under nominally identical conditions. The Sadek and Simiu (2002) method was used to obtain statistics of pressure peaks from observed pressure time histories (unless otherwise stated). Because estimates obtained from this approach are based on the entire information contained in the time series, they are more stable than estimates based on single observed peaks. For the evaluation of these estimated values, the peak value with 85% probability of not being exceeded in one hour of full spectrum wind was selected. The peak pressure coefficient was normalized by the three second gust dynamic pressure as follows:

$$Cp_{peak} = \frac{P_{peak}}{\frac{1}{2}\rho U_{3s}^2} \quad (2)$$

where $P_{peak}$ is the peak pressure, and $U_{3s}$ is the peak 3-s gust at the reference height. For the WOW the wind speed $U_{3s}$ was obtained using time scale $\lambda_t = 0.7$ ($\lambda_t = (\lambda_L = 0.5)/\lambda_V = 0.71$ (based on Froud Number Similarity)), meaning that $512 \times 3 \times 0.7 = 1075$ data points were required for its determination. The peak value of the $U_{3s}$ was obtained by performing moving averages. Data were low-pass filtered at 30 Hz equivalent to 21 Hz full scale.

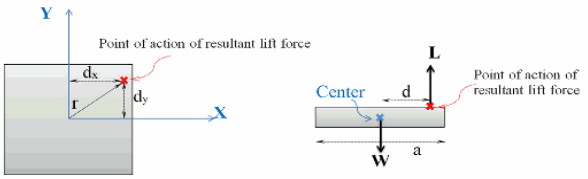


**Fig. 8.** Definition of the point of action of the resultant lift force.

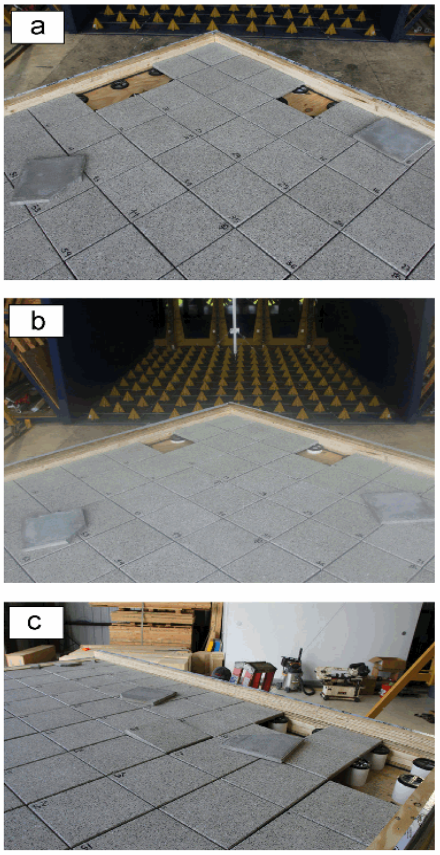


**Fig. 9.** Failure of roof pavers during wind blow-off tests: (a) $G/H_s = 0.25$, (b) $G/H_s = 0.083$, and (c) $G/H_s = 0.028$.

**Table 2**
Failure wind speeds and failure mechanisms.

| Test number | 1st failure wind speed (m/s) | 2nd failure wind speed (m/s) |
|---|---|---|
| **Wind Uplift 1** | **37.2:**paver 1 wobbling, paver 21 lifted off | **40:** paver 1 wobbling, paver 4 lifted off<br>**43:** paver 1 wobbling, paver 31 lifted off |
| **Wind Uplift 2** | **34:** pavers 1, 11 wobbling | **37.3:** pavers 4, 21 lifted off |
| **Wind Uplift 3** | **28:** pavers 1, 2 wobbling<br>**30.7:** paver 1 lifted off | **34:** pavers 3, 4 wobbling<br>**37:** pavers 2, 21 lifted off |

To properly design and secure the most critical pavers in place, it is necessary to know the wind-induced loads acting on individual pavers under the designed wind speed. It should be noted that the highest suction on the paver does not necessarily occur at the center of the paver. This means that even for cases where the total uplift force is less than the weight of the paver, the weight of

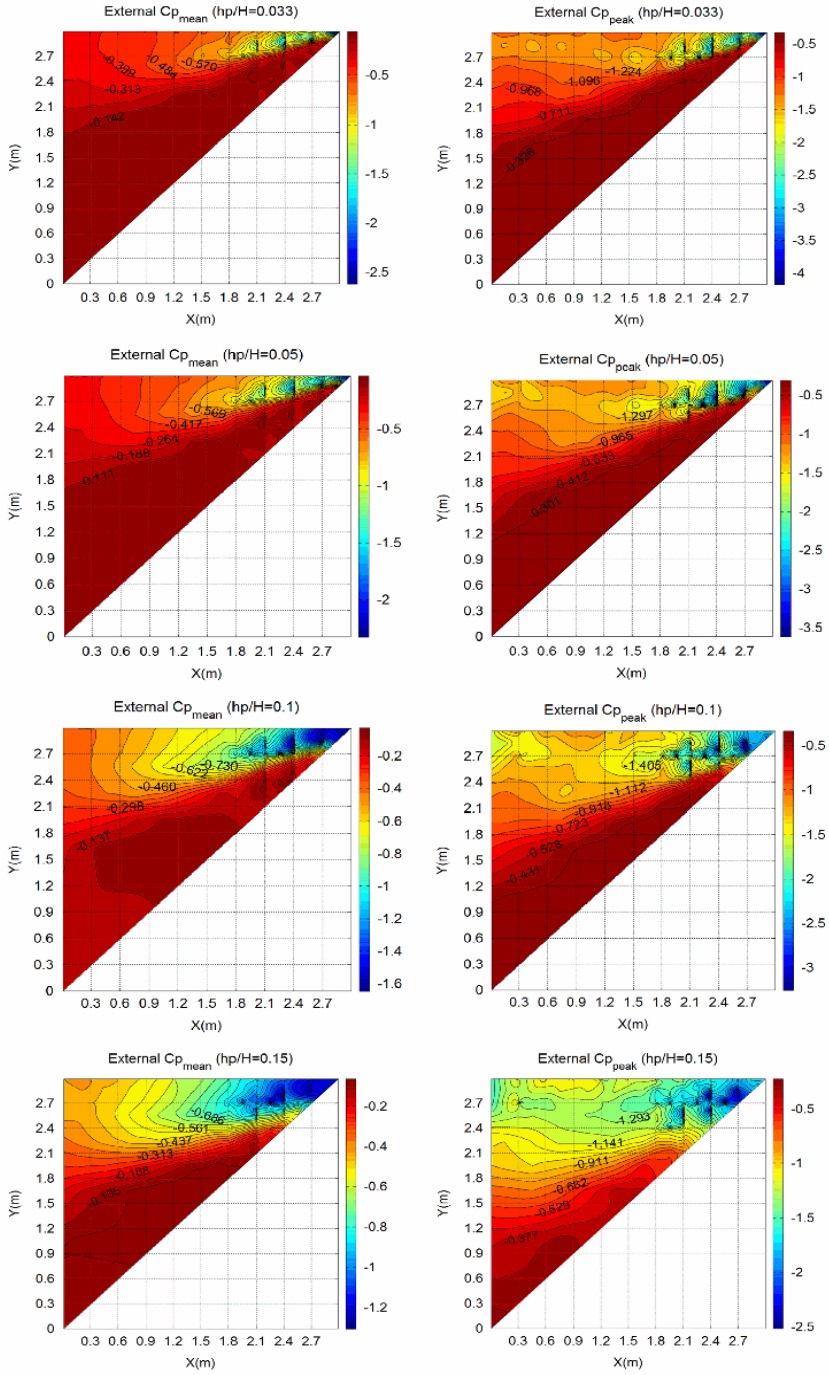


**Fig. 10.** External $Cp_{mean}$ and $Cp_{peak}$ ($G/H_s$=0.083).

the paver might not overcome the corresponding overturning moment. The overall wind uplift load, $L(t)$, and lift coefficient, $C_L(t)$, acting on any single paver are obtained as

$$L(t)=\frac{1}{2}\rho U^2 \iint_{A_{paver}} Cp_{net}(t,x,y)\,dA \quad (3)$$

$$C_L(t)=\frac{L(t)}{\frac{1}{2}\rho U^2 A} \quad (4)$$

where $A$ is the surface area of the paver and $Cp_{net}(t)=Cp_{ext}(t)-Cp_{int}(t)$ is the net total pressure coefficient defined as the instantaneous difference between the external and the corresponding underneath pressure coefficients at the same location. The overturning moment and moment coefficient about a selected axis are obtained from

$$M(x,y,t)=\frac{1}{2}\rho U^2 \iint_{A_{paver}} Cp_{net}(t,x,y)\times d(x,y)\times dA \quad (5)$$

$$C_M(t)=\frac{M(t)}{\frac{1}{2}\rho U^2 A a} \quad (6)$$

where $a$ is the width of the paver and $d(x,y)$ is the moment arm defined as the distance from the selected axis to each point on the paver (Fig. 8). Another important parameter is the point of action of the uplift force (Fig. 8). Having the net lift, $L$, and moments $M_x$ and $M_y$, offsets of point of action of lift from the center are

$$d_y=M_x/L;\quad d_x=M_y/L \quad (7)$$

The blow-off takes place when the moment caused by the uplift force is equal to the moment from the paver weight, $W$. Therefore, the critical wind velocity $U_{CRIT}$ at which blow-off occurs is calculated from

$$\frac{1}{2}\rho U_{CRIT}{}^2 C_L A\left(d+\frac{a}{2}\right)=W\times\frac{a}{2} \quad (8)$$

From which it can be deduced that

$$U_{CRIT}=\sqrt{\frac{a}{2(d+\frac{a}{2})}\times\frac{W}{\frac{1}{2}\rho C_L A}}\ (d \text{ is the larger of } d_x \text{ and } d_y) \quad (9)$$

## 4. Results and discussion

### 4.1. Wind blow-off test results

Table 2 shows the failure wind speeds and the failure mechanism for wind blow-off tests (see Table 1 for each test characteristics). 1st failure wind speed is defined as the wind speed at which minor displacement and/or limited failure (wobbling of pavers and/or 1 paver lifted off) was observed. 2nd failure wind speed corresponds to the situation when more failure occurred (2 or 3 pavers were lifted off). The failure in each case is shown in Fig. 9.

The results showed that by increasing the spacer height ($H_s$), the failure wind speed decreases. This is in agreement with studies of Bienkiewicz and Endo (2009) who showed that increasing the height $H_s$ while having a constant edge-gap between the pavers increases the net pressures on the pavers which may be regarded as lowering the failure wind speed. The location of the failure was in all cases near the edge of the roof (Fig. 9). Pavers 1, 2, 3, 4, 11, 21, and 31 were the most critical pavers. The pressure tap layout (Fig. 7) was decided based on the wind blow-off tests for detailed evaluation of the pressure distribution over the roof and the most critical pavers.

### 4.2. Pressure measurement results

#### 4.2.1. Effect of relative parapet height ($h_p/H$)

*4.2.1.1. External pressure distribution.* Fig. 10 shows the surface plots of the external mean and external peak pressure coefficients for various relative parapet height ratios ($h_p/H$). The peak values correspond to the estimated peak value for each tap during the test and do not occur simultaneously on all taps.

Results in Fig. 10 show that pavers close to the edges and corners of the roof are subjected to the highest local negative pressures. It can be seen that the highest local mean suction pressure coefficient is reduced by about 50% by changing $h_p/H$ from 0.033 to 0.15. The width of the zone of high suctions caused by the conical vortices increases and their strength decreases with taller parapets. This trend is in agreement with the results obtained by Kind (1988) on the effect of parapet height on worst mean suction pressure coefficient for a 1:20 scale low-rise building.

Several studies have been done on the effect of parapets on the external pressure coefficients on flat roofs (Kopp et al., 2005; Stathopoulos, 1982; Stathopoulos and Baskaran, 1987). In order to put the current data in context with the previously published data, it was attempted to compare the external pressure coefficients with those obtained in the literature. Table 3 shows the characteristics of the experiments used for comparison. Note that comparisons

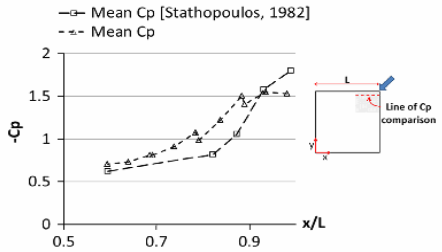


**Fig. 11.** Comparison of external $Cp_{mean}$ ($h_p/H=0.1$; $G/H_s=0.083$) with Stathopoulos (1982).

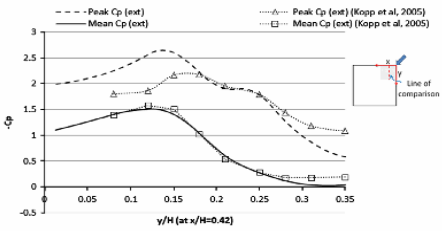


**Fig. 12.** Comparison of external $Cp$ ($h_p/H=0.1$; $G/H_s=0.083$) with Kopp et al. (2005).

**Table 3**
Characteristics of the experiments used for comparison between external pressure coefficients.

| | $H$ (m) | $h_p/H$ | Plan aspect ratio | Terrain | Scale | Wind direction |
|---|---|---|---|---|---|---|
| **Current study** | 3.48 | 0.1 | 1 | Suburban | 1/2 | 45 |
| Stathopoulos, 1982 | 9.8 | 0.122 | 3 | Suburban | 1/250 | Most critical, from tests for 0–90 is presented |
| Kopp et al., 2005 | 4.6 | 0.1 | 1.5 | Open | 1/50 | 325 |

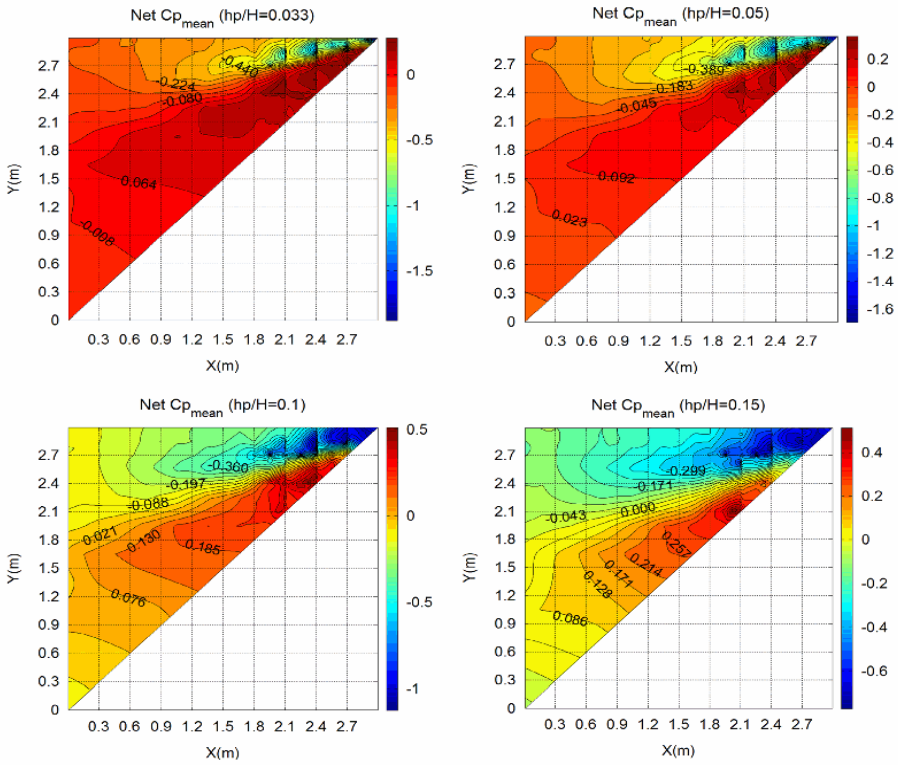


**Fig. 13.** Net $Cp_{mean}$ ($G/H_s$=0.083).

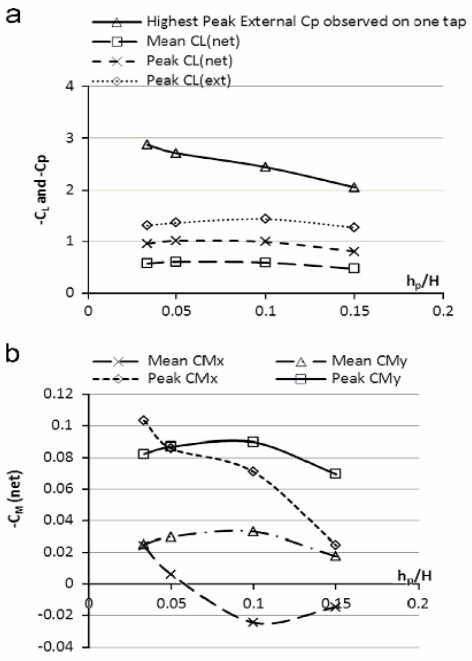


**Fig. 14.** Variations of (a) $C_{Lnet}$ and (b) $C_{Mnet}$ on paver 21 with $h_p/H$ ($G/H_s$=0.083).

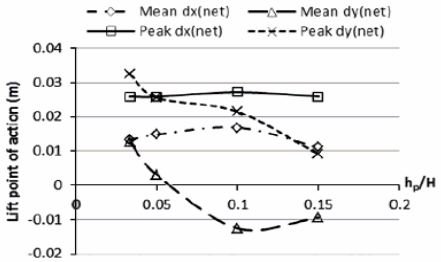


**Fig. 15.** Variation of $L_{net}$ point of action on paver 21 with $h_p/H$ ($G/H_s$=0.083).

pertain to the closest possible match of geometric and exposure configurations as found in the literature and could not be performed for exactly similar test configurations. Comparison was limited to the corner region where 45° wind direction usually dominates the behavior of peak suctions and since 45° was the only angle tested in the present research.

Fig. 11 shows the external mean pressure coefficients measured at the edge taps of the building with the corresponding values from the literature (Stathopoulos, 1982). Note that in the latter reference the published values are the highest ones as obtained from all the wind directions tested, rather than those at 45° only. However, close to the corner the 45° case dominates. It can be seen that the values obtained in the present work are generally in a good agreement with those from Stathopoulos (1982).

As explained previously, the peak values presented in this paper are normalized to the 3-s gust wind speed. In order to be able to

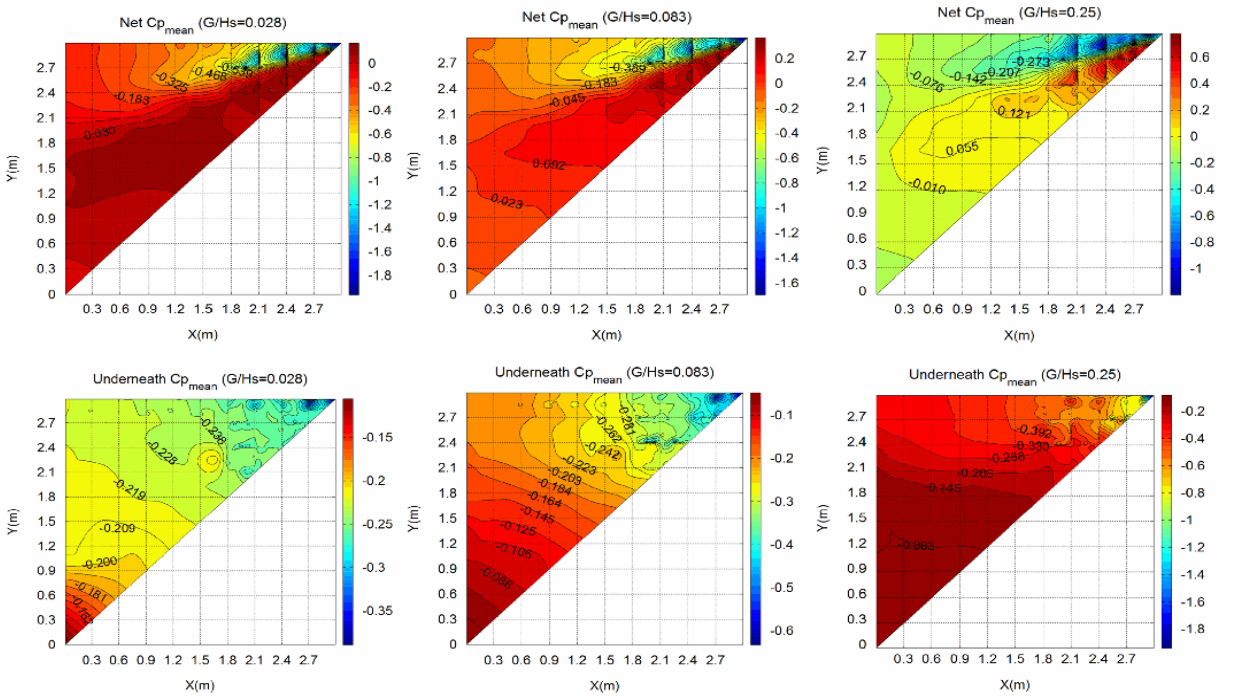


**Fig. 16.** Underneath $Cp_{mean}$ and net $Cp_{mean}$ ($h_p/H=0.05$).

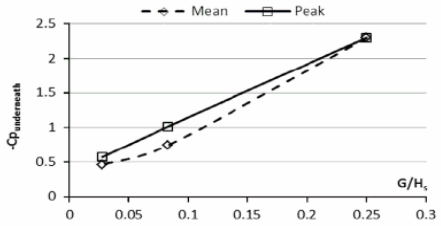


**Fig. 17.** Highest underneath $Cp$ ($h_p/H=0.05$).

compare our peak pressures with those obtained in wind tunnel by Kopp et al. (2005) the procedure explained by Pierre et al. (2005) was used to calculate the equivalent wind tunnel pressure coefficient

$$(GCp)_{eq} = \frac{q_H \hat{C}p}{q_{10m,\,3s} K_{zt} K_h K_d I} = F_{WT} \hat{C}p \qquad (10)$$

where $\hat{C}p$ is the peak coefficient based on the mean hourly wind speed measured at the eave height in a wind tunnel, $q_{10m,\,3s}$ and $q_H$ are the dynamic wind pressures at heights of 10 m and $H$, respectively, as given in the ASCE 7-10, $K_{zt}$ is the topographic factor, $K_h$ is the exposure factor, $K_d$ is the directionality factor and $I$ is the importance factor. The factors $K_{zt}$, $K_d$ and $I$ were set to unity. The coefficient $F_{WT}$ was given as 0.38 for $H=4.6$ m in the open country terrain which was used to re-reference the peak pressure coefficients obtained by Kopp et al. (2005) for comparison purposes. Fig. 12 shows the comparison between the mean and peak pressure coefficients obtained in the current study with the corresponding values in Kopp et al. (2005). The comparison was limited to corner region along the line of $x/H=0.42$ from the windward corner of the roof as defined by Kopp et al. (2005). Results show that the mean pressure coefficients are in very good agreement with the results in

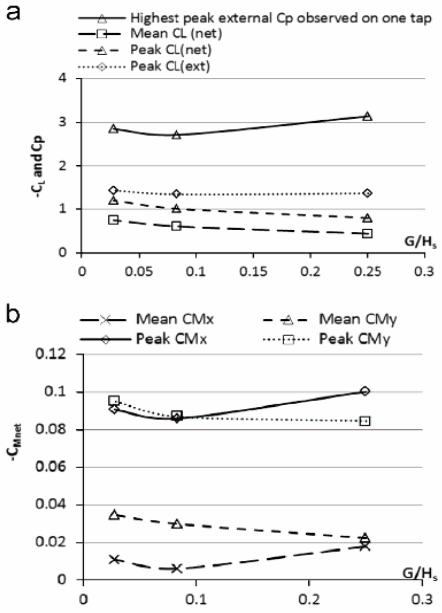


**Fig. 18.** Variation of: (a) $C_{Lnet}$ and (b) $C_{Mnet}$ on paver 21 with $G/H_s$ ($h_p/H=0.05$)

Kopp et al. (2005). The differences in the peak pressure coefficients are probably due to different building geometries, different terrains, and Reynolds number effect. Higher peak pressures are generally

expected for suburban terrain as compared to open terrain results for similar building configurations.

External pressure coefficients measured in this paper are in very good agreement with an earlier full-scale study performed in 6-fan Wall of Wind facility at FIU on concrete roof pavers (Aly et al., 2012). It is to be noted that although the 45° cornering wind is usually considered as the most critical direction for pavers, very localized higher suctions than seen at 45° can occur in small regions near the roof edges for other wind directions (Aly et al., 2012), but apparently the size of the effected region is too small to be the most critical case for pavers.

*4.2.1.2. Net pressure distribution.* Fig. 13 shows the variation of net pressure coefficients for various relative parapet height ratios ($h_p/H$) showing that taller parapets ($h_p/H > 0.1$) reduce the net $Cp_{mean}$ on the roof. This was mainly due to reductions made on the mean external pressure coefficients. However, results show that low parapets might significantly increase the peak roof corner suctions for oblique wind directions (Bienkiewicz and Meroney, 1988; Stathopoulos and Baskaran, 1987).

Fig. 14 shows the variation of the net uplift force coefficient and the net pitching moment coefficient on paver 21 with $h_p/H$. Results show that in contrast to local suctions, the net uplift and the net moment on a paver are both less sensitive to parapet height. For example, in going from $h_p/H$ from 0.033 to $h_p/H$ in the range of 0.05 to 0.10, the values of both $C_{Lnet}$ and $C_{Mnet}$ are increased which makes the range $h_p/H = 0.05$ to 0.10 the worst case scenario among the parapets considered for this study.

The variation of the location of the point of action of the net uplift force with relative parapet height ($h_p/H$) is plotted in Fig. 15. It shows that increasing the parapet height to above $h_p/H$ from 0.1 to 0.15 moves the point of action of the net uplift force more towards the center of the paver while the lift coefficient also decreases. This situation can be interpreted as an improved wind performance for higher parapets. Thus from the current study it was found that a relative parapet height ratio of 0.15 could significantly reduce the suction pressure on pavers under conical vortices. It also reduces the offset distance of the point of action of the lift force from the center of the paver.

*4.2.2. Effect of pavers' edge-gap to spacer height ratio ($G/H_s$)*

Fig. 16 shows the surface plots of the underneath mean and net mean pressure coefficients for various $G/H_s$ ratios. Results presented in Fig. 16 show the effect of edge-gap to spacer height ($G/H_s$) ratio on the wind loading of roof pavers. It can be seen that in these cases also pavers close to the edges and corners of the roof are subjected to the highest negative pressures which is mainly due to the wind-induced conical vortices. Compared to external pressures, the values of underneath pressures acting on the lower surfaces of the pavers are low in magnitude and exhibit more uniformity. For lower $G/H_s$ ratios (larger height spacers), the underneath pressure becomes nearly uniform, probably due to the lower flow resistance underneath the pavers. As concluded by Bienkiewicz and Endo (2009), the $G/H_s$ ratio affects the underside pressures such that the higher the ratio, the lesser the net pressure on the pavers. Fig. 17 clearly shows that increasing the $G/H_s$ ratio results in higher suctions underneath the pavers.

Fig. 18 shows the variation of the net uplift force coefficient and the net pitching moment coefficient on paver 21 with $G/H_s$. The results show that increasing $G/H_s$ ratio reduces the net uplift force coefficient on the paver but the pitching moment is less sensitive to this parameter. The variation of the location of the point of action of the net uplift force with $G/H_s$ ratio is plotted in Fig. 19. For higher $G/H_s$ ratios, the point of action of the lift force is more offset from the center of the paver.

Comparing the results presented in Figs. 18 and 19 shows that even though by increasing the $G/H_s$ ratio the lift force is more offset from the center of the paver, nonetheless its value decreases in such a way that an overall better wind performance is observed for higher $G/H_s$ ratio.

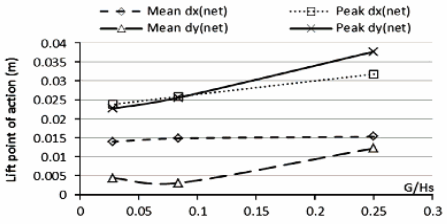


**Fig. 19.** Variation of $L_{net}$ point of action on paver 21 with $G/H_s$ ($h_p/H = 0.05$).

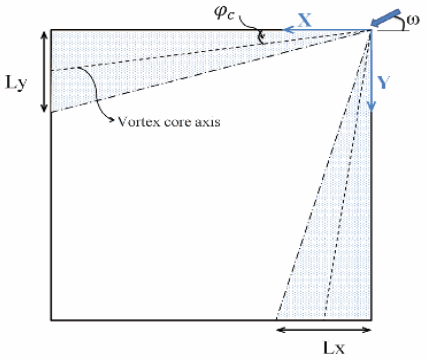


**Fig. 21.** Defining vortex core angle.

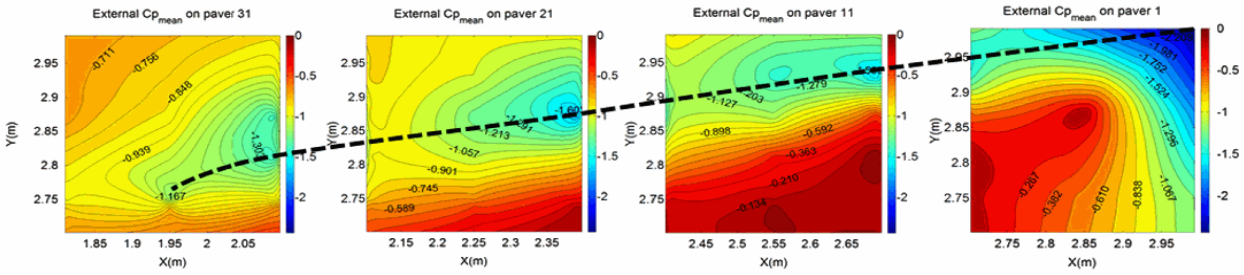


**Fig. 20.** External $Cp_{mean}$ on critical pavers ($G/H_s = 0.083$, $h_p/H = 0.05$).

*4.2.3. Effect of pressure tap resolution on aerodynamic lift and moment results*

Fig. 20 shows the external mean pressure distribution on pavers 1, 11, 21 and 31 and the line indicates the path of the corner vortex. It is noteworthy that the highest suctions are observed at the upwind edge of each paver. It is hypothesized that this is due to the interaction of the high velocity rotating flow caused by the corner vortex with a vertical flow coming out of the upwind end of the paver. Wind lift-off tests showed that paver 1 wobbled but did not fail, whereas paver 21 failed (corresponding to Wind Uplift 2 in Table 2). Results showed that the magnitude of the mean and peak uplift coefficients for paver 21 (mean $C_{Lnet}=-0.6$, peak $C_{Lnet}=-1.0$) was higher than that for paver 1 (mean $C_{Lnet}=-0.25$, peak $C_{Lnet}=-0.76$). This was because the size of the high suction zone relative to the paver size was bigger for paver 21 than for paver 1 (Fig. 20). The aerodynamic mechanisms that cause uplift are quite complex, involving significant interaction between the external flow and the internal flow into and out of the gaps between pavers. This interaction can increase the offset of the lift force from the center of the paver. As pointed out by Gerhardt et al. (1990), the impact of vortices on pavers significantly depends on the size of the paver relative to the width of the corner vortex. If the paver is much larger than the width of the vortex then the impact is reduced since only a small fraction of the paver area is affected by the high suction. Also, if the paver is much smaller than the width of the vortex then, even if it is sitting in a high suction zone, the pressure equalization effect of the gaps at its edges substantially reduces the difference in pressure between top and bottom surfaces. However, if the paver and vortex widths are similar the net uplift will tend to be at a maximum.

Banks et al. (2000) proposed an empirical equation valid for incident wind angle of $\omega=30$–$70°$ to calculate the vortex core angle: $\varphi_c=2.94\,e^{0.0297\,\omega}$ (Fig. 21). The vortex core angle measured during experiments for $G/H_s=0.083$, $h_p/H=0.05$ case, was 11.31° which was in a very good agreement with the results obtained from $\varphi_c=2.94\,e^{0.0297\times45°}=11.2°$ (Banks et al., 2000).

Fig. 22 shows the contour plot for the $h_p/H=0.05$ and $G/H_s=0.25$ case in which the same pressure tap layouts as for pavers 2, 3, and 4 were considered for paver 11, 21, and 31. This results in loss of detail and the resulting pressure patterns resemble some of the earlier patterns obtained by other workers (Kind and Wardlaw, 1982) who had less density of taps available to them at the time of their experiments. It appears that a fairly high density of taps is required to capture all the detailed aerodynamic effects.

In order to find the effect of the tap arrangement and required resolution for pressure taps on the critical pavers, six different tap layouts were evaluated, the results of which are plotted in Fig. 23. The results show that having the pressure taps near the edges, especially those edges which are perpendicular to the parapet, is quite necessary for capturing an accurate measurement of high suctions.

Figs. 24 and 25 show the net uplift force and net moment coefficients on paver 21 for different tap layouts defined in Fig. 23.

The results demonstrate that the net uplift force coefficient and net moment coefficient are sensitive to the resolution and arrangement of the pressure taps. Figs. 24 and 25 also show that there might be significant differences in the calculated lift and overturning moment obtained from a particular layout. Case (f) shows the tap layout used in this study on critical pavers with 30 pressure taps (15 taps on top and 15 taps on bottom). The results show that inaccuracies can occur when having low resolution of pressure taps. High suction areas can be missed as is the case of Tap Layout a, or lift can be overestimated as in Tap Layout d. The latter is mainly because one of the taps captured a very high local suction on the paver. Integrating such local high suction using a large tributary

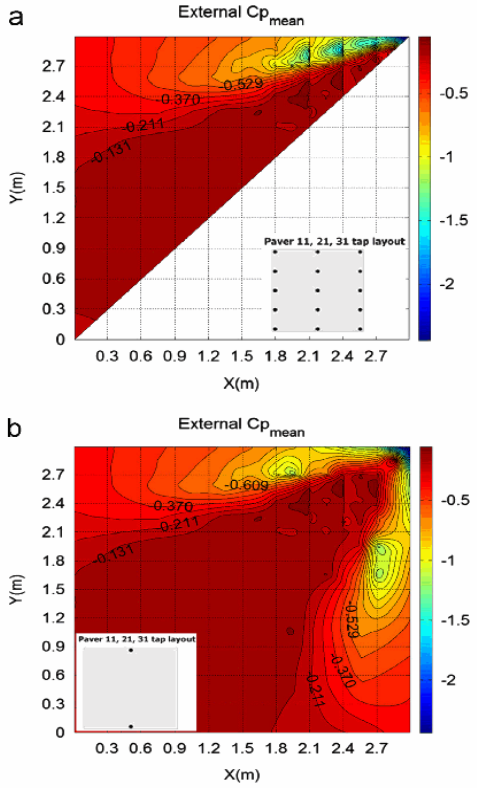


**Fig. 22.** External $Cp_{mean}$: (a) high density of pressure taps and (b) low density of pressure taps ($h_p/H=0.05$, $G/H_s=0.25$).

area and neglecting the effect of pressure gradient can lead to overestimation of the lift. The results of this study show that to obtain accurate measurements of aerodynamic lift and moment a high density of taps is needed, higher than typically used in the past. If the analysis requires higher degrees of accuracy, it is recommended that additional pressure taps be added evenly on lines perpendicular to the corresponding building edge. Of course vortices do not only occur at roof corners but can also occur at setbacks and next to roof obstructions, and similar detailed pressure patterns can be expected at these discontinuities in building geometry.

*4.3. Comparison with wind blow-off tests and practice based on ASCE 7-10 exterior pressures*

The highest external single tap pressure coefficients and the external area averaged pressure coefficient ($C_{Lext}$) observed on the most critical paver (paver 21) obtained for different cases (Table 1) were also compared to component and cladding external pressure coefficients for roofs as given in ASCE 7-10 (2010). Chapter 30 of ASCE 7-10 provides the peak pressure coefficients for components and claddings. For gable roofs with slope $\theta\leq7°$ the peak external pressure coefficient for corner Zone 3 for tributary areas less than 0.9 $m^2$ is given as −2.8 in Fig. 30.4-2A (ASCE 7-10, 2010). The highest single tap peak suction coefficients observed in the present tests for all cases ranged from −4.1682 for $h_p/H=0.033$ and $G/H_s=0.083$ to −3.5486 for $h_p/H=0.15$ and $G/H_s=0.083$ in the corner zone. Being single tap values, they correspond to much

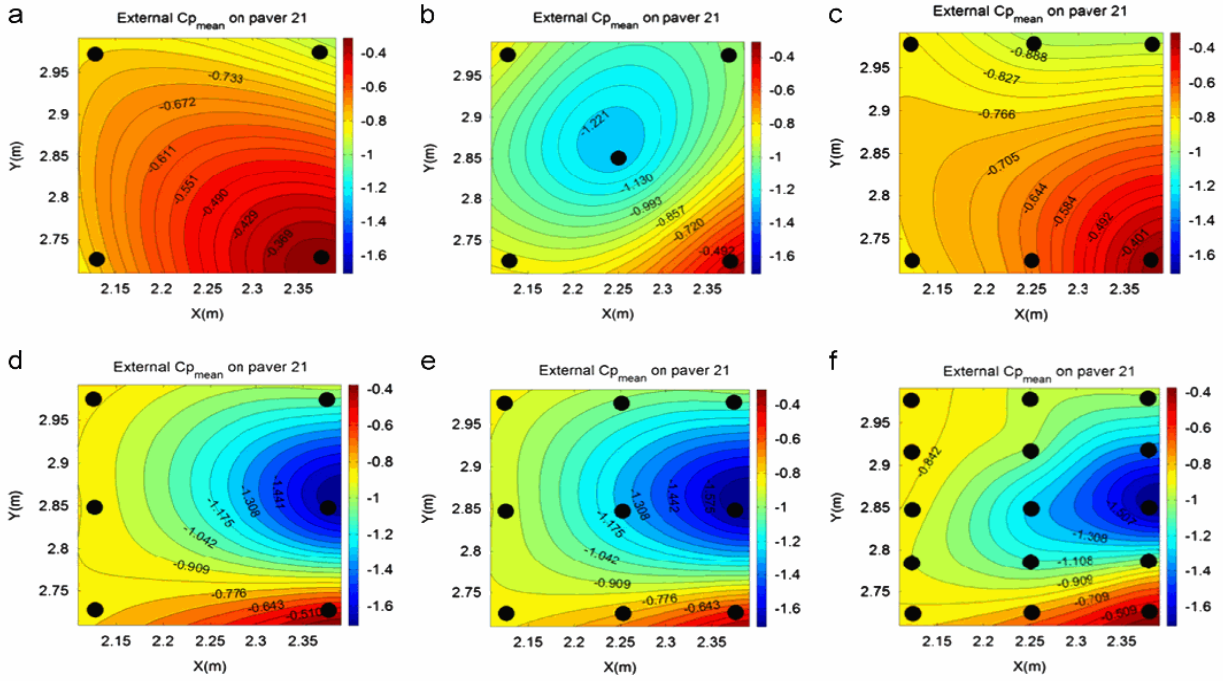


**Fig. 23.** Effect of pressure tap layout on external $Cp_{mean}$ ($h_p/H=0.05$ and $G/H_s=0.25$).

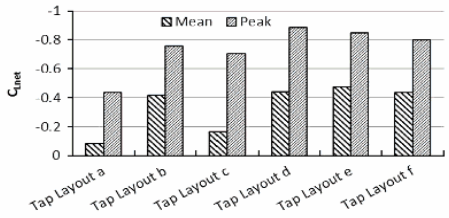


**Fig. 24.** $C_{Lnet}$ for different pressure tap layouts ($h_p/H=0.05$; $G/H_s=0.25$).

smaller tributary area than 0.9 $m^2$ and so would be expected to be somewhat higher in magnitude than the ASCE 7 value. The highest peak external lift coefficients ranged from −1.44 for $h_p$/H=0.05 and $G/H_s=0.028$ to −1.26 for $h_p/H=0.15$ and $G/H_s=0.083$. The underneath pressure coefficients required for calculating the net pressure coefficients are not dealt with in ASCE 7-10. One informal practice is to assume the underneath pressure coefficient to be zero (FPHLM study on tiles, 2005, Volume II, p. 55) and that the net uplift force acts on the center of the paver.

In order to see the overall effect of high local *Cp* values on the failure wind speeds, the critical wind blow-off speeds were calculated from the pressure measurements using Eq. (9) and compared to those obtained from the wind blow-off tests (Table 4) and the wind blow-off speeds calculated from a typical informal practice based on ASCE 7-10 exterior pressures (i.e. using the ASCE 7-10 external pressure coefficients, taking the effective internal pressure as zero and simply assuming that the net uplift acts at the paver's center). Results calculated from pressure measurements are for paver 21 which was shown to be one of the most critical in all three cases. The values recorded for the wind blow-off tests correspond to the case where both wobbling of pavers and first failure were observed. For the practice based on ASCE 7-10 exterior pressures, wind blow-off speed values are calculated using $GCp=-2.8$ (external pressure coefficient in Zone 3 for $A_{eff}=0.09\ m^2 \le 0.9\ m^2$).

Results show that quite good agreement exists between the results from wind blow-off tests and those obtained from mean $C_{Lnet}$ values. This means that although high peak suctions were observed on critical pavers, which can cause instantaneous wobbling, the fluctuations did not last long enough to actually cause lift off. The best agreement between the blow tests and the pressure measurements would be obtained by calculating the lift based on the mean coefficient plus a small contribution from the fluctuations. The critical wind blow-off value calculated using ASCE 7-10 exterior pressures is clearly conservative in comparison to the current experiments.

Table 5 shows equalization factors, as defined by Geurts (2000), for different $G/H_s$ ratios for the critical paver 21. A value of 0.6 was proposed by Geurts based on full-scale pressure measurements. Comparison between the results shows the present values ranging around 0.6. The results presented in Geurts (2000) were for a single $G/H_s$ ratio. The present results indicate the value 0.6 may underestimate the ratio on pavers with low $G/H_s$ ratios. The results presented in this paper are for 45° cornering winds only which is the most critical for paver lift-off on a flat roof. The equalization factor may well be a function of wind direction and Geurts' results covered various wind directions. For the purposes of codification the concept of an equalization factor is useful but it needs also to take account of the results in Table 4. These results show that the best correlation with observed blow off speeds is obtained using the mean $C_{Lnet}$, not the peak $C_{Lnet}$. It appears that most of the fluctuations in $C_{Lnet}$ do not last long enough to disturb the paver. Therefore a more meaningful factor for codification purposes is likely to be the ratio of mean $C_{Lnet}$ (or perhaps mean plus a small contribution from fluctuations) to the peak *Cp* that is provided in codes for cladding design. Future work is in progress to explore

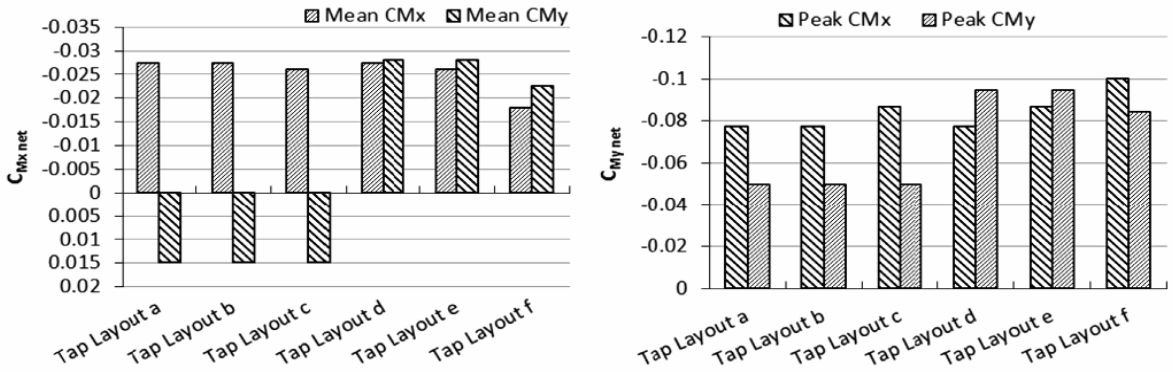


**Fig. 25.** $C_{Mnet}$ for different pressure tap layouts ($h_p/H=0.05$; $G/H_s=0.25$).

**Table 4**
Critical wind blow-off speed.

| Test | Critical wind blow-off speed (m/s) | | | |
|---|---|---|---|---|
| | **Practice based on ASCE 7-10 exterior pressures** | **Wind blow-off tests** | **Pressure measurement tests** | |
| | $\left(U_{CRIT}=\sqrt{\frac{W}{\frac{1}{2}\rho C_{p\,net} A}}\right)$ | | $\left(U_{CRIT}=\sqrt{\frac{a}{2(d+\frac{a}{2})}\times\frac{W}{\frac{1}{2}\rho C_{Lnet\ or\ peak}A}}\right)$ | |
| | | | Based on mean $C_{Lnet}$ | Based on peak $C_{Lnet}$ |
| **$G/H_s=0.25$** | 17.6 | 37.2 | 41.84 | 29.14 |
| **$G/H_s=0.083$** | | 35.7 | 35.72 | 26.8 |
| **$G/H_s=0.028$** | | 30.7 | 32.24 | 24.7 |

*22 (m/s) for $GCp=-1.8$ (external pressure coefficient in Zone 2 for $A_{eff}=0.09\ m^2 \le 0.9\ m^2$).

**Table 5**
Equalization factor based on $G/H_s$.

| $G/H_s$ | $\frac{\text{Mean } C_{Lexc}}{\text{Mean } C_{Lnet}}$ | $\frac{\text{Peak } C_{Lexc}}{\text{Peak } C_{Lnet}}$ | Geurts (2000) $\frac{Cp_{exc}}{Cp_{net}}$ |
|---|---|---|---|
| 0.25 | 0.49 | 0.58 | 0.6 |
| 0.083 | 0.68 | 0.75 | |
| 0.028 | 0.77 | 0.83 | |

this aspect in more detail, as well as the effects of building geometry, paver size, $G/H_s$ ratio and $h_p/H$.

## 5. Conclusions and future work

The wind loading mechanism of concrete roof pavers was investigated in this project. Wind blow-off tests and pressure measurements were carried out on a square portion of a flat roof for the critical wind direction that generates corner vortices. The experiments were performed in the Wall of Wind, at FIU. The influence of an edge parapet on net uplift pressures was also explored. Increasing the pavers' edge-gap to spacer height ratio improves the system behavior. A certain relative parapet height in the range $h_p/H=0.10$–$0.15$ exists in which the uplift loads reach the worst case values. The results demonstrated that the net uplift force and moment coefficients are sensitive to the resolution and layout of the pressure taps. The location and spacing of pressure taps needed to accurately resolve the uplift pressures were investigated. A larger number of taps than typically used in the past was found to be needed. Based on the information gathered in the current tests and review of the literature, guidelines suitable for codes and standards are being developed for the design of roof pavers. These guidelines will need to incorporate appropriate factors of safety in order to achieve the normal levels of reliability used in the design of building envelopes. Similar phenomena observed for the roof pavers affect roof tiles and shingles, further complicated by the profiles of the particular tile and shingle systems used. The large-scale testing methods used in the present investigation are also applicable to these other roofing systems and provide new insights through accurately reproducing critical aerodynamic effects at full scale, or close to full scale Reynolds numbers.

## Acknowledgments

We would like to greatly appreciate the Tile Tech Company for providing us with concrete roof pavers and the pedestal system required for the wind blow-off tests. This research was supported by the Florida Division of Emergency Management (DEM) and the National Science Foundation (NSF) (NSF Award no. CMMI-1151003) through the 12-fan Wall of Wind flow simulation and large-scale testing of roof pavers. The help offered by the Wall of Wind manager, Walter Conklin and the Research scientists, Roy Liu Marquis and James Erwin, is greatly acknowledged. We would also like to acknowledge the great help received from the graduate research assistant, Ramtin Kargarmoakhar.

## References

Aly, A.M., Bitsuamlak, G.T., Chowdhury, A.G., 2012. Full-scale aerodynamic testing of a loose concrete roof paver system. Eng. Struct. 44, 260–270.
Amano, T., Fujii, K., Tazaki, S., 1988. Wind loads on permeable roof-blocks in roof insulation systems. J. Wind Eng. Ind. Aerodyn. 29, 39–48.
AS 1170.2, 2011. Australian/New Zealand standard: structural design actions, Part 2: wind actions, Standards Australia/Standards New Zealand, Sydney, Australia.
ASCE 7-10, 2010, Minimum Design Loads for Buildings and Other Structures, American Society of Civil Engineers, ASCE, Virginia.
Banks, D., 2011. Measuring peak wind loads on solar power assemblies. In: Proceedings of the 13th International Conference on Wind Engineering.
Banks, D., Meroney, R.N., Sarkar, P.P., Zhao, Z., Wu, F., 2000. Flow visualization of conical vortices on flat roofs with simultaneous surface pressure measurement. J. Wind Eng. Ind. Aerodyn. 84, 65–85.
Bienkiewicz, B., Endo, M., 2009. Wind considerations for loose-laid and photo-voltaic roofing systems, Structures Congress, Austin, Texas. pp. 2578–2587.
Bienkiewicz, B., Meroney, R.N., 1988. Wind effects on roof ballast pavers. J. Eng. Struct. 114, 1250–1267.
Bienkiewicz, B., Sun, Y., 1992. Wind-tunnel study of wind loading on loose-laid roofing system. J. Wind Eng. Ind. Aerodyn. 43, 1817–1828.

Bofah, K.K., Gerhardt, H.J., Kramer, C., 1996. Calculations of pressure equilibration underneath loose-laid, flow permeable roof insulation boards. J. Wind Eng. Ind. Aerodyn. 59, 23–37.

Cheung, J.C.K., Melbourne, W.H., 1986. Wind loads on porous cladding. In: Proceedings of the 9th Australasian Fluid Mechanics Conference, Auckland. pp. 308–311.

Cheung, J.C.K., Melbourne, W.H., 1988. Wind loading on a porous roof. J. Wind Eng. Ind. Aerodyn. 29, 19–28.

DEUTSCHE NORM, 2001-03. DIN 1055-4, Einwirkungen auf Tragwerke, Teil 4: Windlasten.

Fu, T.-C., 2013. Development of Effective Approaches to the Large-Scale Aerodynamic Testing of Low-Rise Building. Florida International University, Miami, Florida, USA.

Fu, T.-C., Aly, A.M., Chowdhury, A.G., Bitsuamlak, G., Yeo, D., Simiu, E., 2012. A proposed technique for determining aerodynamic pressures on residential homes. Wind Struct. 15, 27–41.

Gerhardt, H.J., Janser, F., 1995. Windbelastung belufteter Fassadensysteme. Bauingenieur 70, 193–201.

Gerhardt, H.J., Kramer, C., Bofah, K.K., 1990. Wind loading on loosely laid pavers and insulation boards for flat roofs. J. Wind Eng. Ind. Aerodyn. 36 (Part 1), 309–318.

Geurts, C.P.W., 2000. Wind loads on permeable roof covering products. In: Fourth Colloquium on Bluff Body Aerodynamics and Applications, Ruhr Universität Bochum. pp. 511–514.

Ho, T.C.E., Surry, D., Morrish, D., Kopp, G.A., 2005. The UWO contribution to the NIST aerodynamic database for wind loads on low buildings: Part 1. Archiving format and basic aerodynamic data. J. Wind Eng. Ind. Aerodyn. 93, 1–30.

Holmes, J.D., 2007. Wind Loading of Structures. Taylor & Francis, New York.

Irwin, P., 2009. Wind engineering research needs, building codes and project specific studies. In: Proceedings of the 11th Americas Conference on Wind Engineering.

Irwin, P., Cooper, K., Girard, R., 1979. Correction of distortion effects caused by tubing systems in measurements of fluctuating pressures. J. Wind Eng. Ind. Aerodyn. 5, 93–107.

Katsuchi, H., Yamada, H., 2011. Study on turbulence partial simulation for wind-tunnel testing if bridge deck. In: Proceedings of the 12th International Conference on Web Engineering, ICWE 2012, Amsterdam, Netherlands.

Kind, R.J., 1988. Worst suctions near edges of the flat roof tops with parapets. J. Wind Eng. Ind. Aerodyn. 31, 251–264.

Kind, R.J., 1994. Predicting pressure distribution underneath loose laid roof cladding systems. J. Wind Eng. Ind. Aerodyn. 51, 371–379.

Kind, R.J., Wardlaw, R.L., 1982. Failure mechanisms of loose laid roof insulation systems. J. Wind Eng. Ind. Aerodyn. 9, 325–341.

Kopp, G.A., Banks, D., 2013. Use of the wind tunnel test method for obtaining design wind loads on roof-mounted solar arrays. J. Struct. Eng. 139, 284–287.

Kopp, G.A., Surry, D., Mans, C., 2005. Wind effects of parapets on low buildings: part 1. Basic aerodynamics and local loads. J. Wind Eng. Ind. Aerodyn. 93, 817–841.

Kramer, C., Gerhardt, H.J., 1983. Wind loads on permeable roofing systems. J. Wind Eng. Ind. Aerodyn. 13, 347–358.

Kumar, K.S., Stathopoulos, T., 1998. Spectral density functions of wind pressures on various low building roof geometries. Wind Struct. 1, 203–223.

Lin, J.X., Surry, D., 1998. The variation of peak loads with tributary area near corners on flat low building roofs. J. Wind Eng. Ind. Aerodyn. 77–78, 185–196.

Lin, J.X., Surry, D., Tieleman, H.W., 1995. The distribution of pressure near roof corners of flat roof low buildings. J. Wind Eng. Ind. Aerodyn. 56, 235–265.

Melbourne, W.H., 1980. Turbulence effects on maximum surface pressures—a mechanism and possibility of reduction. Wind Eng. 1, 541–551.

NBCC, 1995. User's Guide-NBC 1995, Structural Commentaries (Part 4), National Research Council of Canada, Ottawa, Canada.

NEN EN 1991-1-4/NA 1991, Eurocode: Actions on structures—General actions—Part 1.4: Wind Actions.

Pierre, L.M.S., Kopp, G.A., Surry, D., Ho, T.C.E., 2005. The UWO contribution to the NIST aerodynamic database for wind loads on low buildings: Part 2. Comparison of data with wind load provisions. J. Wind Eng. Ind. Aerodyn. 93, 31–59.

Richards, P.J., Hoxey, R.P., Connell, B.D., Lander, D.P., 2007. Wind-tunnel modelling of the Silsoe cube. J. Wind Eng. Ind. Aerodyn. 95, 1384–1399.

Saathoff, P.J., Melbourne, W.H., 1997. Effects of free-stream turbulence on surface pressure fluctuation in a separation bubble. J. Fluid Mech. 337, 1–24.

Sadek, F., Simiu, E., 2002. Peak non-Gaussian wind effects for database-assisted lowrise building design. J. Eng. Mech. 128, 530–539.

Smith, T., McDonnald, J., 1991. Roof Wind Damage Mitigation: Lessons from Hugo. American Society of Civil Engineers, New York

Stathopoulos, T., 1982. Wind pressure on low buildings with parapets. J. Struct. Div. 108, 2723–2736.

Stathopoulos, T., Baskaran, A., 1987. Wind pressures on flat roofs with parapets. J. Struct. Eng. 113, 2166–2180.

Stathopoulos, T., Baskaran, A., 1988. Turbulent wind loading on roofs with parapet configurations. Can. J. Civ. Eng. 29, 570–578.

Sun, Y., Bienkiewicz, B., 1993. Numerical simulation of pressure distributions underneath roofing paver systems. J. Wind Eng. Ind. Aerodyn. 46–47, 517–526.

Tieleman, H.W., 2003. Wind tunnel simulation of wind loading on low-rise structures: a review. J. Wind Eng. Ind. Aerodyn. 91, 1627–1649.

Trung, V., Tamura, Y., Yoshida, A., 2009. Study on wind loading on porous roof cover sheets on a low-rise building: effects of parapet height and underneath volume. In: Proceedings of the 11th Americas Conference on Wind Engineering, San Juan, Puerto Rico.

Trung, V., Tamura, Y., Yoshida, A., 2010. Numerical computation for lower surface pressures on a porous sunshade roof cover sheet. In: Proceedings of the Fifth International Symposium on Computational Wind Engineering (CWE2010), Chapel Hill, North Carolina, USA.

Yamada, H., Katsuchi, H., 2008. Wind-tunnel study on effects of small-scale turbulence on flow patterns around rectangular cylinder. In: Proceedings of the 4th International Colloquium on Bluff Bodies Aerodynamics & Applications, Italy.

Yeo, D., Chowdhury, A.G., 2013. Simplified wind flow model for the estimation of aerodynamic effects on small structures. J. Eng. Mech. 139, 367–375.